# Biomimetic Bi-Pedal Humanoid: Design, Actuation, and Control Implementation with Focus on Robotic Legs

MICHAEL LOUIS OKYEN

Thesis submitted to the faculty of the Virginia Polytechnic Institute and State University in partial fulfillment of the requirements for the degree of

Master of Science

In

Mechanical Engineering

Shashank Priya, Chair

Steve Southward

Alfred Wicks

April 5, 2013

Blacksburg, VA

Keywords: humanoid, biomimetic, legs, mechatronics, hydraulics

Biomimetic Bi-Pedal Humanoid:

Design, Actuation, and Control Implementation with Focus on Robotic Legs

Michael Louis Okyen

## ABSTRACT

The advancements made in technology over the past several decades have brought the field of humanoid robotics closer to integration into the everyday lives of humans. Despite these advances, the cost of these systems consistently remains high, thus limiting the environments in which these robots can be deployed. In this thesis, a pair of low-cost, bio-mimetic legs for a humanoid robot was developed with 12 degrees of freedom: three at the hip, one at the knee, and two at the ankle. Prior to developing the robot, a survey of the human-sized robotic legs released from 2006-2012 was conducted. The analysis included a summary of the key performance metrics and trends in series of human-sized robots. Recommendations were developed for future data reporting that will allow improved comparison of different prototypes. The design of the new robotic legs in this thesis utilized human anatomy data to devise performance parameters and select actuators. The developed system was able to achieve comparable ROM, size, weight, and torque to a six-foot tall human. Position and zero-moment point sensors were integrated for use in balancing, and a control architecture was developed. A model of the leg dynamics was created for designing balancing and walking algorithms. In addition, hydraulic actuators were evaluated for use in humanoid robotics, and testing was conducted in order to create a position control methodology. Finally, a predictive deadband controller was designed that was able to achieve accuracy of less than one degree using a valve with slow switching speed.

# Acknowledgements

I need to thank everyone who has been a part of this great journey in my life. I certainly would not have made it through without the guidance, assistance, motivation, and friendship I received from the people I have worked with, especially Nick Thayer, Eric Baldrighi, Mike Stevens, Matthew Paluszek, Stephen Powell, and Noah Philipson. Working with 38 senior design students over the past three years has been one of the greatest experiences of my life. Thank you for the hard work, for all the late nights, for all the laughs, and for the friendships that will last a lifetime.

I would also like to thank my advisor, Dr. Priya for giving me the opportunity to learn and grow into the engineer and person I am today. Despite all of your responsibilities, I always felt that you would make time for me, and I continually felt your trust in my judgment. I have never met anyone who is harder working, and I have no doubt that your research will continue to change the world!

I have also been blessed with a wonderful family and friends who have supported me through every stage of my education. To my parents- thank you for everything you have done for me and given me as we've journeyed together through the past seven years. To my friends, thank you for all your encouragement and for all the joy you've brought to my life.

Thank you everyone!

# Contents

## Chapter 1

## Chapter 2



## Chapter 3

## Appendices

# List of Figures

# List of Tables

# Chapter 1

# Introduction

For centuries, humans have attempted to develop a mechanical copy of their own bodies. While our goals have varied from entertainment to science to military use, the overall objective has remained the same: to create a robot that is able to emulate what humans are able to do. The world is laden with inventions which surpass almost any particular human capabilities, whether that is an automobile's speed, power, and range; an industrial machine's precision in manufacturing; or a computer's ability to process massive amounts of data. However, no invention is able to match the vast capabilities of man in one system, as cars are unable to climb stairs, machines only produce what they are created to fabricate, and computers only calculate as they have been programmed. As better tools have been developed, increasingly more of the tedious or repetitive tasks are conducted by machines, allowing humans to dedicate time to our unique capacities: critical and creative thought. The desire to have one machine that can perform the functions of humans with the same capacity has driven the development of humanoid robots. Walking legs are critical for many of the functions that are important towards achieving this goal.

## 1.1 Justification for Walking Robotics

Most of the systems investigated in the literature for locomotion have relied on wheels instead of legs. However, with the progress made in development of actuators and computers, legged robots now offer several advantages over their wheeled counterparts. Typically wheels have been designed to move on flat surfaces with limited inclines. Rougher terrains were largely impassable or needed treaded vehicles, which are also limited. Conventionally wheeled systems have a large contact area and need continuous contact with the ground to apply torque only in one direction that is normal to the point of contact between the wheel and ground in the direction of rotation. However, the form of most wheeled vehicles, having all sets typically rotating in one direction with some or all being able to pivot around a vertical axis, makes controlling their movement considerably simpler than legs with more degrees of freedom (DOF). Further, because

all of the supplied energy goes directly into propelling the vehicle, wheels would be more efficient for movement in a straight direction on a flat surface than a leg, which uses energy to lift in the vertical direction (assuming negligible frictional losses).

### 1.1.1 Establishing Criterion for Selection of Legged Robot

To establish the criterion for developing a legged robot, the comparative advantages of the wheeled and legged robots first must be established. A review of the current literature mostly provides the justification for legs in qualitative and subjective terms. Generally, the literature suggests allowing a robot to operate in human environments without adapting the environment to the robot (e.g., Chew, Tay, Smit, & Bartneck, 2010). However, environments are continually adapting to new technology, be it elevators and ramps for wheelchairs, or wireless internet for communication devices; thus, simply stating the environment is insufficient rationale. Thus, an attempt was made to systematically provide a justification for research on bi-peds, beginning with the definition of stability.

### 1.1.2 Defining Stability

In general, wheeled robots have been accepted as more stable platform than their legged counterparts. A system that is stable is defined as the one that will not lose its balance. If a static system with no outside forces being applied to it has only a single point (i.e., an infinitesimally small place in space) in contact with the ground, then the only time in which that system is balanced is when the center of mass (COM) is exactly above that point. If the system has two points of contact (POC), then the balance is only achieved when the COM is somewhere along the line between the two points (Figure 1.1.1). If three or more POCs are present in the system, they will form the support polygon, which we will refer to as the base of support (BOS; Figure 1.1.1). As long as the COM remains within the BOS in the X-Y plane, stability will be maintained if the system is at rest and not under influence of outside forces.

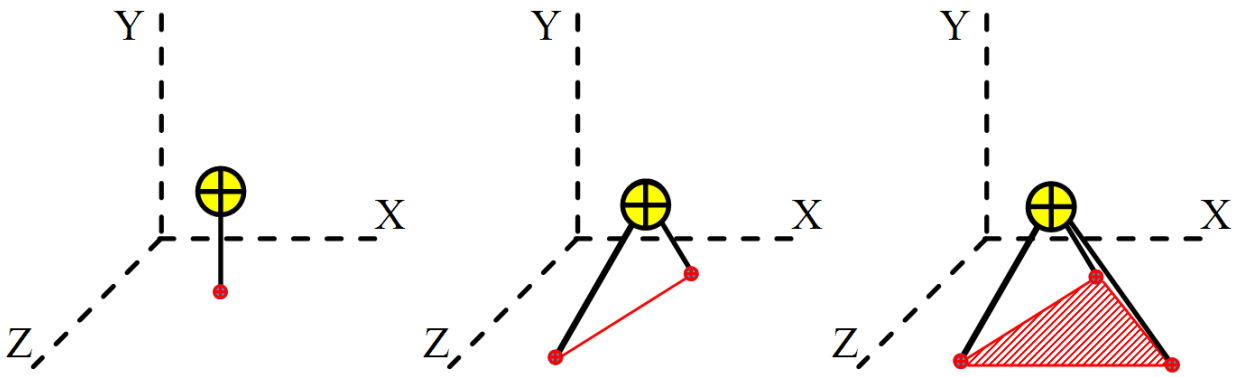


**Figure 1.1.1. BOS for one, two, and three points of contact. The BOS is shown by the dot at the bottom of the segment and the line connecting them. The support polygon would continue to grow with additional POCs.**

However, if the system is not at rest or any outside forces are applied, then the center of pressure (COP), or zero moment point (ZMP) as it is commonly referred to in robotics, must remain inside the BOS. Although the distribution of forces between the POCs and the ground is complex, Erbatur, Okazaki, Obiya, Takahashi, and Kawamura (2002) have provided an analysis of the stability (p. 431, as cited in Tak, Song, & Ko, 2001; see Figure 1.1.2) which reflects some important considerations. Erbatur et al. (2002) define ZMP as the location of the point where the net force, including the inertial and gravitational forces, has no component except in the vertical direction (perpendicular to the ground (as cited in Tak et al., 2001).

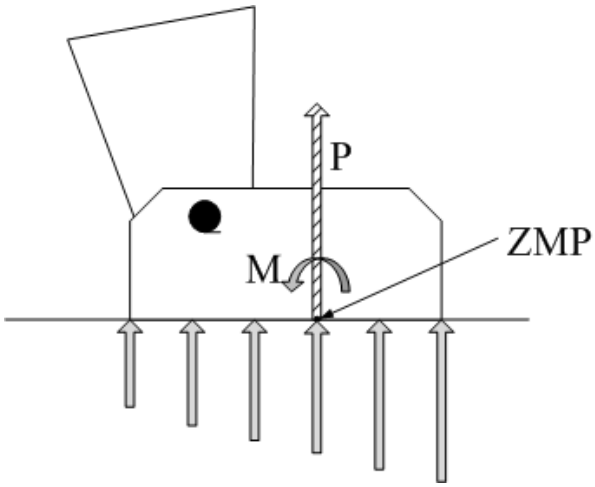


**Figure 1.1.2. ZMP underneath a foot. Figure adapted from Erbatur et al. (2002). The forces on the bottom of the foot can be approximated by the force P and moment M at any point.**

If a wheel is a perfectly round disk which is infinitely small, it would contact a perfectly flat surface at only one infinitely small point. However, actual wheels deform, as does the ground, so the contact points will be infinite in number in the area between the wheel and ground, as they will be for the area under the contact points for legged robots. The BOS for any system will be the largest polygon that can be drawn through the points of contact with the ground, as is displayed in Figure 1.1.3. Therefore a system will be more stable if it has a larger BOS than a robot of the same form with a smaller BOS. From here forward POC will refer to the whole part of the robot that is making contact with the ground whether that is a foot or tire.

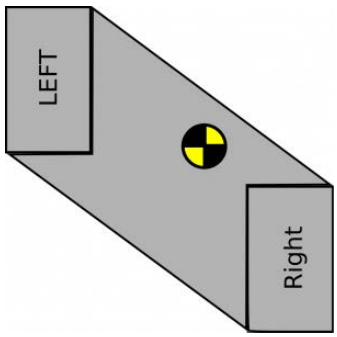


**Figure 1.1.3. Base of support for robotic feet. The support polygon is the area under and between the POCs. The system will remain stable as long as the COP is within this area, as is shown.**

### 1.1.3 Defining Wheeled vs. Legged Robots

With the definition of stability established, a comparative analysis of legged and wheeled robot can be developed. A *legged robot* has the ability to actively move a point of contact in the vertical direction, in contrast to a *wheeled robot*, which uses wheels as the primary method of force transmission and cannot actively move any of its points of contact in the vertical direction (see Figure 1.1.4). These definitions were developed to distinguish a system that can lift one of its wheels off the ground using a segment of various shapes from one whose wheels are static, because lifting a segment would enable a system to potentially walk or move up to a higher level. It is important to note that legged robots do not necessarily walk as their primary means of movement. *Walking robots* will be defined as legged robots that primarily translate by moving segments in the vertical direction rather than using rotating wheels. Hybrid robots also exist, utilizing both legs and wheels (see Figures 1.1.5 and 1.1.6).

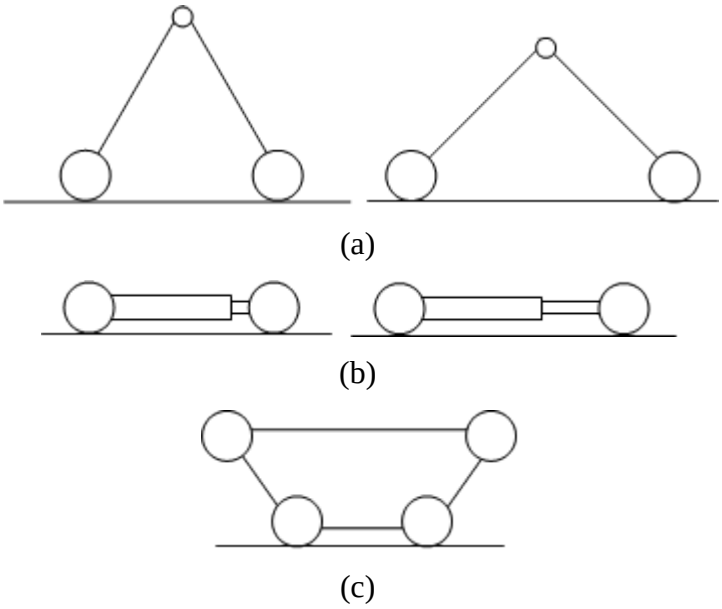


**Figure 1.1.4. Examples of wheeled robots. (a) a robot with a raised DOF that changes the distance between the wheels by adjusting the angle between the segments, but cannot lift a wheel off of the ground. (b) a system that uses a prismatic joint to similarly change the distance between the wheels. (c) a system with fixed wheels, but because some are raised, the BOS can change when the higher wheels come into contact with a surface. Although the wheels do not move, this is still considered a wheeled robot.**

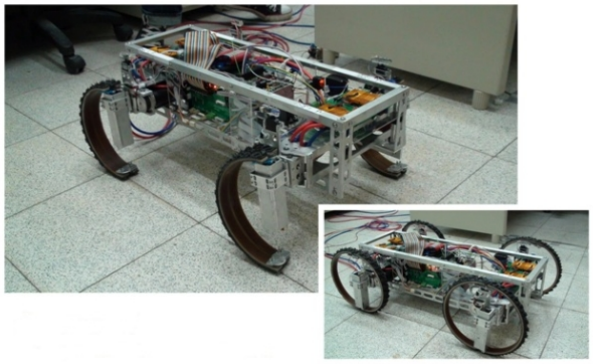

**Figure 1.1.5. Leg-wheel hybrid robot. This robot can either have four legs, which rotate and move POCs off the ground, or as a wheeled robot, where the wheels are always in contact (Shen et al., 2009, p. 4682). Figure reprinted by permission, © 2009 IEEE. (see Appendix A).**

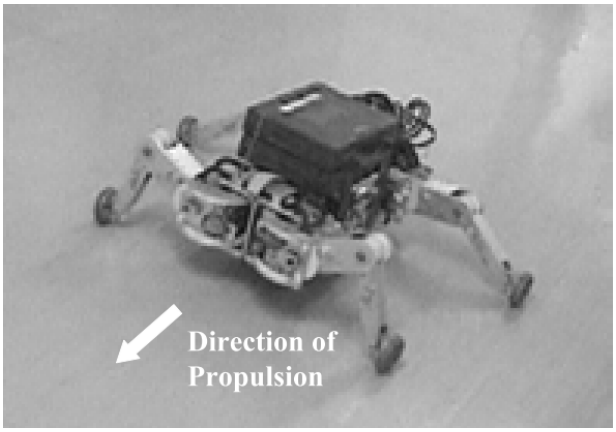


**Figure 1.1.6. Roller-walker robot. This robot is able to move by walking or using the passive wheels on the end of each leg, which rotate down to contact the ground (Endo & Hirose, 2011, p. 979). This would also be classified as a legged robot, because it is able to lift its POCS. However, if the wheels could not be lifted, it would be classified as a wheeled robot despite having appendages that move. Figure reprinted by permission, © 2012 Taylor & Francis (see Appendix A).**

Because the legged robots can move a POC vertically, they have two distinct advantages over wheeled robots. First, the robots are able to actively change their BOS by varying the number of POCs. For example, a four-legged robot would be able to lift one POC if that point began to slip. Second, legs allow movement in a discontinuous path. A wheel must move along a

continuous line from one point to another, while a leg can be lifted, moved, and set down. These two advantages allow legged robots to perform tasks that wheeled robots cannot. Mobility on uneven surfaces such as rocky or wooded terrain can be a complex task for wheeled vehicles. Legs allow a robot to step over obstacles or step up to a higher plane such as when navigating stairs. Being able to move a POC to an area with more traction is critical when handling diverse environments. Consequently, while wheeled robots appear to have a definitive edge when moving on flat surfaces, legged robots are more adaptive and in turn can handle a wider variety of situations. In the next section a discussion on the choice of legs over wheels is presented.

### 1.1.4 Justification for Two Legs over More Legs

Walking robots come in a variety of forms. Over the past 25 years, many of the humanoids that have been developed are bipedal, which has both advantages and disadvantages when compared to the walking robots with more legs. Systems with six legs or more have the advantage of being able to maintain stability by keeping at least three POCs on the ground at all times (Bräunl, 2008). However, two-legged robots will have a smaller footprint than other robots, which allows them to navigate in tighter spaces. It is also the minimum number of limbs necessary; fewer legs also means a smaller number of joints to design and control in addition to less weight. However, the most important reason for a biped is the resemblance to the human form (Lebouvier, 2011). If a two-legged robot is able to maneuver in the similar fashion as a person, it could be used in identical situations and environments. This would allow robots to perform tasks which are considered menial and repetitive or are dangerous and pose risk towards the health of humans. The use of bipedal legs as prosthesis could also be a possibility in the near future. Moreover, researchers have also cited the ability to study human kinematics by developing robotics to mimic the motions such as Wabian (Ogura, Aikawa, Shimomura, Kondo, & Morishima, 2006). Behnke (2008) points out that the goal of developing humanoid robots is to create robots that work in close cooperation with humans in the same environment that we designed to suit our needs. Coradeschi et al. (2006) detail the potential roles of humanoid robots by stating that robots are only now becoming commonplace in everyday life for the general population but will eventually begin to permeate schools, homes, and healthcare. Furthermore, they contend that developing robots with similarity to humans will facilitate the adoption of the systems for people without a depth of knowledge of the technology (Coradeschi et al., 2006).

When the nearly limitless capability of humans is considered, it seems as though only a biped would be able to fulfill this goal.

In addition to the scientific reasons for developing bipedal robots, a significant part of the rationale comes down to the psychological desire of humans to build systems that resemble themselves. The Idaho National Laboratory (n.d.) describes the human fascination with humanoid robots functioning beyond that of mere automation, citing classic writings by Homer as early examples of this trend. Thus, the natural inclination for people is to incorporate human-like attributes in any tools, ranging from hammers to cellular phones to vehicles. It seems that human nature desires objects to interact, as is seen with the technology that permeates science fiction (Behnke, 2008; Idaho National Laboratory, n.d.; Lebouvier, 2011; National Public Radio, 2007). As Coradeschi et al. (2006) agree, humans have a tendency to expect human-like attributes (e.g., human emotions and motivations) to manifest in robots.

It is likely that this desire to humanize robotics also greatly influences the level of public interest in humanoid robots. Although little by way of empirical research has commenced on the subject, some discussion has been held regarding the malleability of the public's interest level. Lebouvier (2011) notes that while fictional writings have primarily focused upon the human desire to seize the role of the creator, little has been written concerning the link between the development of robotic technology and society. In addition, Hiroshi Ishiguro has discussed our high expectations of humanoid robots; we often attribute human personality to the inhuman, which drive our attraction to humanoids and androids (Coradeschi et al., 2006).

Noel Sharkey, a well-known British robot expert, said to be the man from whom the history of intelligent robots stemmed, notes in an Australian newspaper article that while people have been trying to re-create themselves throughout history, the rationale for doing so is an important yet unanswered question (Reikert, 2005). Similarly, Stacey and Suchman (2012) while discussing the relationship between automation and animation touch on human nature and our response to robots. The authors discuss Jessica Riskin, a historian of automata's (e.g., see Riskin, 2003) thoughts on our capacity to "humanize" mechanics when presented with a human-like object, and in turn the reciprocal relationship inherent in this interaction: our interpretations of what it is to be human are shaped by our interactions with humanoid machines, and likewise our interpretation of what it is to machine is affected (Stacey & Suchman, 2012). Herein lies a potential threat: the boundary between machine and human is obscured.

However, although these sentiments are likely to be among the greatest justifications for developing a walking biped, further investigation is outside the scope of this research. As Lebouvier (2011) describes it,

> [o]ur inability to describe adequately just what it is that makes us unique deeply engages us as few other scientific or philosophical questions can. In their capacity to compel us to look at ourselves, humanoid robots might be considered the ultimate technological artifact. (Lebouvier, 2011, p. 3)

### 1.1.5 Applications for Walking Robots

Systems which translate using legs have traditionally taken inspiration from nature, and the types of legged robots have followed the biological trend of extreme diversity in architecture. The range of designs spans from systems that are large with four legs like Big Dog by Boston Dynamics which weighs over 100 kilograms (Wooden et al., 2010) to very small with six legs, such as the 2.4 gram RoACH, which was developed at the University of California (Hoover, Steltz, & Fearing, 2008). A humanoid robot has been defined as a machine in which "perception, processing and action are embodied in a recognizably anthropomorphic form in order to emulate some subset of the physical, cognitive and social dimensions of the human body and experience" (Idaho National Laboratory, n.d., para. 14)]. Within this group, many of the robots are much smaller than a human, such as Virginia Tech's DARwIn (Muecke & Hong, 2007) and NAO (Gouaillier et al., 2009) developed at Aldebaran Robotics. Because of their small stature and light weight, these bipeds tend to be less expensive to implement. However, their size also limits their capability, which is why considerable research has been performed on robots closer to human size and strength.

Chevallereau et al. (2009) explain that the areas of use for bipedal robots focus around service, dangerous terrains, defense, and medical prosthesis. Service robots could be used to assist at personal residences with daily chores, particularly for an aging population. Dangerous terrains such as fires or car accidents present hazards on a daily basis where a humanoid could potentially assist in the most dangerous tasks. The Defense Advanced Research Projects Agency (DARPA) in the United States announced the DARPA Robotics Challenge in 2012, and the tasks that the systems will be required to perform focus on disaster response (DARPA, 2012, 2013).

DARPA also funds the development of the humanoid PETMAN by Boston Dynamics (2012), whose stated purpose is to test clothing for chemical protection. Humanoid soldiers have been included in film and movies for decades (Lebouvier, 2011; National Public Radio, 2007), and many of the currently developed systems could be used to supplement or replace members of the armed forces in the future. Medical prosthesis, as previously mentioned, could also benefit, although a pair of connected legs would probably be less common than replacing several segments of one leg or the lower leg from the knee down. Despite these projections, as androids continue to advance, the number of jobs they could fulfill will only grow with cost reductions and increases in functionality.

### 1.1.6 Justification for the Presented Design

The focus of this work was on developing a pair of robotic legs as part of a humanoid robot. The overall purpose is for the system to be used in two applications: as a laboratory assistant to conduct experiments and as an elderly assistant. In a laboratory setting, developing a system which could conduct experiments remotely with a high level of adaptability could open the door for more collaboration and equipment sharing in scientific studies. As an elderly assist robot, the largest gains would be providing care to older people with everyday tasks, including movement, dressing, and taking medication. The goal in both situations would focus around initially developing a semi-autonomous system with a human in the loop to control the robot and over time move towards higher levels of autonomy.

The robotic legs are important to accomplishing these goals for several reasons:

1. Environments in which the robot will be expected to perform will continue to be occupied by people, and therefore a goal will be to minimize the changes needed to accommodate the robot. Walking, bending over, and maneuvering in tight spaces will be required capabilities.
2. Stairs and obstructions will be present in both scenarios, especially if the system matures to the point of being integrated into private homes.
3. For elderly assistance, patients may feel more comfortable if the system more closely resembles a human. The same may be true for those working in the laboratory.
4. In both situations, the cost of current humanoid robots will continue to prevent their widespread integration into daily life.

## 1.2 Survey of Full Size Bipedal Humanoid Robots

### 1.2.1 Criteria for Survey

To understand the trends in bipedal robots and the typical parameters of design, a survey was conducted on the recently developed *full-sized humanoids*, which are defined here as robots meeting the following parameters:

1. Primarily walks on two legs
2. At least 1 m in height with an upper body, or 0.5 m to the waist without an upper body
3. Released between January 1, 2006 and June 30, 2012

Because the focus of this thesis is on humanoid robots, only those systems with two legs are included. Robots that can walk on two legs but primarily walk on four or use wheels were excluded from this survey. Smaller robots are not able to perform many of the human tasks due to the lack of reach and strength. Because computational technology is evolving at an unprecedented rate and the goal here is to summarize the state-of-the-art, only the newest systems are included.

### 1.2.2 Data Collection

A difficulty in performing this survey was the diversity of data reported from each research group. Many research teams have not published the results in peer-reviewed journals, and other researchers have not provided quantitative information about their components using terms like *servomotors* instead of specifying the type of motor. Data collected for this analysis was taken from scholarly publications, official websites of the developing groups, and from publications in reputable newspapers and magazines. Six humanoids were not included in the analysis due to the lack of verifiable data, and are listed in Table 1.2.1. PETMAN is widely accepted as one of the premier walking humanoids developed to date; however, as videos on Youtube.com were the primary sources of information, it was removed from the analysis. Common robot description parameters are included, and later suggestions for data that can be included in the future are presented. Due to the large number of publications included in this survey, the citations for each robot are included in Appendix B.

**Table 1.2.1. Biped robots not included due to lack of verifiable data**

| Robot Name | Developers |
|---|---|
| BHR5 | Beijing Institute of Technology |
| E-nuvo | ZMP, Inc. and Nippon Institute of Technology |
| KIBO 3.0 | KIST |
| NASH | Nanyang Technological University |
| PETMAN | Boston Dynamics |
| SURENA 2 | Tehran University |

**Table 1.2.2. Survey of qualitative data on full size bipedal robots**

| Robot Name | Developers | Latest Release | Purpose* | Actuator Type |
|---|---|---|---|---|
| ASIMO | Honda Motor Company | 2011 | 2,3 | Unknown DC |
| ATOM | FutureBots Humanoid Lab | 2010 | 1,2,3 | Unknown DC |
| BHR 2 | Beijing Institute of Tech. | 2006 | 2 | Unknown DC |
| BHR 3 | Beijing Institute of Tech. | 2010 | 2 | 0 |
| BHR 4 | Beijing Institute of Tech. | 2012 | 2 | 0 |
| CB | Sarcos | 2006 | 4 | Hydraulics |
| Charli-L | RoMeLa | 2010 | 6 | Brushed DC |
| Charli-2 | RoMeLa | 2011 | 6 | Brushed DC |
| COMAN | Italian Institute of Tech. | 2011 | 6 | 0 |
| DLR Biped | DLR | 2010 | 2 | Brushless DC |
| HRP 3 | Kwada Industries | 2007 | 2 | Unknown DC |
| HRP4 | Kwada and Aist Industries | 2010 | 2 | Unknown DC |
| HUBO2(KHR4) | Kaist | 2008 | 6 | Brushless DC |
| KBHR | Kangawa University | 2011 | 2 | Brushed DC |
| LOLA | Inst. of Appl. Mechanics and Tech. University Munich | 2008 | 2 | Other Electric |
| MAHRU 2 | KIST | 2006 | 2 | Brushed DC |
| MAHRU 3 | KIST | 2007 | 2 | Brushed DC |
| MAHRU R | KIST | 2009 | 2 | Brushed DC |
| MAHRU Z | KIST | 2010 | 2 | Brushed DC |
| REEM B | Pal Robotics | 2008 | 2,5 | Brushed DC |
| Running Robot | Toyota Motor Company | 2009 | 6 | 0 |
| Violin Playing Robot | Toyota Motor Company | 2007 | 2 | 0 |
| WABIAN 2R | Waseda University | 2009 | 4 | Unknown DC |
| Suralp | Sabancı University | 2010 | 2 | Unknown DC |

*Note*: * 1 = defense, 2 = assistance, 3 = industrial, 4 = medical, 5 = social; ** legs only.
*Note:* References for each robot are included in Appendix B.

Two of the robots, COMAN and the DLR Biped, were included despite the lack of an upper body. Several systems are part of a series developed by the same research team, but only the releases since 2006 were included in Table 1.2.1. Purpose or role for the robots was grouped according to common trends. The types of actuators used were inconsistently reported in literature with results varying explicit details such as model numbers to more ambiguity, such as referring only to *hydraulic actuators* or *servomotors,* as noted above. Because the literature is often ambiguous as to whether or not the published weight accounts for batteries, the table below includes the reported weights without distinguishing tethered from un-tethered.

**Table 1.2.3. Survey of quantitative data on full size bipedal robots**

| Robot Name | Weight (kg) | Height (cm) | Max Speed (km/h) | Total DOF | Waist DOF | Leg DOF |
|---|---|---|---|---|---|---|
| ASIMO | 48 | 130 | 9.0 | 57 | 1 | 6 |
| ATOM | 73 | 158 | 0.0 | 48 | 0 | 7 |
| BHR 2 | 63 | 160 | 0.0 | 32 | 0 | 0 |
| BHR 3 | -- | -- | 0.0 | -- | 0 | 7 |
| BHR 4 | 63 | 165 | 0.0 | 32 | 0 | 0 |
| CB | 92 | 158 | 0.0 | 50 | 3 | 7 |
| Charli-L | 12 | 141 | 0.8 | 21 | 0 | 5 |
| Charli-2 | 12 | 141 | 1.4 | 25 | 1 | 6 |
| COMAN | 17 | 67 | 0.0 | 15 | 3 | 6 |
| DLR BIPED | 50 | 143 | 0.5 | 12 | 0 | 6 |
| HRP 3 | 68 | 161 | 2.0 | 42 | 2 | 6 |
| HRP4 | 39 | 151 | 1.6 | 34 | 2 | 6 |
| HUBO2 (KHR 4) | 45 | 130 | 2.0 | 41 | 1 | 6 |
| KBHR | 60 | 162 | 0.7 | 29 | 3 | 6 |
| LOLA | 55 | 180 | 3.3 | 25 | 2 | 7 |
| MAHRU 2 | 70 | 155 | 0.0 | 31 | 1 | 6 |
| MAHRU 3 | 62 | 150 | 1.3 | 32 | 1 | 6 |
| MAHRU R | 50 | 135 | 0.0 | 34 | 0 | 6 |
| MAHRU Z | 60 | 150 | 0.0 | 35 | 1 | 6 |
| REEM B | 60 | 147 | 1.5 | 51 | 0 | 6 |
| Running Robot | 50 | 130 | 7.0 | -- | 0 | 7 |
| Violin Playing Robot | 56 | 152 | 0.0 | -- | 0 | 0 |
| WABIAN 2R | 64 | 150 | 1.9 | 41 | 2 | 7 |
| Suralp | 101 | 164 | 0.0 | 29 | 1 | 6 |
| **Mean** | 55.2 | 146.9 | 2.5 | 34.1 | 1.14 | 6.19 |
| **StDev** | 20.9 | 21.0 | 2.5 | 11.5 | 0.80 | 0.59 |
| **StDev % of mean** | 38% | 14% | 97% | 34% | 70% | 9% |

*Note:* References for each robot are included in Appendix B.

Table 1.2.3 displays quantitative data describing the survey of robots in form and performance. The maximum speed of each robot included in Table 1.2.3 is the highest reported either for walking or running. This is the only consistently-reported active metric of performance. The total DOF is a measure of the DOF of the whole robot, including the upper body and hands. Waist DOF can include rotating or bending the torso and is not necessarily required to be adjacent to the hips because the human spine moves along its length. Leg DOF includes DOF at the foot, such as a "toe" joint in WABIAN.

### 1.2.3 Survey Results

The results of the survey revealed many interesting trends. As previously stated, several additional robots were found on websites but are not included in the analysis here due to the lack of sufficient data.

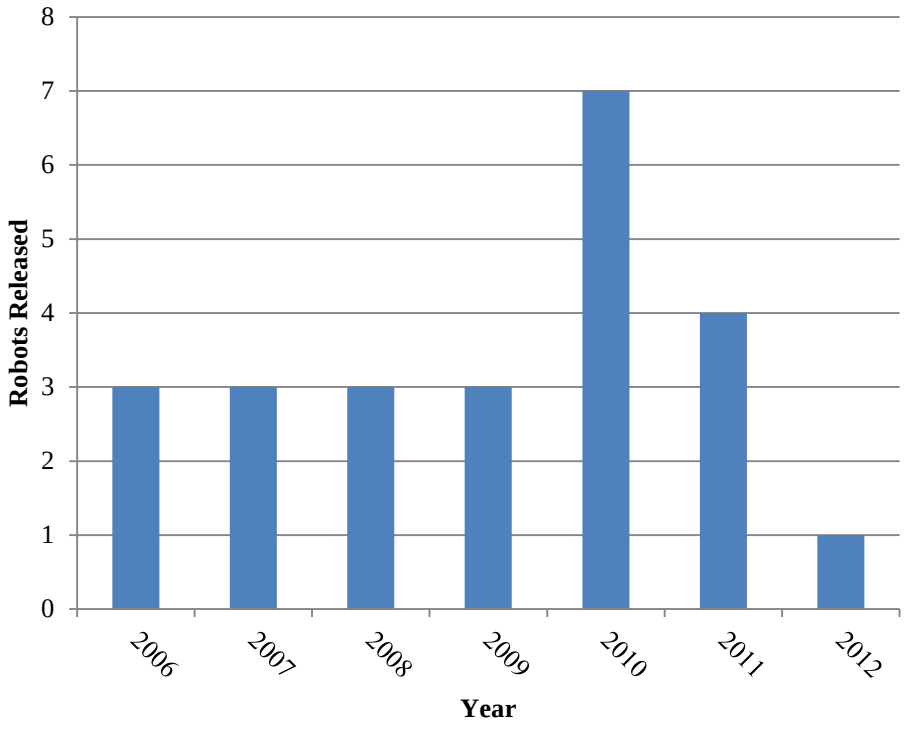


**Figure 1.2.1. Number of robots released by year. The number of robots released in 2012 would likely be higher if the second half of the year was included.**

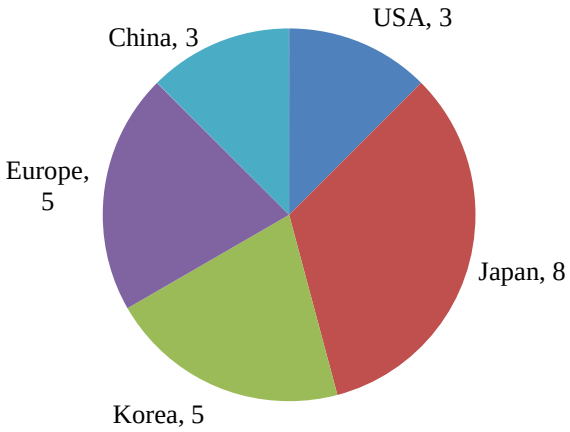


**Figure 1.2.2. Distribution of robots by region. Because Japan and Korea release such a large number of robots, they were each separated from the rest of Asia. Turkey, which is in both Europe and Asia, was included in the count for the latter.**

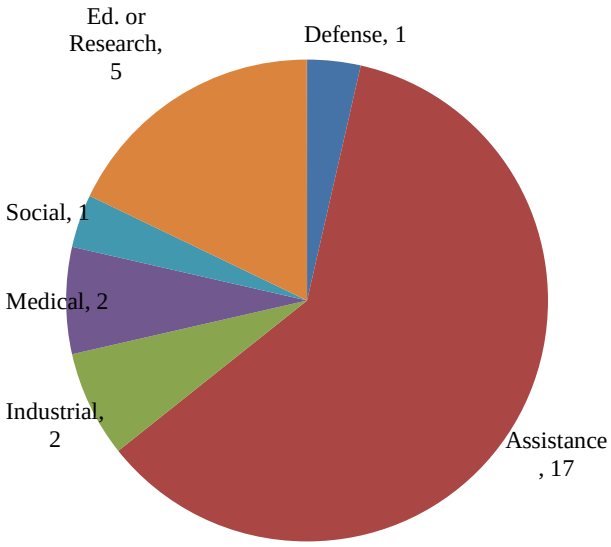


**Figure 1.2.3. Distribution of robot purposes. Robots could qualify for multiple categories, and zero robots were found to focus on defense.**

The distribution of robots for each year was fairly consistent and showed that development was continuous between 2006 and 2012 (see Figure 1.2.1). From Figure 1.2.2 it is clear that Japan leads the world in biped development, with Korea and Europe also producing a large number of the humanoids. The United States has made some contributions, but what may possibly be its best robot, the defense-focused PETMAN, was not included (as was previously mentioned) due to the lack of reliable data. Stairs in homes may be the cause for the large portion of biped robots focused on assistance, as Figure 1.2.3 demonstrates.

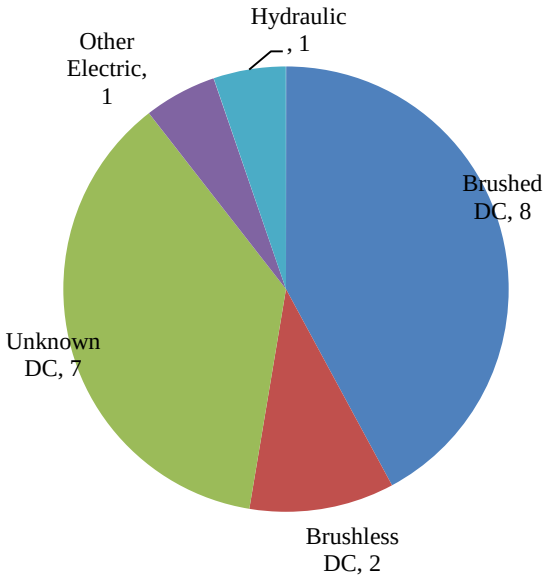


**Figure 1.2.4. Distribution of actuators used. Many research teams were not specific about the type of actuators used and were therefore not included. A common trend was to only specify a "servomotor" which could refer to several actuators.**

The trend in actuators heavily favored electric motors, and brushed DC motors seemed to be the most prevalent (see Figure 1.2.4). Brushed DC motors have the advantage of possessing simpler drives than other types of motors, such as brushless motors (Park, Kim, Lee, & Oh, 2005). This is caused by the fact that brushed motors, as the name suggests, use brushes to alternate the current, while brushless motors use external electronics to supply the alternating current directly (Chevallereau et al., 2009). Hydraulics supply a very high power/weight ratio and are more powerful, but are also nonlinear and more complex to control than electric motors

(Caldwell, Medrano-Cerda, & Goodwin, 1995; Hollerbach, Hunter, & Ballantyne, 1992). However, because of their strength, hydraulics can be used as direct-drives without gears. Without the difficult to determine losses due to friction in gearing systems, the force output can also be determined by measuring the pressure in the piston. Pneumatic humanoids did not appear in the survey, which may be due to the difficulties with the compressibility of air. All of these data provided valuable and useful information towards the selection of the actuators for leg design considered in this thesis.

**Table 1.2.4. Mean values of robotic parameters**

| | **Weight (kg)** | **Height (cm)** | **Max Speed (km/h)** | **Total DOF** | **Waist DOF** | **Leg DOF** |
|---|---|---|---|---|---|---|
| **Mean** | 55.2 | 146.9 | 2.5 | 34.1 | 1.14 | 6.24 |
| **Std Dev** | 20.9 | 21.0 | 2.5 | 11.5 | 0.80 | 0.53 |
| **Std Dev % of Mean** | 38% | 14% | 97% | 34% | 70% | 8% |
| **Typ. US Male Values** | 88[1] | 176[1] | 37.6[2] | 70[3] | 3[4] | 8[4] |

*Note*. These data are also displayed in the above Table 1.2.3. The average values did not include data that was not reported, including situations where the maximum speed was not reported in literature. [1]Human weight and height data from McDowell, Fryar, Ogden, and Flegal (2008). [2]Max speed was calculated by taking the speed during world record for the 100 m dash (USA Track & Field, 2012). [3]Simplification by counting six for each leg, four for each arm, two for each wrist, three for the back, three for the neck, and 20 for each hand. [4]Human waist and leg DOF data from Chaffin, Andersson, and Martin (999).

Table 1.2.4 shows the mean and standard deviation for each of the parameters in Table 1.2.3. The weights of the robots were focused around 55 kg. CHARLI-L and CHARLI-2, which were developed at Virginia Tech, were the lightest full-body robots, each weighing under 12.5 kg, and Suralp was the heaviest at 100 kg. COMAN, which has only legs, weighs only 17.3 kg. COMAN, CHARLI-L, CHARLI-2, and Surlap are the only four systems more than two standard deviations from the mean. The mean (55.2 kg; see Figure 1.2.3) was still significantly less than the weight of the typical US male (88 kg).

The heights of the robots were considerably more consistent, with a standard deviation of only 14% of the mean. This is likely due to most groups desiring humanoids to be close enough to human height to allow for performance in a wide variety of tasks while maintaining a center of mass closer to the ground than the average adult male in the US (which is approximately 30 cm taller). Although the human body has a very high number of DOF (the spinal column alone has dozens), the motions can be approximated to the 70 DOF shown in Table 1.2.4. Humanoids are beginning to approach this human capability, with ASIMO being the closest. As Table 1.2.4 indicates, most robots included one DOF in the waist, which was typically the yaw or torso rotation. Six DOF in the legs are required to generate three-dimensional human-like walking: hip yaw, pitch, and roll (i.e., rotation, flexion/extension, and abduction/adduction), knee pitch (i.e., flexion/extension), and ankle pitch and roll (i.e., dorsiflexion/plantar flexion and inversion/eversion; Chevallereau et al., 2009, p. 49). All but seven of the robots had six DOF in the leg, with CHARLI-L being the only system incorporating five DOF. The other six robots had seven DOF, each including an additional toe joint.

The maximum speed of the robots clearly lags behind the fastest human, defined here as the average speed of the world record 100 m dash. In 2009, Usain Bolt set the world record by completing a 100 m dash in 9.58 seconds (USA Track & Field, 2012). Max speed was reported in only 13 of the groups. It is assumed that several of the robots without reported speeds would be significantly lower than the 2.5 km/h, but this could not be confirmed without empirical evidence.

### 1.2.3.1 Trends in Series of Robots

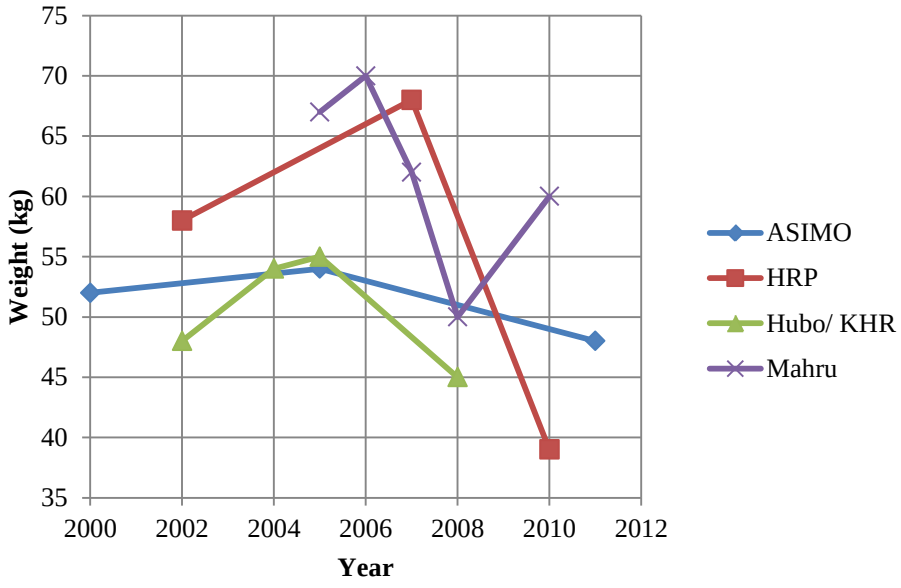


**Figure 1.2.5. Robot weight by year. Data from before 2006, which was not included in Table 1.2.2, is cited in Appendix C.**

As Figure 1.2.5 demonstrates, the weight of each surveyed robot increased in the second iteration, and in three of the four systems the weight of the newest robot was lower than the previous iteration. These changes correspond to each robot increasing in height (see Figure 1.2.6), and the DOF increasing in all the systems except for Mahru from the first to the second iterations (Figure 1.2.8).

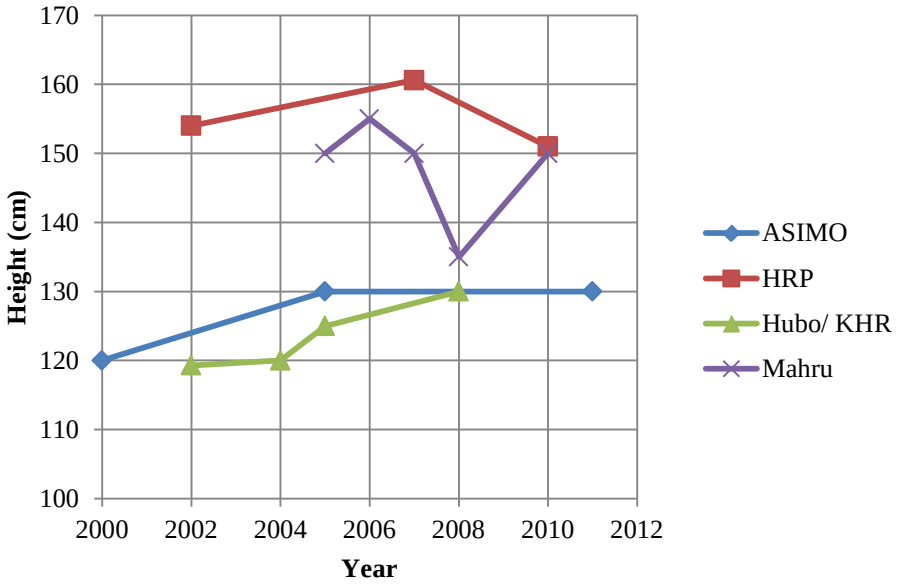


**Figure 1.2.6. Robot height by year. Data from before 2006, which was not included in Table 1.2.2, is cited in Appendix C.**

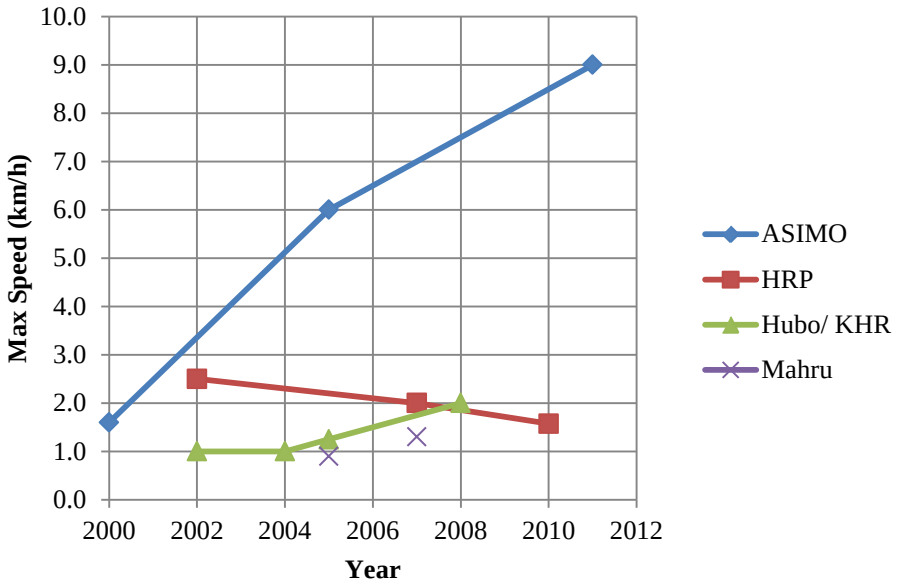


**Figure 1.2.7. Robot max speed by year. Maximum speed of the robot was considered the fastest walking or running speed reported. Data from before 2006, which was not included in Table 1.2.2, is cited in Appendix C.**

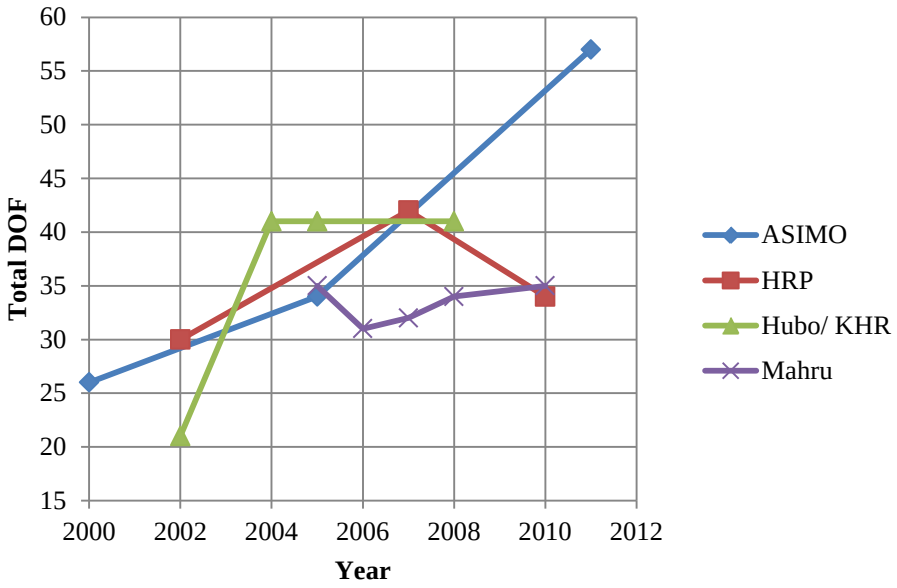


**Figure 1.2.8. Robot total DOF by year. Total DOF refers to the DOF of the entire body – the legs, torso, arms, head, and hands. Data from before 2006, which was not included in Table 1.2.2, is cited in Appendix C.**

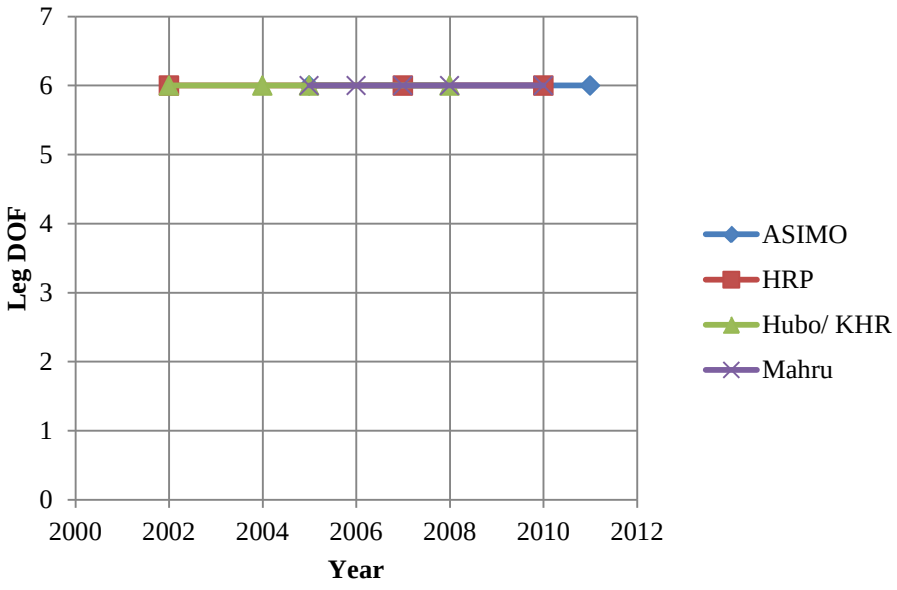


**Figure 1.2.9. Robot leg DOF by year. Data from before 2006, which was not included in Table 1.2.2, is cited in Appendix C.**

The preceding plots show that few definitive trends exist in the development of these humanoids (Figure 1.2.5, Figure 1.2.6, Figure 1.2.7, Figure 1.2.8 and Figure 1.2.9). ASIMO showed by far the greatest increases in both speed and total DOF (Figure 1.2.7 and Figure 1.2.8). Perhaps the most interesting trend shows that walking speed did not increase greatly for three of the systems, and that HRP actually decreased its walking speed (Figure 1.2.7). This trend is most likely due to the humanoids' end goal; thus, with "Assistance" cited as the primary purpose, achieving running would likely not be a critical capability for performing common human tasks. Consequently, the focus may have instead shifted towards higher dexterity and stability. The DOF in the leg remained at six for all the systems, as was the general trend shown in Table 1.2.4. It should be noted that although the systems exhibited an increase in overall DOF and therefore full system complexity, none changed the number of actuators in the legs (see Figure 1.2.8 and Figure 1.2.9, respectively). This implies that most of the dramatic near-future developments for walking are unlikely to involve system architecture; instead the focus is on the new computational algorithms and software.

## 1.2.4 Trends in Joint Design

### 1.2.4.1 Lower Back (Waist)

Bipedal locomotion is possible without movement in the waist; however, the survey illustrates that the majority of full-sized humanoid robots contain at least one or more DOF in their waist (Table 1.2.3). When discussing the waist DOF there are only three possible degrees than can occur: roll, pitch, and yaw. Few humanoids feature all three of these degrees, although they do exist in some systems (e.g., CB, COMAN, and KBHR).

Implementing a waist into a humanoid design can assist in achieving increased anthropomorphism and humanoid functionality. This enables humanoids to bend at their waist when standing up from a seated position, or to twist their waist during a fast walk. A waist also allows for heightened abilities with regards to upper body mobility, enabling the humanoid to interact with its surroundings while leaving its legs in a fixed position. According to Ogura et al. (2006), the designers of WABIAN-2R, the movement of the torso is used to compensate for position errors during grasping or making contact with other surfaces. WABIAN-2R has a 2-DOF waist and 2-DOF trunk; the waist consists of a roll and yaw joint and the trunk including a

pitch and roll joint assembled over the waist. The trunk motions are used to maintain its balance when walking to compensate for the ZMP. In addition to the WABIAN-2R, humanoids such as ASIMO, HRP-4, HUBO 2, and MAHRU-Z are all examples of robots with DOF in their waist.

#### 1.2.4.2 Hip Trends

Chevallereau et al. (2009) state that the human hip is a ball-and-socket joint and has three DOF, as was mentioned above. One hip architecture is often referred to as the "cantilever beam" structure, which has the yaw rotation offset from the center of the leg (see Figure 1.2.10). HRP-3 and COMAN feature this design. In general, this seems to be an architecture that is fading from popular use. More common is the in-line hip design, where all three DOF of the hip align with the leg center, which is also seen in Figure 1.2.10. KBHR, WABIAN-2, HUBO 2, and HRP-4 all use in-line hips, among others. DLR, which designed their leg based off a previously developed robotic arm, used a very unique design featuring two yaw degrees and a pitch degree (Ott et al., 2010). Although the order of the DOF varied, the survey shows that all of the biped robots that have been developed have three hip DOF.

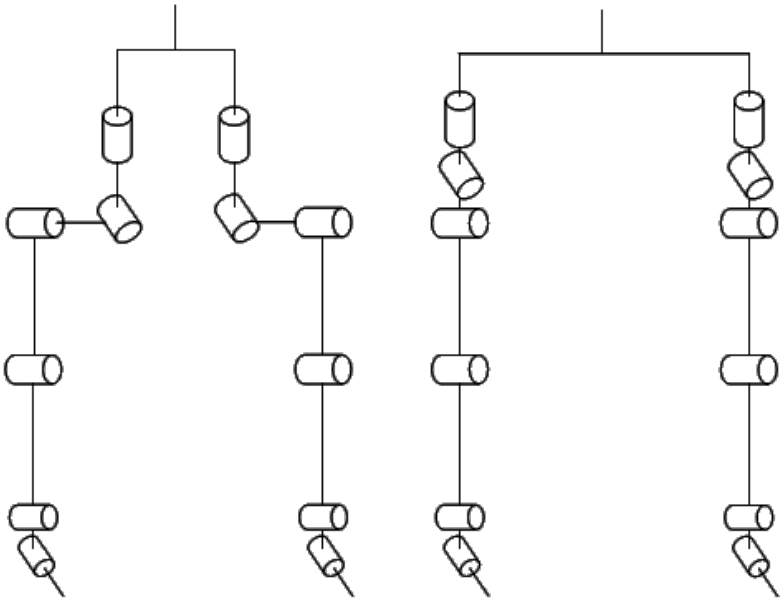

**Figure 1.2.10. Examples of hip joint designs. The left shows a cantilever beam architecture while the right shows an in-line architecture.**

#### 1.2.4.3 Knee Trends

Although the human has two DOF (Chaffin et al., 1999), the ROM of the medial/lateral rotation is relatively small and is typically assumed not to be necessary for robotic walking (Chevallereau et al., 2009). Human knees also cannot be defined by a fixed single axis relative to the other joint segments, but rather have a various radius of curvature during pitch; however, this again is not necessary for humanoid robots (Chevallereau et al., 2009). All of the researched humanoids for which data was collected have the single pitch DOF in the knee with a fixed axis.

#### 1.2.4.4 Foot and Ankle Trends

The ankle has both a pitch (dorsiflexion/plantar flexion) and roll (inversion/eversion) DOF. Chevallereau et al. (2009) state that the ankle roll is critical to be used in conjunction with the hip roll to move the ZMP smoothly in the lateral direction during walking. The survey showed that all the humanoids include both ankle DOF except CHARLI-L, which did not include roll. Humans also use the toes to push off and perform the toe-off, heel-strike walking motion. However, only six of the robots in the survey include a toe joint, and all of these have total seven DOF in the leg, as seen in Table 1.2.3.

#### 1.2.4.5 Walking/Running Capabilities

Though ASIMO is able to reach an incredible running speed of 9km/h, humanoid ambulation still seems to lack human-like characteristics. The majority of humanoids walk with a bent knee due to mechanical or algorithm limitations. WABIAN-2R is one of the few that is able to walk with straight legs. Also, as mentioned in the previous section, humanoids lack the ability to mimic the toe mechanism produced in human ambulation. This is one of the reasons that most of the robots pick their feet straight up to walk, rather than perform the toe-off, heel strike motion of humans which may save a significant amount of energy. Overall, many humanoids are capable of walking and a few can run, but much work is needed to achieve efficiencies accomplished by human ambulation.

### 1.2.5 Analysis of Survey Data

One method that was used to analyze the data was the Body Mass Index (BMI), which is a metric developed by the National Institutes of Health (1998) to assess human weight and levels of obesity. BMI is a ratio of the mass to the height squared using SI units, and the same method

was used to find the BMI for the robots. NIH has developed five classes, as shown in Figure 1.2.11, to categorize the relative health risks. Although a BMI between 25-29.9 is classified as Overweight, 32.6% (National Institutes of Health, 1998, p. 8, 10) of Americans between ages 20-80 were in this classification.

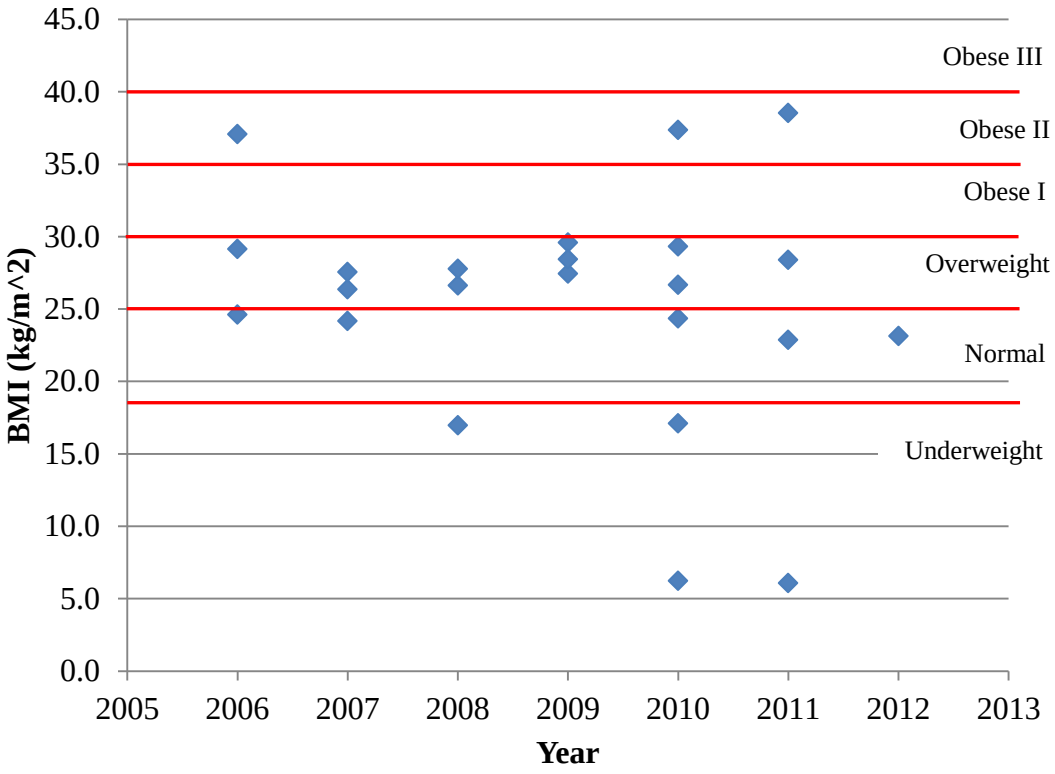


**Figure 1.2.11. BMI by year. The two outliers were CHARLI-L and CHARLI-2 with a BMI of 6.2 in 2010 and 6.1 in 2011, respectively. Data from before 2006, which was not included in Table 1.2.2, is cited in Appendix C.**

BMI was used as an analysis parameter because it is a ratio of weight that normalizes the size of the robots and can be easily compared to the large amounts of human data available. Interestingly, almost half of the robots were also in the Overweight category, and over two-thirds of the robots had a BMI between 22.5-30. As the robot becomes taller, the actuators will need to be stronger to lift heavier limbs and to handle centers of masses that will be further away from the joint. Because most groups used similar actuators, which are among the heaviest components, and are of relatively similar heights, it is logical that the normalized size of the robots would be

similar. CHARLI-L and CHARLI-2 use small robot servomotors which are very light and therefore have the lower BMI.

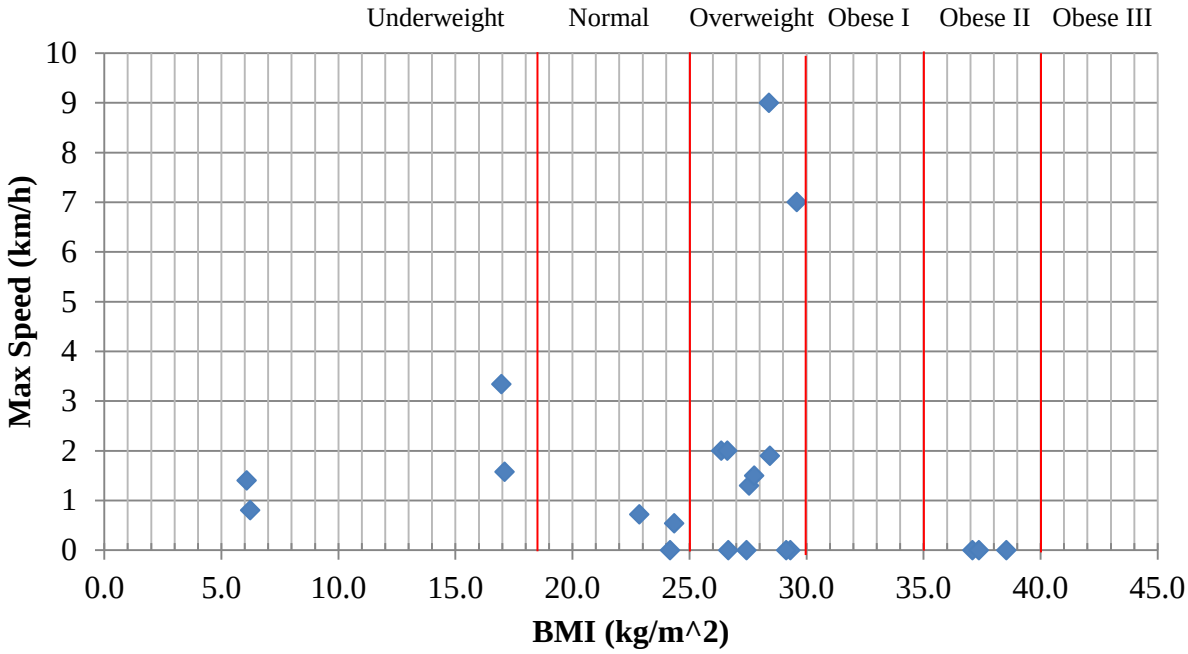


**Figure 1.2.12. Body Mass Index vs. Max Speed. The divisions were determined by the National Institutes of Health (1998). The maximum speed was plotted as zero if the actual value was not reported to show the trend in BMI. Data from before 2006, which was not included in Table 1.2.2, is cited in Appendix C.**

The max speed of the robots does not seem to be connected to the BMI since all but two of the robots that reported a max speed were within one standard deviation of the mean speed, yet 7/23 robots were more than one standard deviation from the BMI mean. This can be seen in Figure 1.2.12.

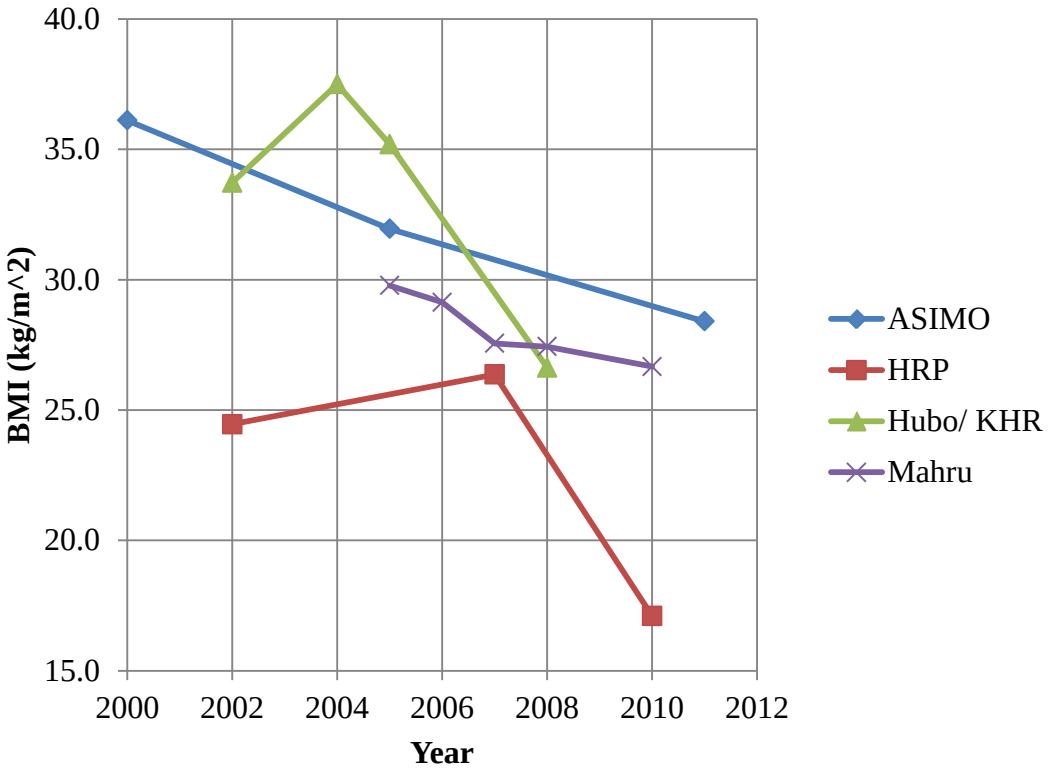


**Figure 1.2.13. Body Mass Index (BMI) by year. Data from before 2006, which was not included in Table 1.2.2, is cited in Appendix C.**

Looking at how the series of robots evolved in terms of BMI shows a definitive downward trend. As the researchers understand better the needs and limitations of their designs, it is safe to assume that they are doing a better job in optimizing and reducing the weight. Computational technology also continues to get smaller and lighter, so the amount of weight for on-board computing will continue to decrease for the same processing power. HRP-4 is the only robot not close to the Overweight range since 2006. Perhaps the most impressive robot is ASIMO, which has a BMI similar to other robots, but is able to run at 9 km/h, as seen in Figure 1.2.12.

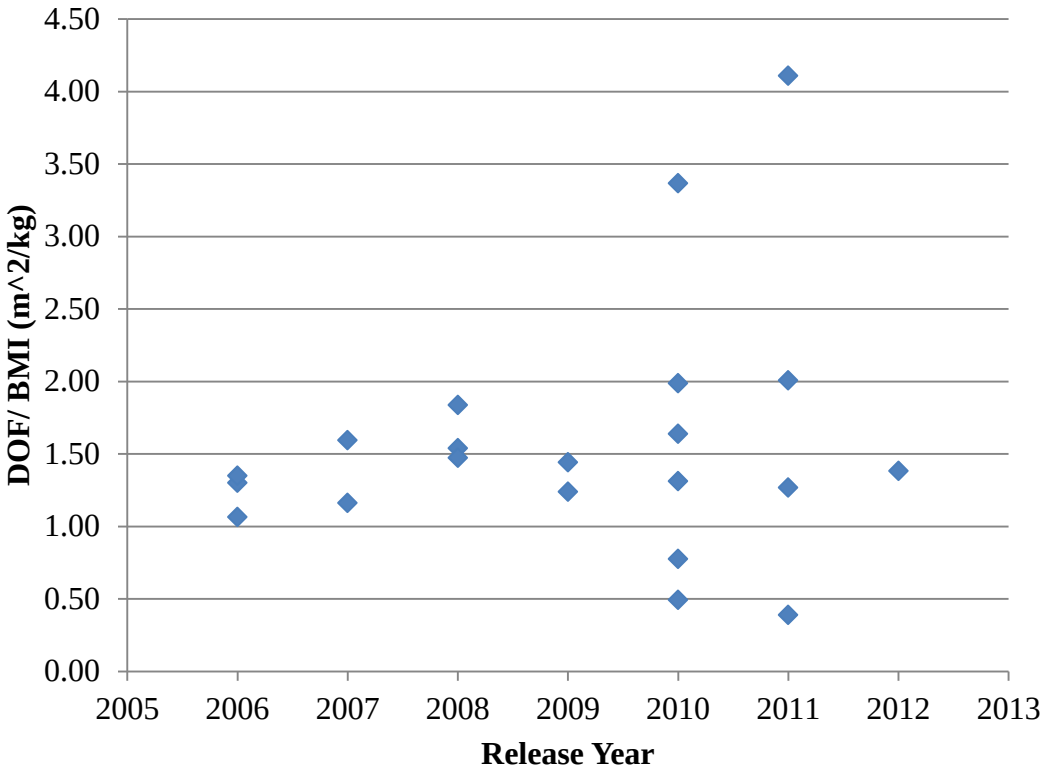


**Figure 1.2.14. DOF/ BMI by year. Data from before 2006, which was not included in Table 1.2.2, is cited in Appendix C.**

Since DOF is one parameter that indicates capability, seeing that the ratio of DOF/BMI by year in Figure 1.2.14 is fairly consistent shows that robots tend to have about the same capability for a specific size robot.

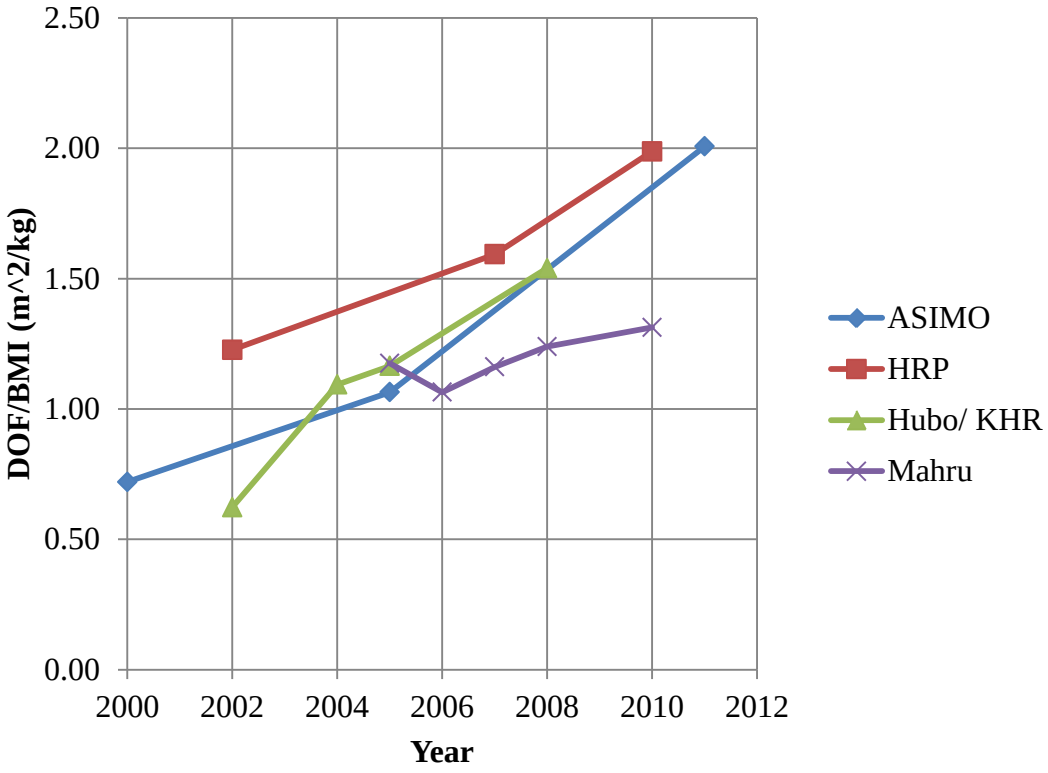


**Figure 1.2.15. DOF/BMI by year for robot series. Data from before 2006, which was not included in Table 1.2.2, is cited in Appendix C.**

Plotting the DOF/BMI ratio for the series of robots shows a much clearer trend than the group as a whole, presumably because the weight of robots tends to decrease as number of iterations increases and capability follows an inverse relationship. However, it is interesting that the DOF is increasing faster than the BMI is decreasing. More DOF typically means more actuators to create the motion, and of course more actuators mean more weight. With the same types of actuators being used, weight can only be decreased so low. Additionally, since none of these systems changed the DOF in the legs and the leg actuators tend to perform the primary load bearing, it is safe to assume that the increase in DOF is primarily due to increases in arm or hand motions.

### 1.2.6 Suggestions for Future Data Reporting

Throughout the process of producing the survey, a strong trend of inconsistency in information published was found for the humanoid robots. One of the biggest holes was left by the exclusion of Petman by Boston Dynamics, which has a plethora of videos online but very little information officially published. Only the purpose of the system was available on the company website, despite reports that the robot has one of the top speeds at over 7 km/h (Boston Dynamics, 2012). The lack of accessible information makes future developments in the field more difficult. If the following information was included by all groups, it would be easier for others to understand and advance bipedal robots.

1. Robot name
2. Developer
3. Date of first release
4. Release date
5. Names and date of previous robots in series with a clear explanation of the differences between the previous and current prototype
6. Purpose of robot (i.e. military, assistance, industrial, medical, social)
7. Weight and height of whole humanoid
8. Weight and length of humanoid with of individual body segments (foot, leg, arm, torso, head)
9. Total DOF with diagram illustrating each DOF
10. Range of motion, max torque, and angular velocity for each DOF (theoretical and/or experimental)
11. Walking and running speed
12. Actuation and gear type and model (DC brushless/brushed motors, hydraulics, and electric)
13. Force and torque sensor locations
14. Type of controllers
15. Balancing method (ZMP, torque control)
16. Compliance components included
17. Power source, type of battery, and battery life

18. Composition material
19. Unique physical and task performing capabilities as well as special features for upper body and lower body

### 1.2.7 Survey Conclusions

Using the previous survey data, several conclusions can be drawn about the status of humanoid bipedal robotics. Asia has remained the world leader in development of humanoid robots, both in number and in having the robot with the highest DOF and running speed. The complexity of the robots has continued to rise with the increase in DOF, as robots are continuing to strive towards matching human capability. Since the DOF in the leg has remained consistent over time and most robots use the same arrangement, advances in hardware besides a decrease in weight have not been the major factors in moving the field forward. The relative size of humanoids seems to change with iterations by the same researchers, but most robots remain around the same level. Walking speed seems to either be a metric that is not being focused on or a problem that has not been largely solved by the majority of researchers. A major breakthrough for bipeds may come if the toe joint of several systems can be better used to mimic the walking gait of humans. Finally, this survey shows that while the number of biped robots worldwide remains relatively small, the groups working in the field are distributed across the globe, and they are continuing to develop new designs to drive the field of humanoid robotics closer to the goal of integration into our daily lives.

### 1.2.8 Discussion of Future Biped Trends

To analyze the issues facing researchers, the goal must be kept in mind. Since most of these robots want to use the legs to walk in human environments, vast increases in speed over today's systems are not necessary for most of these tasks. So long as robots are able to walk around a home or office and maintain balance, most of the human world is accessible to them. The majority of the tasks that people perform don't require running or carrying extremely heavy loads. For this reason, it seems appropriate to expect that algorithm over hardware development will be the driving force for future advancement.

The field of bipedal humanoids is broad and global, but advances in technology and software throughout the coming years will enable systems to move towards human capability. Current actuators and gears are expensive, which is one factor leading to the small number of groups developing large humanoids. Perhaps the greatest current technological challenge exists in battery capacity. Walking bears the weight of the whole robot and therefore requires significant energy, and robots will always be limited in capability as long as they are tethered or have short battery life. Computational technology continues to advance at an extremely high rate and with it the ability to process increasingly complex algorithms. The development of software with more efficient walking gaits will also increase battery life. New actuators including piezoeletrics, shape memory alloys, and electroactive polymers among other technologies still need considerable advances until they will be able to match the torque output of more conventional components, so the foreseeable future is likely to focus around more optimized, custom electric motors and hydraulics (and potentially pneumatics).

# Chapter 2

# Mechanical Design of the Legs

The mechanical design of the leg was focused on developing a pair of robotic legs that would match the size of a male who is 183 cm (6 feet) tall. A priority was placed upon the reduction of cost by using conventional gear drives and reducing the overall complexity. Legs in many of the humanoids previously mentioned have been developed over several years of research and are based upon a common drive mechanism. Thus, there was an attempt made in this chapter to take a new route in the design because if a lower cost leg system could be developed, it would have a greater chance of being commercialized for social applications. Three generations of designs for the leg were developed, and the final version is described here in detail.

## 2.1 Human Data Research

With the primary goal to develop biomimetic legs, human parameters were first identified through a literature survey. The most important metrics were the size, range of motion (ROM), maximum torques, and maximum velocities of each segment or joint. The goal was to match the size to human segment length while attempting to minimize the radial width. Human length, weight, and ROM were well documented and established, as large studies are relatively simple to conduct and clear trends have been established in literature. The torques and velocities are much more difficult parameters to establish because of the nonlinear behavior of muscles and variation in human performance. To establish the baseline values for these two parameters, data was researched from both in biomechanics literature on human motion and from the Wabian 2-LL, one of the very few humanoids for which the information on velocity and torque has been reported.

### 2.1.1 Human Size and ROM

The size of each segment was established using data from Roebuck, Kroemer, and Thomson (1975). The size was based upon the previously mentioned 183 cm overall height for the whole robot. Figure 2.1.1 shows the data that was used as a basis.

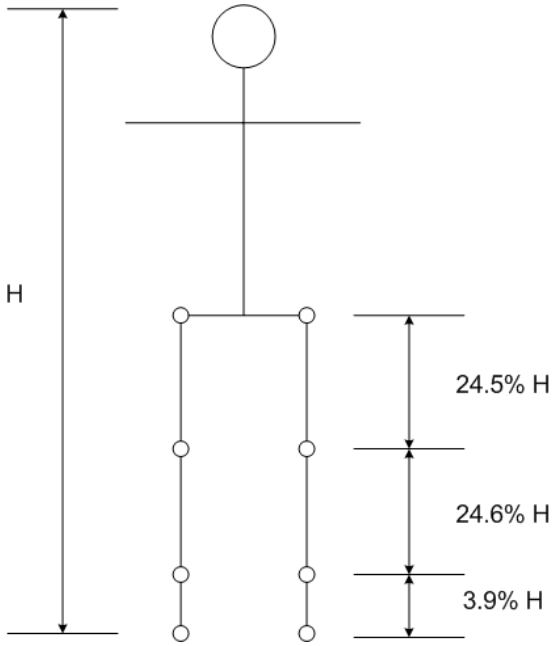


**Figure 2.1.1. Leg segment lengths normalized to overall height, *H*. Segment lengths were adapted from (Roebuck, Kroemer, & Thomson, 1975).**

These trends were then used to derive the segment lengths to achieve the desired robot height. These lengths are shown in Table 2.1.1 below.

**Table 2.1.1. Design goals for the robotic leg segment lengths**

| Segment | Segment Percent of Height | Segment Length (cm/ in) |
|---|---|---|
| **Total Height** | 100 | 183.0/ 72 |
| **Ground to Hip** | 53 | 97/ 38.2 |
| **Thigh** | 24.5 | 44.8/ 17.6 |
| **Shank** | 24.6 | 45.0/ 17.7 |
| **Foot (ground to ankle)** | 3.9 | 7.1/ 2.8 |

Human range of motion found in literature is summarized in Table 2.1.2. Extension/ flexion, abduction/ adduction or eversion/ inversion, and rotation are the same as pitch, roll, and yaw, respectively. Numerous methods have been used in literature to quantify the ROM, and therefore direct comparison among the reports is difficult. The data from Table 2.1.2 was used as a guide to select the desired range for the leg design.

**Table 2.1.2. Typical leg joint ROM of males 30-40 years of age (Roass & Andersson, 1982)**

| Joint | Motion | ROM (degrees) |
|---|---|---|
| Hip | Extension | 9.4 |
| | Flexion | 120.3 |
| | Abduction | 38.8 |
| | Adduction | 30.5 |
| | Internal Rotation | 32.6 |
| | External Rotation | 33.6 |
| Knee | Extension | -1.6 |
| | Flexion | 143.8 |
| Ankle | Dorsiflexion | 15.3 |
| | Plantar flexion | 39.7 |
| | Eversion | 27.6 |
| | Inversion | 27.7 |

## 2.1.2 Human Joint Torques and Velocities

When considering the typical torques and velocities that humans are able to produce at each joint, it is important to note the difference in actuation methods between muscles and motors. DC motors display a linear relationship between torque and current and between velocity and voltage. They will output the same amount of power regardless of position. Conversely, a muscle outputs the most force when it is in the middle of its deformation and decreases as it approaches both its maximum and minimum lengths. Passive tendons and ligaments also apply force when the muscle moves past its middle length, which increases the output force and efficiency since no outside energy is required. Muscles also output more force when they move quickly, and they output significantly more force when they are resisting lengthening than when they are actively shortening (Chaffin et al., 1999). This is further complicated by the fact that more than one muscle acts on a joint at a time. Because of all these factors, establishing an

analogous set of torques and velocities is difficult, however, human data can be used to understand general trends in joint dynamic parameters.

Since the goal of the system was to produce a robot capable of walking, the joint torques and velocities from biomechanics studies on ambulation were researched. A study on modeling of human walking was used to generate the joint torques that humans produce during walking (Besier, Sturnieks, Alderson, & Lloyd, 2003). Since the torque was normalized to body mass, 70 kg was used as an estimator for the data in Figure 2.1.2. Additionally, joint torque and velocity data from the humanoid robot Wabian 2-LL was also considered. Comparison with another robot offers an interesting perspective, as humans may walk differently than robotic legs. It is worthwhile to note here that Wabian 2-LL was designed for a humanoid which was 150 cm tall and had weight of 50 kg, both of which are lower than the desired parameters for the proposed design (Ogura, Aikawa, Lim, & Takanishi, 2004). However, Wabian is a very advanced humanoid that has been under development for many years, so learning from its design parameters was considered as a good exercise.

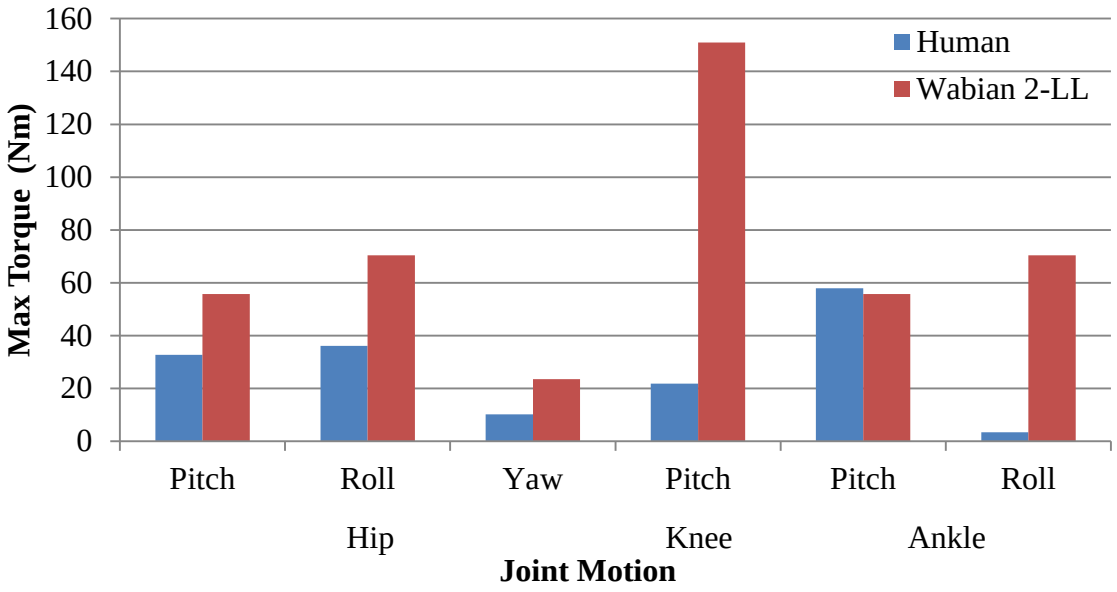


**Figure 2.1.2. Typical max joint torques during walking as reported in (Besier et al., 2003) and the maximum torques of the humanoid Wabian 2-LL (Ogura, Aikawa, Lim, & Takanishi, 2004). The human values were normalized to total mass and 70 kg was used in the calculation for comparison in this figure.**

Joint velocity was more difficult to quantify when considering human walking because it is more dependent upon walking speed. From the findings in Chapter 1, most humanoid robots walk very slowly, with the vast majority under 2 km/h and several under 1 km/h. Walking at the speed of 0.5 km/h would require much lower joint velocities than a typical human walk or that of Wabian's top speed, which was 1.8 km/h (Ogura et. al, 2006) (although this speed was for Wabian 2R, not 2LL for which the values were reported in Figure 2.1.2). To ensure that a robot capable of human-like movement could be achieved, the design was more focused on achieving high torque output and saving costs rather than matching the velocity of Wabian.

## 2.2 Overall Design Concepts and Actuator Selection

The design of the leg was divided into six sections, one for each DOF. Within each section, the actuator selection was performed concurrently with the design. Several components were standard parts, such as shafts, bushings and thrust bearings, to simplify the design and fabrication. Each shaft was a 12mm diameter keyed steel drive shaft and brass bushings were used with these shafts to reduce the friction. Both needle and ball thrust bearings were implemented, depending on the space available, to reduce the friction between parallel rotating faces. By using the same shaft throughout the design, one set of these accessory components was able to be used on the whole system.

### 2.2.1 Actuator Selection

The most important components to select were the actuators for the legs, as the rest of the structure is dependent upon their performance. The maximum actual output for the DC brushed motors was found by estimating the force output of the motor and associated gearing. Brushed motors would output high speeds and low torques, therefore significant gearing was necessary.

Several options were available for gearing, with each having its own advantages in performance. Many of the robots surveyed in Chapter 1 used Harmonic Drive gear heads, which uses a flexible cup and an elliptical wave generator to achieve its gear reduction. These gears have several desirable qualities: large torque-to-weight ratio, high efficiency, large gear ratios, high available torque capacity, and very low backlash. The disadvantages of these gears are the limitation on mounting orientation which must be parallel to the axis-of-rotation of the input

shaft, the requirement for large diameter, and the high financial cost (Chevallereau et al., 2009). Planetary gear heads offer comparable efficiency and a decent torque-to-weight ratio, particularly for those made from ceramic materials. The backlash or the play between the motor output and the gear head shaft, for the planetary gear heads can be significantly higher than those of Harmonic Drive gears, partially due to the fact that the former typically has multiple compounding stages. However, the lower cost of planetary gears and the development of novel algorithms to mitigate the backlash issues (as discussed in Chapter 3) were sufficient reason to use them instead of Harmonic Drive gears. However, due to the high desired torque of each joint and the limitations on motor mounting due to the length of the motor and gear head, additional gearing external to the planetary gears was also considered to increase the maximum output torque and to change the direction of motion.

Calculation was based on motor parameters specified by the manufacturer. The maximum continuous torque is the amount that motor can output consistently without damage. The peak safe output torque was assumed to be twice this amount, since peak loads during walking and balancing would be experienced for only a short period of time in most situations. The no-load speed of the motor is the highest speed the motor can achieve with the rated voltage without having to drive any external loads. However, the actual output from the actuator is dependent upon the loading that is applied because the motor is capable of lower top speeds with increased torque output. Equation 2.2.1 shows the formula used to calculate the motor torques, and Equations 2.2.2 and 2.2.3 show the equations used to calculate the motor velocity based on a given load.

$$T_{output} = T_{MC} * G_{Gh} * \varepsilon_{Gh} * G_{Ge} * \varepsilon_{Ge} * C_{ft} \quad \textbf{2.2.1}$$

$$V_L = T_c * \tau_m \quad \textbf{2.2.2}$$

$$V_o = \frac{(V_{NL} - V_L)}{G\_Gh * G\_Ge} \quad \textbf{2.2.3}$$

The maximum continuous torque is denoted as $T_{MC}$, and the no-load speed is represented as $V_{NL}$. The loss of maximum speed due to loading, motor speed / torque gradient, and motor torque are represented as $V_L$, $T_c$, and $\tau_m$ respectively. The efficiency and gear ratio of the gear heads are

$G_{Gh}$ and $\varepsilon_{Gh}$ respectively. For the external gearing after the gear head, the estimated efficiency is $\varepsilon_{Ge}$ and the gear ratio is denoted by $G_{Ge}$. The torque correction factor, $C_{ft}$, was one if the continuous torque was used or two if double the torque was used representing the conservative and aggressive calculations respectively.

The difficulty in estimating the maximum velocity for a complex dynamic system such as a humanoid robot arises because segment geometry, walking pattern, and outside disturbances are unknown in the early design phases and dictate many of these decisions. Since the velocity and torque output of a DC motor are coupled, the decision was made to emphasize the torque over velocity in the actuator selection. In this early stage of system development, it was hypothesized that a system which was strong enough would still be able to move if its velocity was low, but if the actuators had too low of a torque then movement may not be achievable at all. The uncertainty of load conditions also made estimation of structural strength difficult so it was assumed that the structure would be overdesigned and therefore a bit heavier than optimally needed. The joint torques of Wabian were used as a benchmark to match or exceed for each joint, assuming that Wabian is capable of higher performance (faster speed) movement than this system will achieve and that its structure has been more optimized in weight. Achieving the desired magnitude of torque while maintaining enough speed for movement was one of the main criterion during the motor selection.

The chosen actuators are shown in Table 2.2.1 for all the joints except ankle pitch. All were DC brushed motors manufactured by Maxon Motors. The motors for the knee and hip flexion were chosen to be the same to simplify the design. As such, this allowed the design of each joint to be very similar as well. The hip and ankle roll also used the same motors.

**Table 2.2.1. DC motors selected for design**

| Function | Motor Model, Series | Continuous Torque (mNm) | Nominal Speed (RPM) |
|---|---|---|---|
| Hip Yaw | 310007, RE-30 | 85 | 8050.0 |
| Hip Roll | 148867, RE-40 | 177 | 6930.0 |
| Hip Pitch | 370355, RE-50 | 418 | 5420.0 |
| Knee Pitch | 370355, RE-50 | 418 | 5420.0 |
| Ankle Roll | 148867, RE-40 | 177 | 6930.0 |

The gear heads were chosen with each of the motors to increase the output torque. The greatest limitation was the continuous output torque, which limits the drive output torque. The efficiency of planetary gears is reduced because multiple stages are required to reach the desired gear ratio. The same gear head for the knee and hip flexion was chosen.

**Table 2.2.2. Planetary gear heads selected for design**

| Joint | Gear Head Model, Series | Continuous/ Max Torque (Nm) | Gear Ratio | Max. Efficiency (%) |
|---|---|---|---|---|
| Hip Yaw | 166937, GP-32C | 3/ 3.75 | 28:1 | 75 |
| Hip Roll | 203126 GP-52C | 15/ 22 | 113:1 | 72 |
| Hip Pitch | 110507, GP-62A | 50/ 75 | 181:1 | 70 |
| Knee Pitch | 110507, GP-62A | 50/ 75 | 181:1 | 70 |
| Ankle Roll | 223105, GP-52C | 30/ 45 | 353:1 | 68 |

The external gearing was necessary because of the limited output torque of the planetary gear heads. The worm gear was chosen because it is able to rotate the actuator's direction of rotation by 90 degrees with a high gear ratio. Additionally, the motor had to be placed normal to the outside of the worm gear, while bevel gears require the motor to be normal to the center of rotation. This allowed easier mounting in the hip plate where space was limited. However, worm gears can be very inefficient, so a low efficiency was assumed. The bevel gears were more advantageous in the hip and knee flexion because they have a higher efficiency and the motor orientation was not as limiting. The motors in the hip and ankle roll were mounted parallel to the axis-of-rotation, and therefore spur gears were used to increase the torque. The efficiencies of the bevel and spur gears were both estimated for the calculation.

**Table 2.2.3. External gearing selected for design**

| Joint | Gear Type | Gear Ratio | Assumed Efficiency (%) | Total Gear Ratio |
|---|---|---|---|---|
| Hip Yaw | Worm | 30:1 | 50 | 840 |
| Hip Roll | Spur | 2.5:1 | 95 | 282.5 |
| Hip Pitch | Bevel | 2:1 | 90 | 362 |
| Knee Pitch | Bevel | 2:1 | 90 | 362 |
| Ankle Roll | Spur | 1:2 | 95 | 176.5 |

The ankle pitch was chosen to be driven by a linear actuator to avoid a third large bevel gear system. The Digit actuator from UltraMotion Inc. was found to have adequate performance, but was driven by a HT23-401 model stepper motor from Applied Motion Products. The motor was connected to a ball screw to change the motion from rotary to linear with a maximum force output of 1744 N at 12.7 cm/s. Although the speed of stepper motor is more difficult to be controlled than a DC brushed motor, it also has greater holding torque. The linear actuator was attached normal to a 63.5 mm moment arm when the foot is normal to the shank so that the maximum torque is achieved at this angle. Using this configuration creates a nonlinear torque output due to the change in effective moment arm length as the joint rotates. However, the change is less than 10 degrees and its affect was therefore determined to be small enough such that the linear actuator would still be able to generate enough torque when the moment arm is reduced.

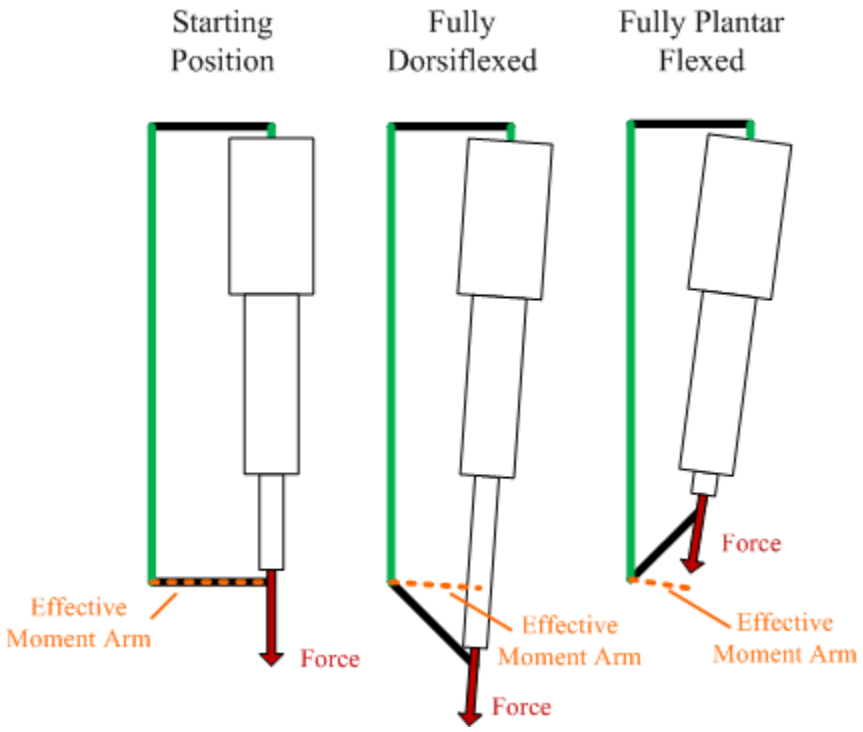


**Figure 2.2.1. Linear actuator model. The ankle is nominally at 90 degrees to the shank, and the relative change of actuator angle is small at both extremes of its movement because the top connection of the linear actuator is very short compared to the length of the actuator.**

The maximum theoretical torques and velocities for the actuator at each joint is summarized below in Table 2.2.4. The maximum velocity for two load cases are also shown, one for the no-load case which is the peak velocity that the motor can achieve and one in which the manufacturer specified maximum continuous torque is applied. The linear actuator was designed not to exceed its peak operating speed, so the ankle pitch velocity was same in both cases. These values are also compared to the previously discussed human and Wabian data in Figure 2.2.2 and Figure 2.2.3.

**Table 2.2.4. Calculated theoretical speeds and torques for each joint**

| Joint | Conservative Max Torque Output (Nm) | Aggressive Max Torque Output (Nm) | Max Velocity Output, No Load (deg/s) | Max Velocity Output, Continuous Torque (deg/s) |
|---|---|---|---|---|
| Hip Yaw | 27 | 54 | 63 | 58 |
| Hip Roll | 32 | 64 | 162 | 149 |
| Hip Pitch | 95 | 191 | 94 | 90 |
| Knee Pitch | 95 | 191 | 94 | 90 |
| Ankle Pitch | 73 | 111 | 143 | 143 |
| Ankle Roll | 20 | 42 | 259 | 239 |

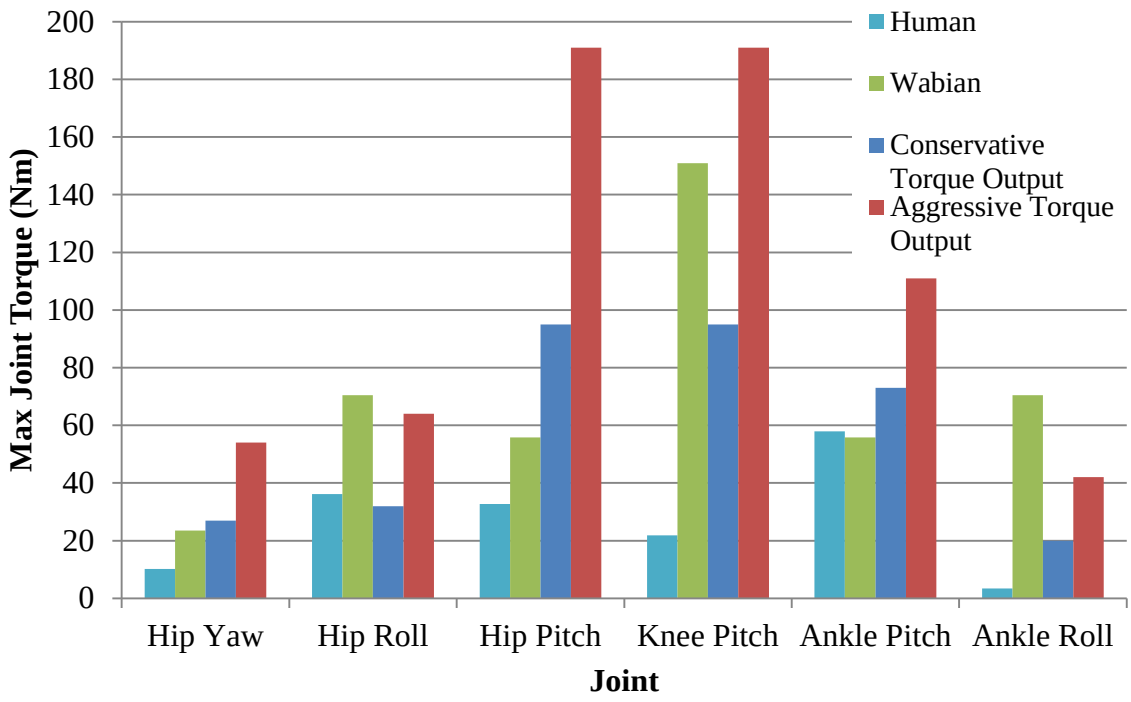


**Figure 2.2.2. Maximum joint torques. The human torques were highest during the walking test (Besier et al., 2003) while the Wabian's values were found from (Ogura, Aikawa, Lim, & Takanishi, 2004).**

The chosen actuators compare well with both the human data and the specifications of Wabian. The conservative torque estimate was greater than the human data for each joint except the hip, where it was slightly lower. The aggressive estimates exceeded Wabian's torque range as well, at all the joints except the hip roll and ankle roll. The knee motion clearly has the highest torque capability in Wabian although the human data shows it has one of the lesser torque values. This is likely due to the fact that humanoid robots tend to keep the knee bent to avoid singularity (Ogura et. al, 2006), while humans use passive dynamics and locking of the knee when straight during walking to reduce the amount of energy (torque) required during walking (Chevallereau et al., 2009).

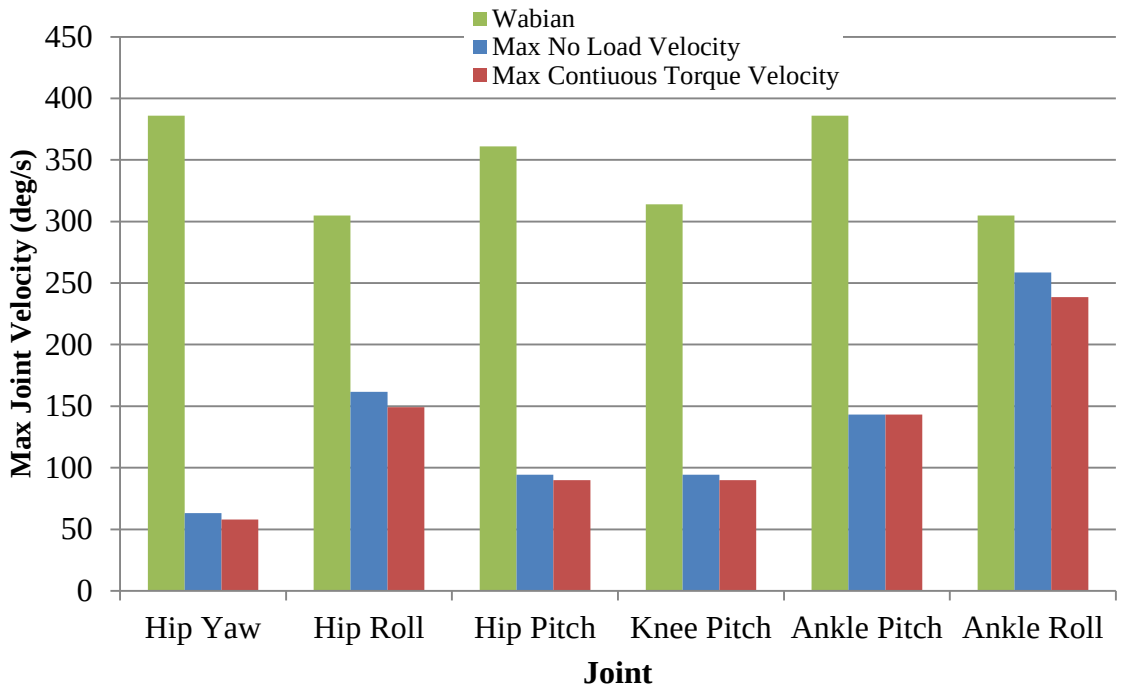


**Figure 2.2.3. Maximum joint velocities. Wabian's values were found from (Ogura, Aikawa, Lim, & Takanishi,, 2004).**

The velocity performance of the actuators did not compare nearly as well to the data from Wabian. The greatest discrepancy was at the hip yaw joint, where the chosen actuators could only achieve 63 degrees / second and Wabian can achieve 386 degrees/ second. However, in this early phase of the leg development, hip rotation was decided not to be used for simple balancing and walking so the difference was not seen as an issue. The bigger potential issue was the speed of the hip roll and pitch. However, since the intent was to use the same actuator for both joints, and the torque at the knee rotation was not excessively greater than that of Wabian, the speed was found to be acceptable. It should be mentioned here that the method by which the maximum values of Wabian were calculated was not discussed by the authors in the literature. The rated power of each of the motors chosen in this study exceeded the power of corresponding motor in Wabian by at least 50% for all the joints except the knee, where the chosen motor has a 33% higher rated power. Without knowing the method used to derive the maximum values for Wabian, the comparative analysis could not be conclusive. However, knowing that the actuator will be strong enough was a good foundation for designing the remainder of the legs.

## 2.3 Hip Plate Design

At the top of the legs, the hip plate serves as the foundation of the whole assembly. It connects the two legs, serves as the connection point for an upper body, and houses the hip rotation motors and gears. A slew gear, which is a type of turntable that has a high load capacity in the axial direction about which the gear rotates, was used to connect the leg to the hip plate as shown in Figure 2.2.5. Atop the slew gear was a mounting plate and then a worm gear. Connecting to the worm gear is a worm, which is driven by a DC brushed motor. The worm gear system has the motion normal to the rotation of the motor. Supports on the front and back of the motor and gear are used to stabilize the motor. The front support is attached with screws to the gear head face, but the back support slides on the motor and only makes contact radially with the motor housing. Figure 2.2.4 shows the design of the hip plate and yaw rotation assembly.

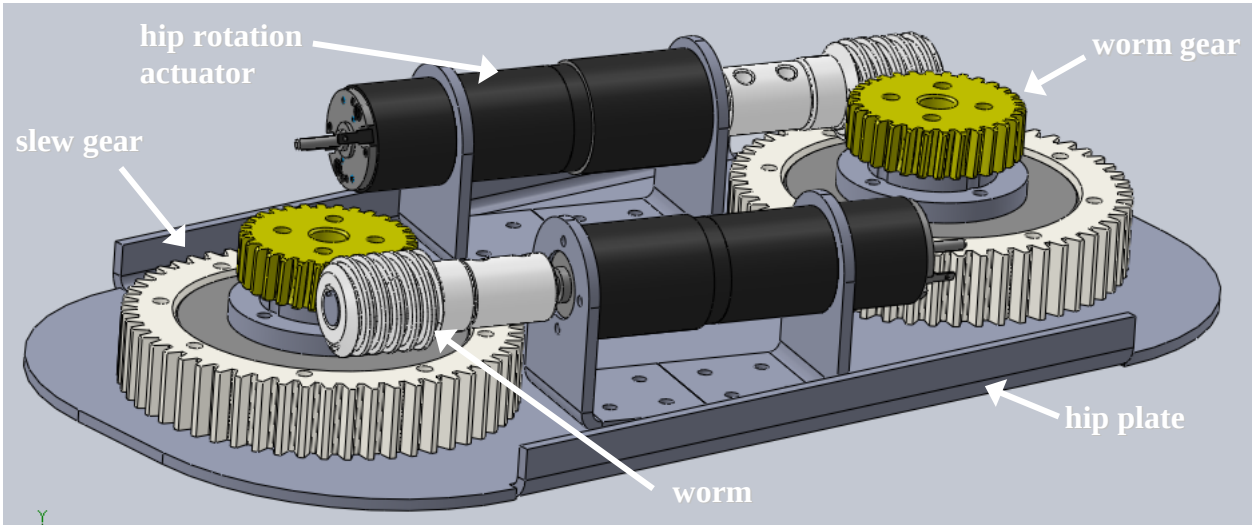


**Figure 2.2.4. Design of the hip plate. The worm gear system rotates 90 degrees into the yaw direction for hip motion. Although the slew gears have teeth around the outside, they were not used for actuation as the outside was rigidly connected to the hip plate.**

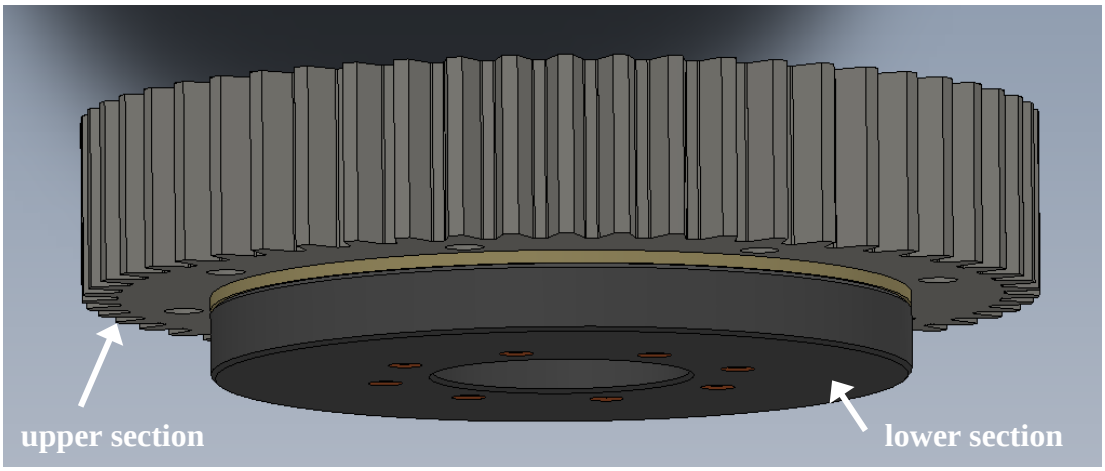


**Figure 2.2.5. The slew gear used in the hip rotation. The lower section extends through the hip plate and connects to the upper hip.**

Yaw rotation at the hip was concluded to be the least important for initial testing, and therefore the joint was locked in place to simplify the control. An “X” shaped piece was used to hold the two pieces of the slew gear together when the gear was not in place as shown in Figure 2.2.6.

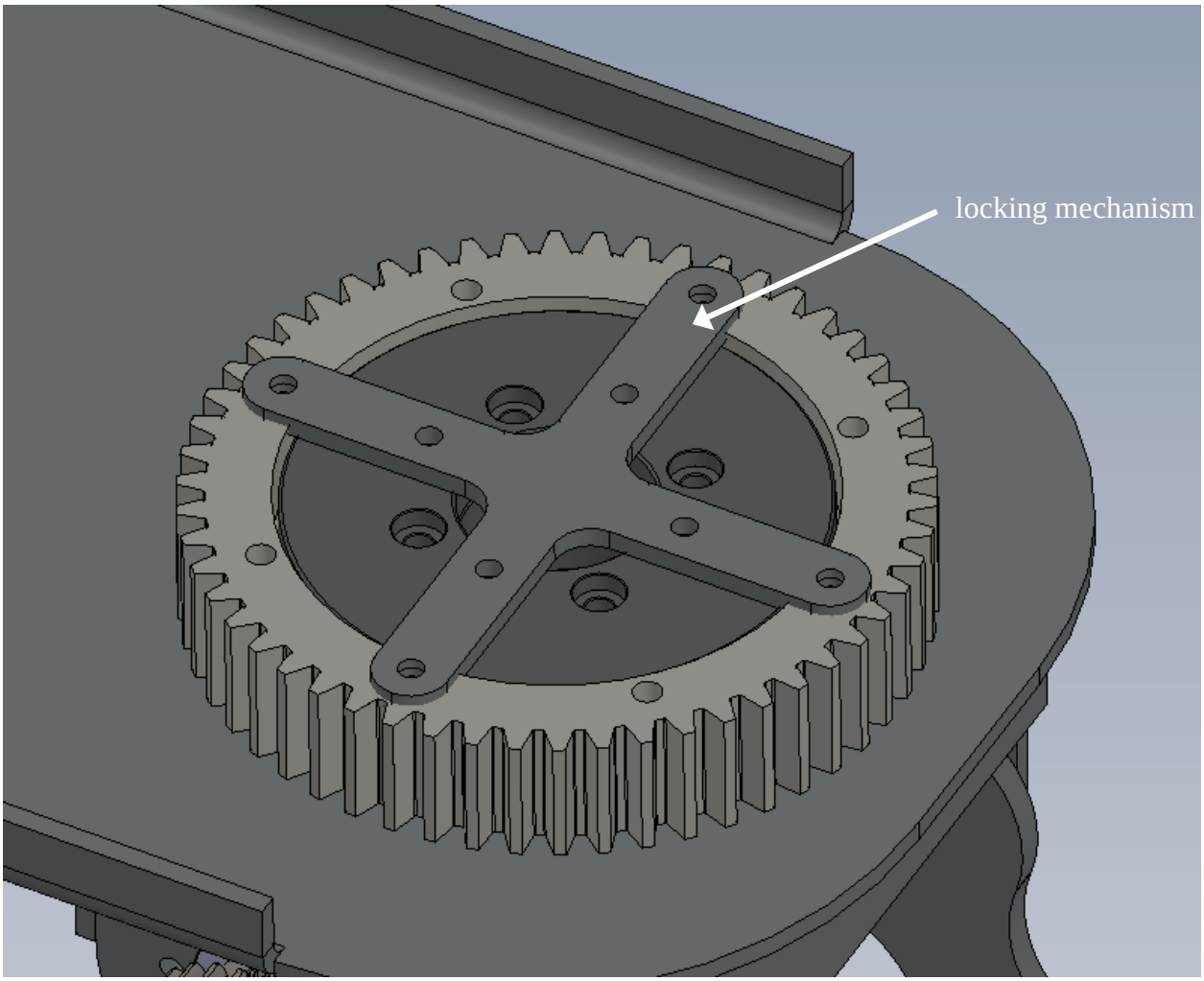


**Figure 2.2.6. The hip rotation locking mechanism.**

## 2.4 Upper Hip Design

Second section of the leg was the upper hip, which connects to the bottom of the slew gear and consists of the hip abduction motor inside a housing and the spur gears. Front and back views of the upper hip can be seen in Figure 2.2.7 and Figure 2.2.8. The motor has a spur gear with a key hole mounted to its output shaft, and the large spur gear is rigidly bolted to the lower hip structure. Thrust bearings were used between the upper and lower hip structures to reduce friction. Because the gear head has a larger diameter than the motor, an aluminum sleeve was bolted on the upper hip structure to support the motor, as shown in Figure 2.2.8. Mechanical stops were implemented to allow the motor to safely operate without damaging critical components.

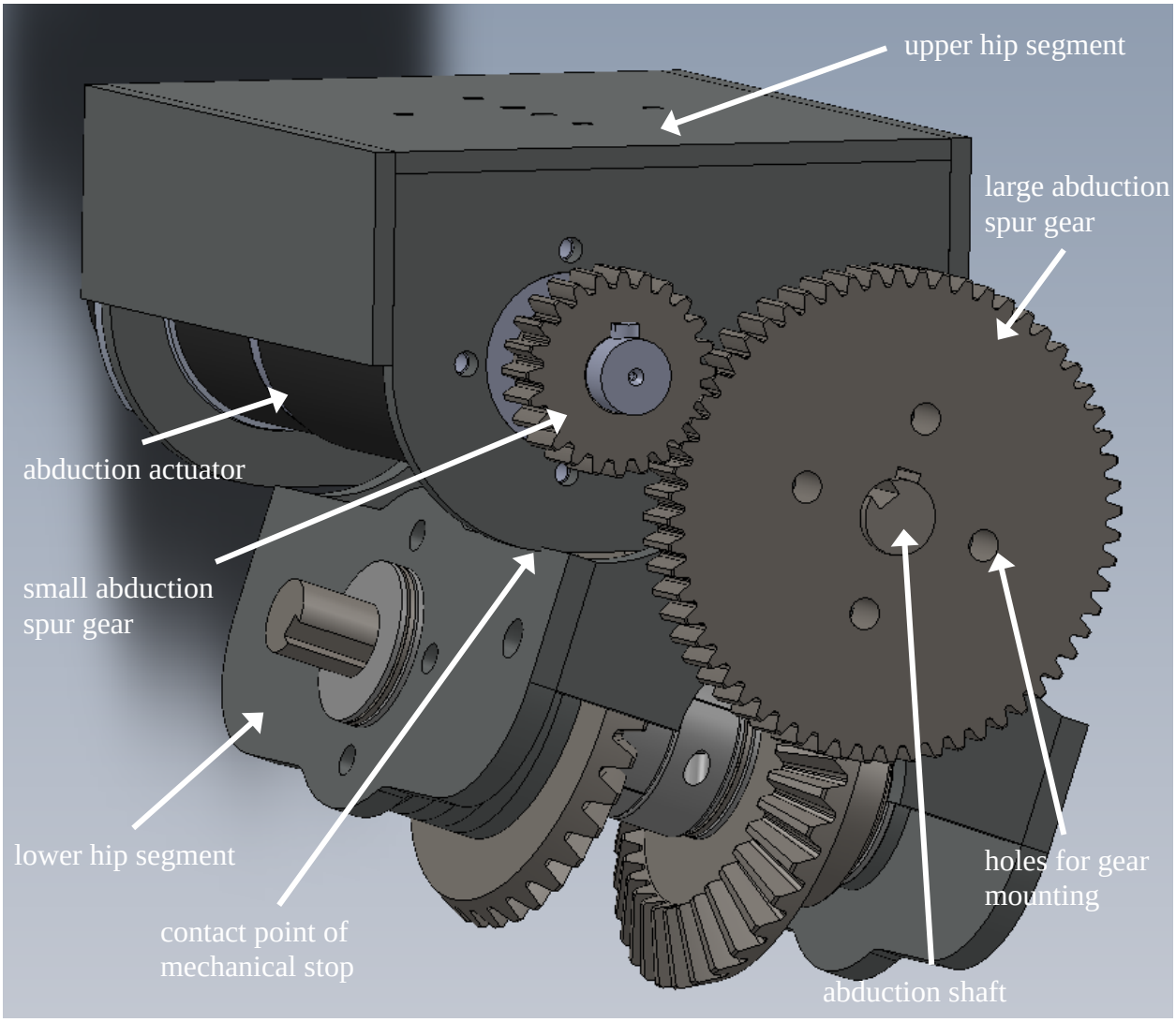


**Figure 2.2.7. Back view of the upper and lower segment from the hip. The turning of the big gear causes the lower hip segment to rotate as well, creating abduction and adduction of the hip. The upper hip structure acts as a mechanical stop.**

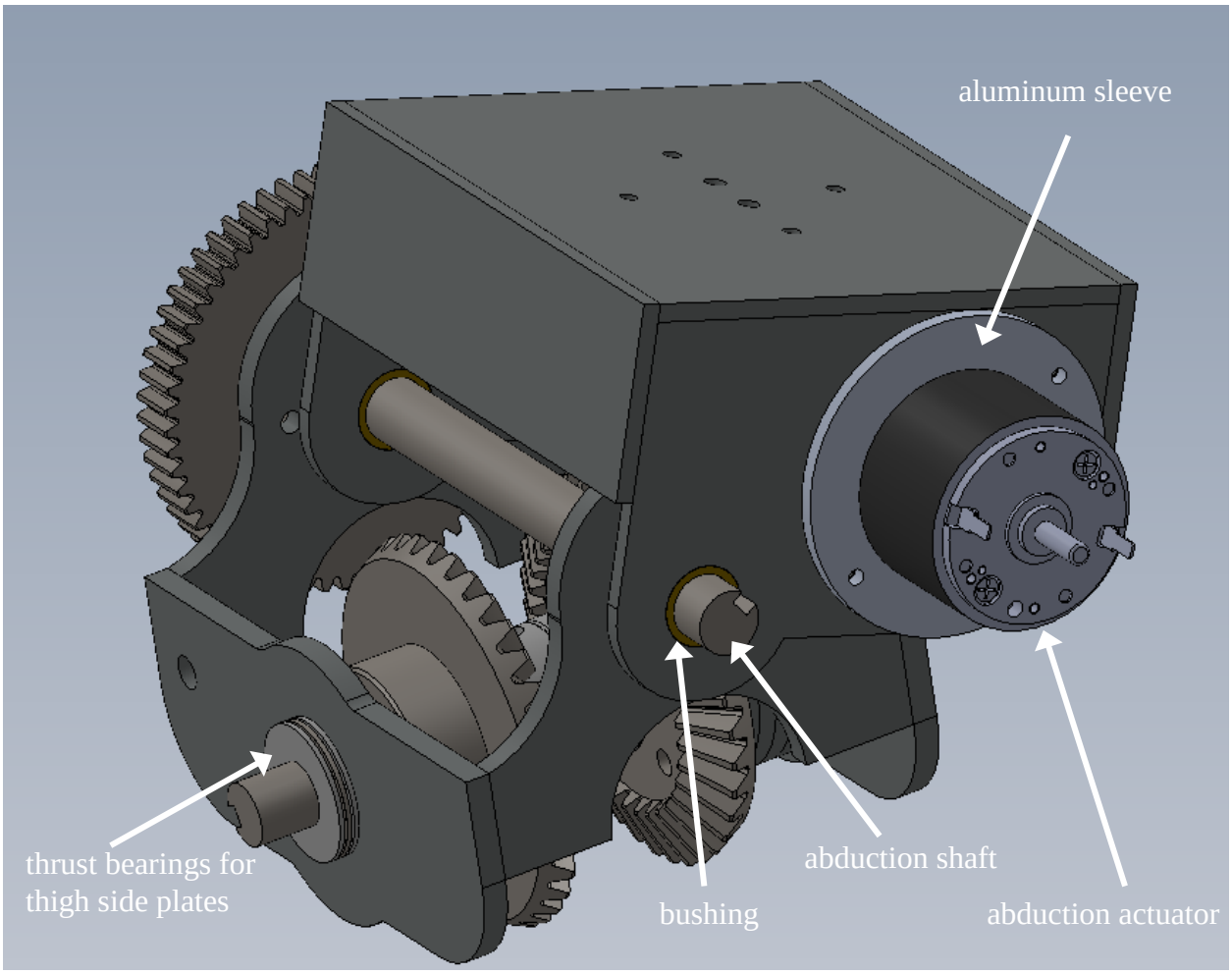


**Figure 2.2.8. Front view of the total hip assembly. In this position, the adduction is in its extreme position and cannot go any further.**

## 2.5 Lower Hip and Thigh Design

The lower hip section attaches on a shaft to the upper hip and is rotated to perform the roll motion of the hip. Contained within the section are the bevel gear assemblies that allow the hip to flex or pitch. Because the human hip has all three DOF at one socket joint, a goal was to minimize the distance between the abduction and flexion shafts as much as the design would allow. The bevel gear without a hub was rigidly bolted to the lower hip structure. The gear was tapped to allow simple assembly, and one of the spacers was keyed to rigidly connect the shaft to the gear for use with the potentiometers for position feedback.

The joints for the knee and hip flexion were designed similarly, since the same gear heads and bevel gears were used. In the hip, the gear which is mounted to the upper hip structure remains stationary while the pinion gear causes the leg to rotate around it. The second bevel gear spins freely and is used to apply an opposing force to the pinion gear so as to avoid bending the gear head shaft. Thrust bearings separate all the moving surfaces.

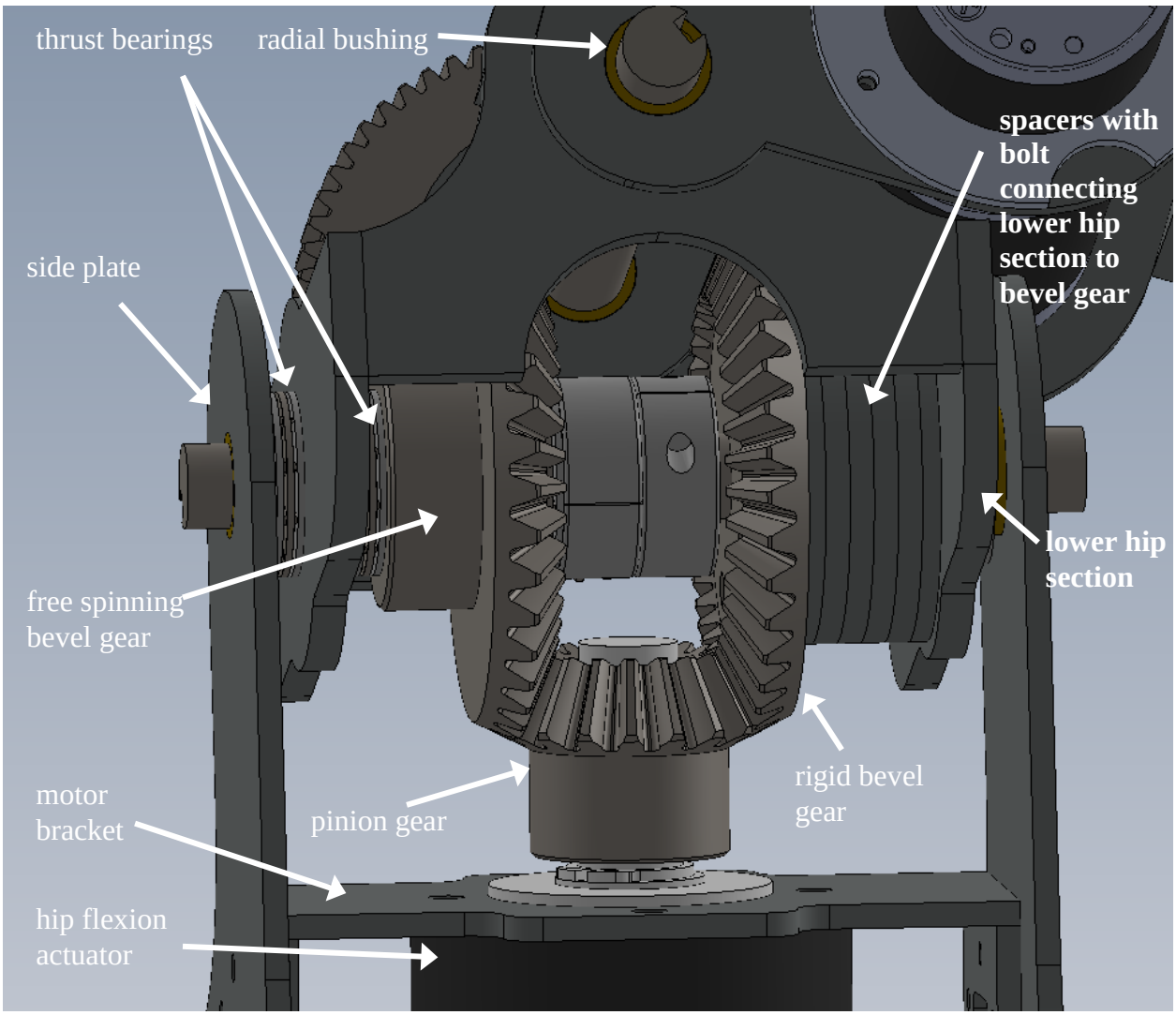


**Figure 2.2.9. The bevel-pinion gear setup that drives flexion and extension of the hip are shown here. The gear that has a removed hub spins freely, while the gear with the hub is bolted to the lower hip segment. When actuated the thigh assembly will rotate relative to the lower hip segment.**

The thigh section houses the motors for both the hip and knee flexion joints. Brackets connect the side plates together and hold the motors in place. A bracket was placed on the front of each motor, and a second bracket was seated around the motor at the back of the gear head. Cutouts were made into the side plates to eliminate weight and allow locations for mounting electronics and wiring.

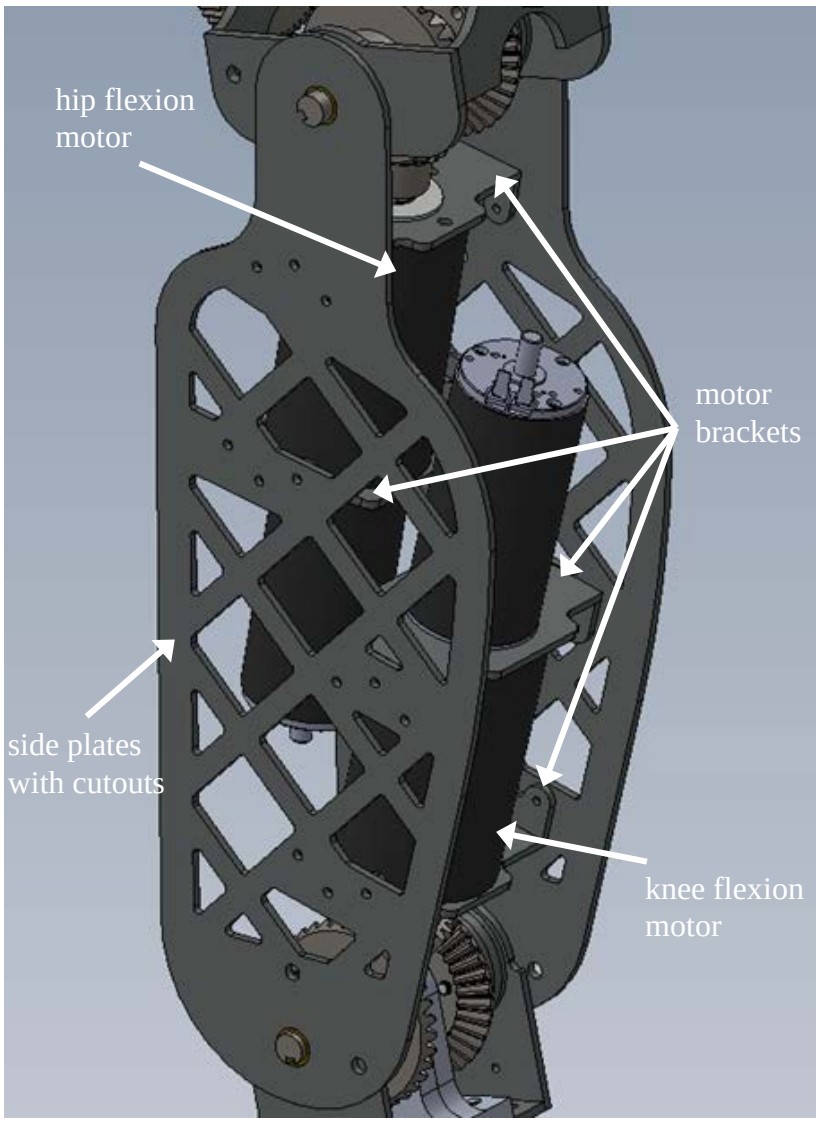


**Figure 2.2.10. Thigh assembly. The side plates were contoured to be narrow near the top to avoid limiting the ROM and to give a human-like appearance. This figure shows the front of the leg on the right of the image.**

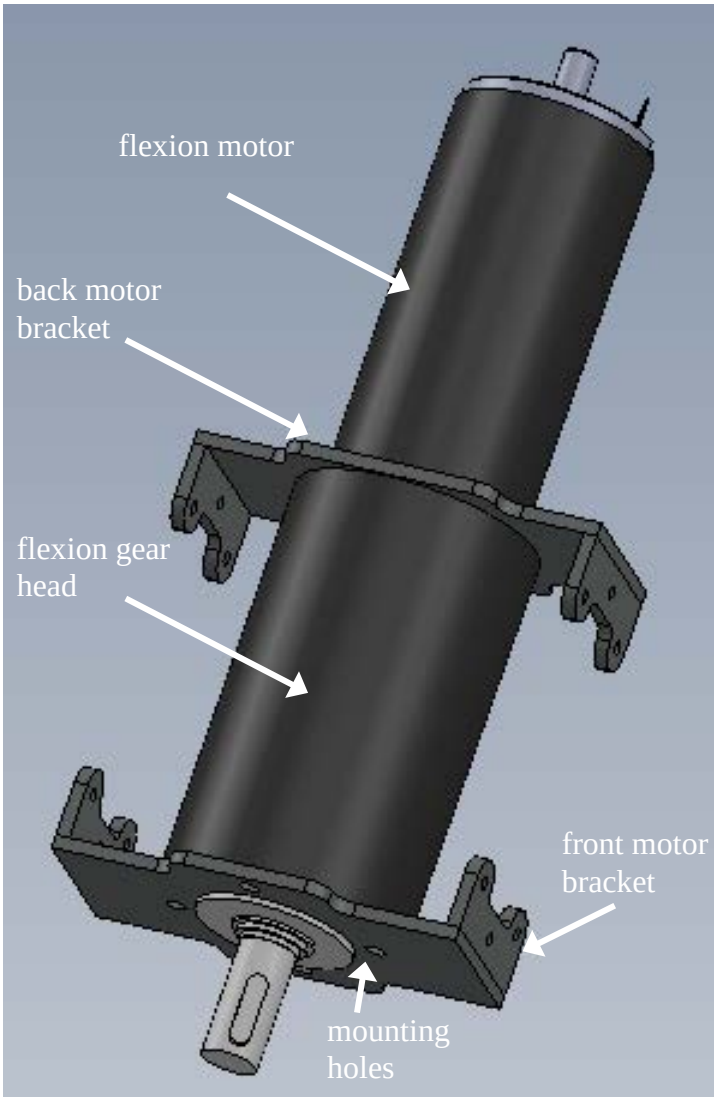


**Figure 2.2.11. Hip and knee flexion motor with brackets. A pair of brackets was used to provide adequate strength. While the front bracket was held in place with four screws into the face of the gear head, the back bracket was not rigidly connected to the actuator but was held in place by sliding around the motor and by connecting to the side plates.**

## 2.6 Knee Design

The knee joint used the same double bevel gear arrangement as the hip flexion, but the rest of the structure varied as shown in Figure 2.2.13. One bevel gear was rigidly connected the inner knee structure to drive the lower leg while the other again spun freely. A central support between the bevel gears, shown in Figure 2.2.12, made from aluminum was used to add support to the knee structure and was also keyed to the shaft for use with the potentiometer. A pair of

bolts through the each side plate was used as the mechanical stops to limit the range of motion and avoid self-damage. The human knee is also locked when straight, so these bolts were important to allow the leg to "lean" on the structure. On the bottom of the knee structure a prosthetic pyramid adapter was mounted to allow for the pylon in the lower leg to be connected, as will be further discussed in the next section.

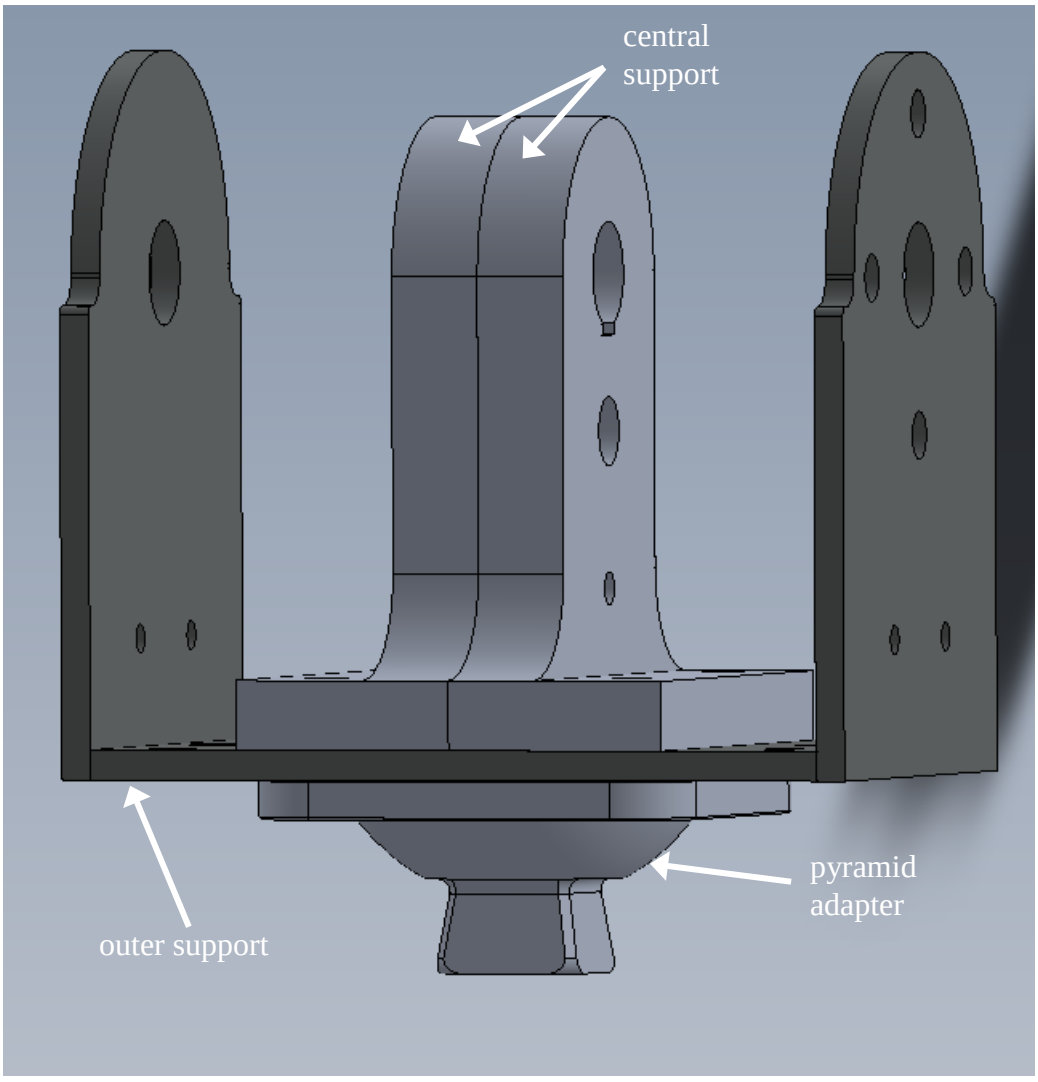


**Figure 2.2.12. The inner knee structure was composed of four components- the two-piece aluminum central support, the outer support, and the pyramid adapter.**

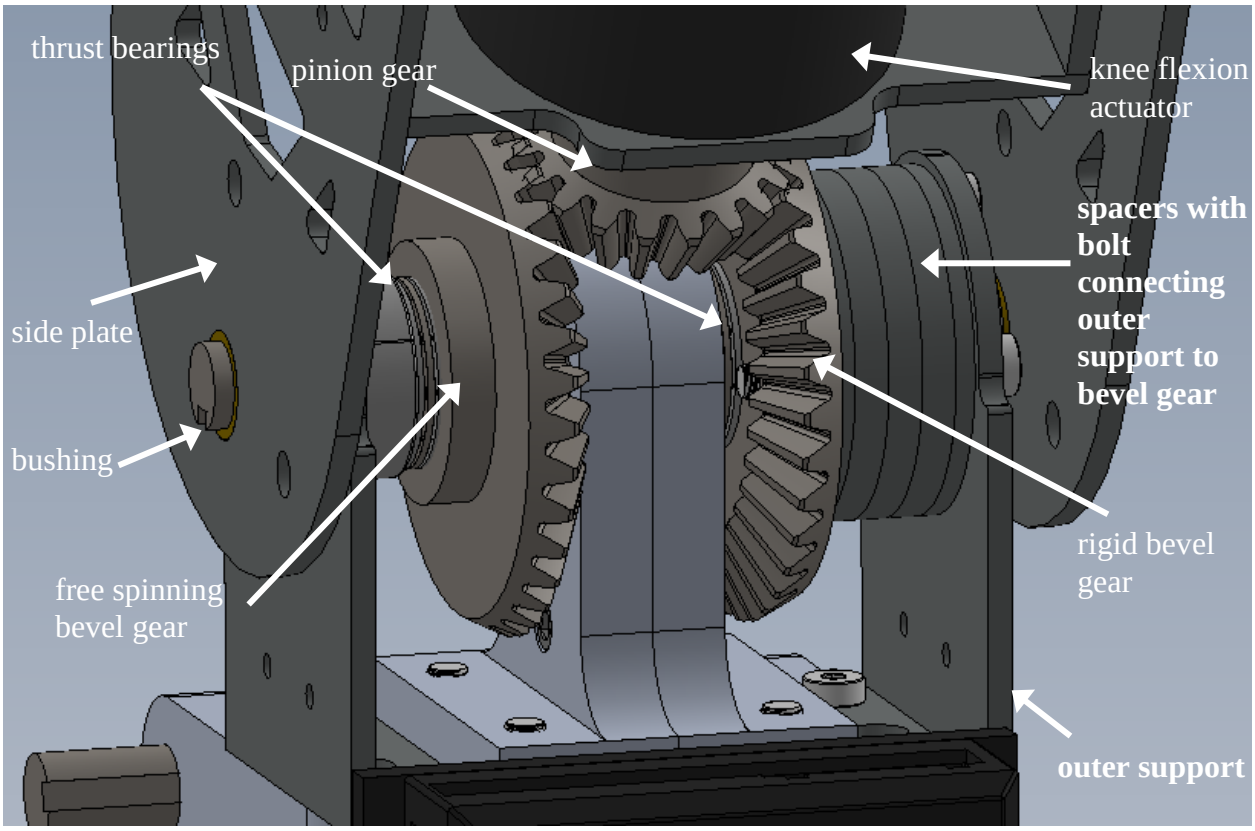


**Figure 2.2.13. Knee joint from the front. The middle support and the outside support share the load bearing of the lower leg. The bolts run from the right side of the outside support through the spacers into the right bevel gear.**

## 2.7 Lower Leg and Ankle Design

As previously mentioned, the lower leg was designed using a pylon structure, which was inspired by prosthetic legs currently in use. This design used a central aluminum tube to reduce weight and prosthetic connectors that allowed the legs to be taken apart quickly. By removing the two screws from the linear actuator beams, the horizontal screw from the pylon connector, the whole lower leg can be removed. The pyramid connector, which is the top piece in Figure 2.2.14, has a four-sided central pyramid that is inserted into the pylon adapter. The four screws on the adapter are tightened onto the pyramid, and in prosthetics the amount each screw is tightened can be used to adjust the relative angle of the pylon to the pyramid adapter. However, these adapters were chosen because they allow quick connection. A single screw running normal

to the pylon was used to tighten the adapter onto the pylon. This assembly was used to connect the lower leg to both the knee and the upper ankle.

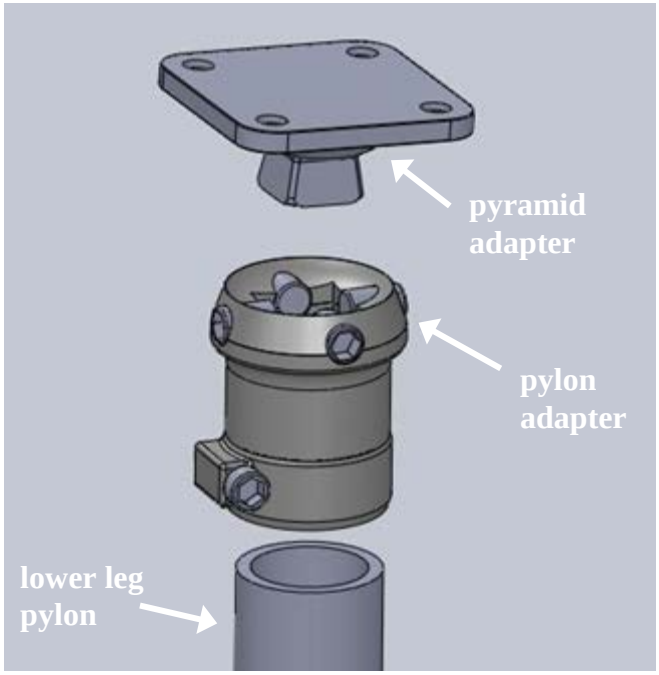


**Figure 2.2.14. Pylon connection to pyramid adapter. The four holes in the pyramid adapter, the top piece above, are used to connect the pylon to the joint. The four holes in the pylon adapter, the middle piece above, tighten on the pyramid faces. The single bolt tightens the pylon adapter to the pylon.**

The linear actuator, which drives the ankle pitch, was attached to the pylon and the outer knee structure. Two aluminum beams connect to the knee structure using an M8 screw each, as shown in Figure 2.2.15. A 12 mm shaft runs horizontally between the beams, with thrust bearings and a rod end between them. The rod end connects to the back of the linear actuator and is locked in place with a nut. Shaft collars on each end secure the whole assembly.

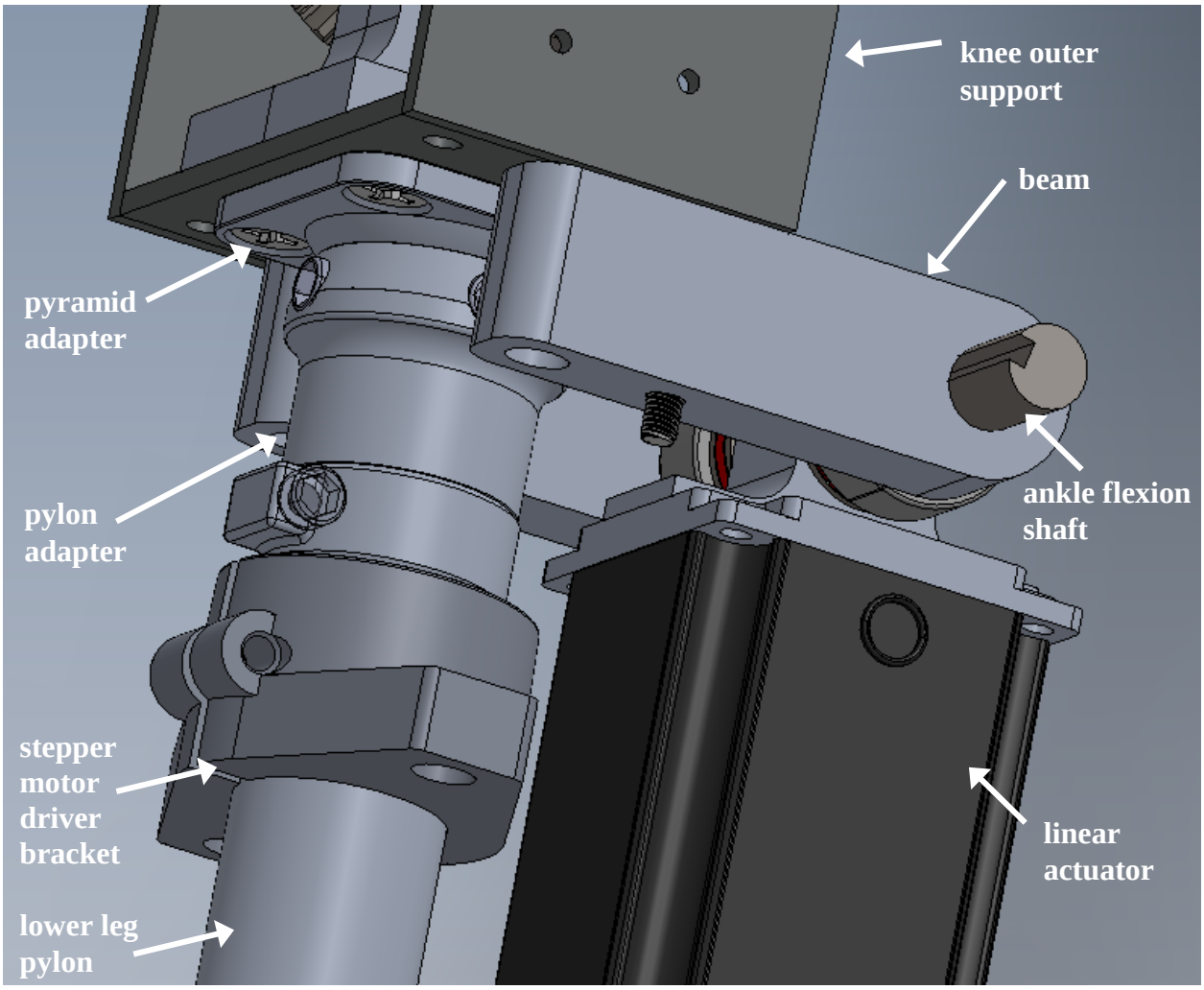


**Figure 2.2.15. Linear actuator attachment as seen from below. Although each beam is only held in place by one screw, the tight fit on the shaft keeps the beams parallel.**

The pylon was sized so that when the foot was normal to the pylon, the linear actuator would be parallel to the pylon and extended in the middle of its stroke so that it could achieve its full range of motion, which was +/- 45 degrees. As previously mentioned, since the moment arm was longest when the linear actuator was in this position, this was also its position of greatest torque output.

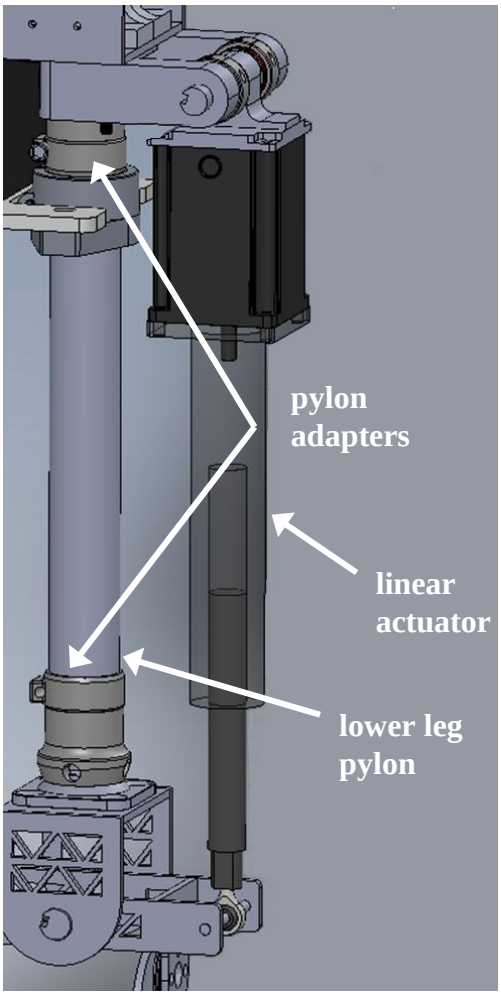


**Figure 2.2.16. Lower leg and linear actuator. The ankle structure was designed so that a hard stop would be reached before the linear actuator reached its limit in either direction.**

The bottom of the pylon connected to the upper ankle structure, which has cut-outs on the side to reduce the weight. The center ankle structure was connected by a 12 mm shaft. The linear actuator had a rod end that connected it to a stainless steel shaft running through the back of the center structure. Spacers on the shaft prevent lateral movement of the rod end, and the center box also features cut outs. The upper structure was designed so that the center structure will make contact with it before the linear actuator reaches its limits, therefore protecting the actuator by acting as a mechanical stop.

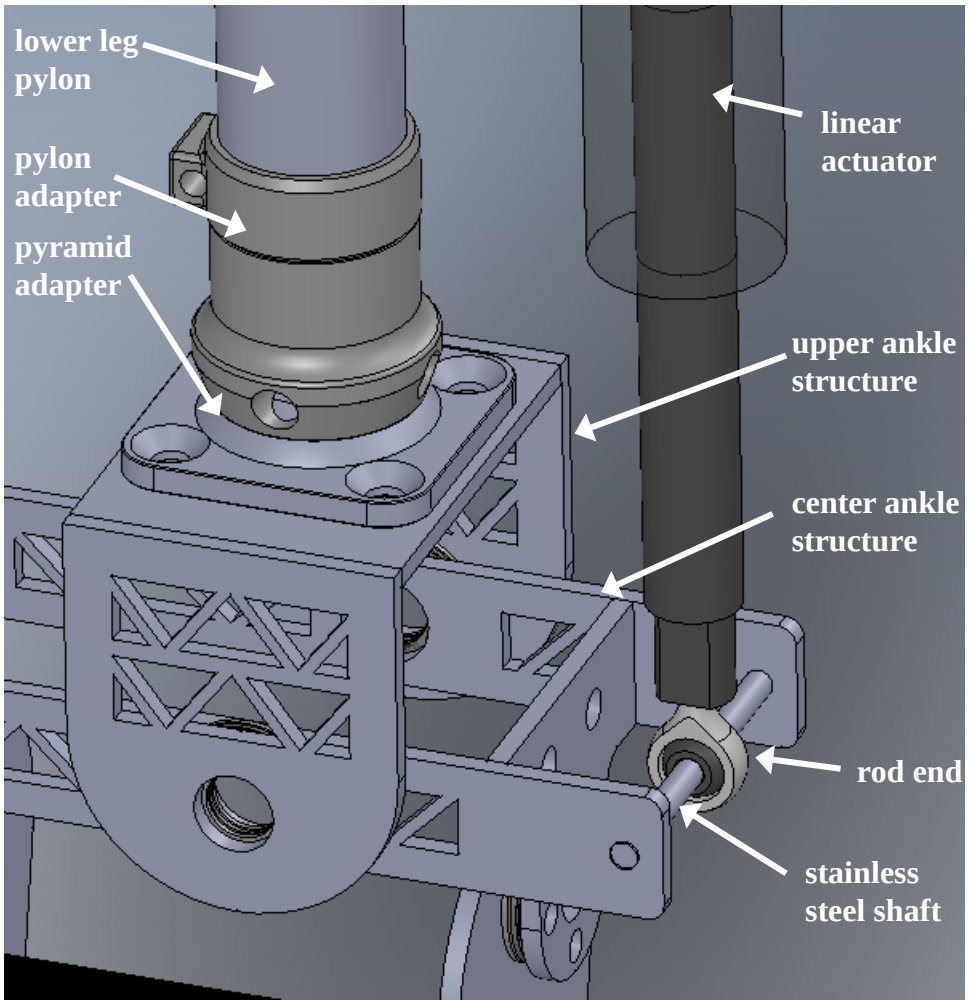


**Figure 2.2.17. Upper ankle assembly. Using a linear actuator allowed the ankle to be minimized in vertical height, since the motor is connected by just a simple pin joint. Many of the robots seen in the survey in Chapter 1 had large ankles that lacked human appearance, and this design also allowed the ankle to be more similar to human anatomy.**

## 2.8 Lower Ankle and Foot Design

The lower ankle assembly consists of the actuator, gearing, and structure for the roll of the ankle. The center structure has a spacer mounted on the front, which is held in place with two M6 screws, as shown in Figure 2.2.18. The small ankle gear was rigidly connected to the threaded holes in the spacer by four M5 screws. The gear head selected for the motor, as mentioned earlier, was used in an early design of the leg and had a gear ratio of 353:1, which

would not provide enough velocity at the joint. Therefore the external gears have a 1:2 ratio to increase the joint speed. To reduce the bending load on the gear head output shaft, a ring was designed to keep the larger gear from pushing away from the smaller gear, as shown in Figure 2.2.19. The motor and gear head were held in place by the foot structures, which were similar to the thigh motor brackets, and were held against the side of the gear head by the center ankle structure. Shaft collars hold the shaft in place from horizontal loads. Two screws hold each foot structure to the footplates using M5 screws.

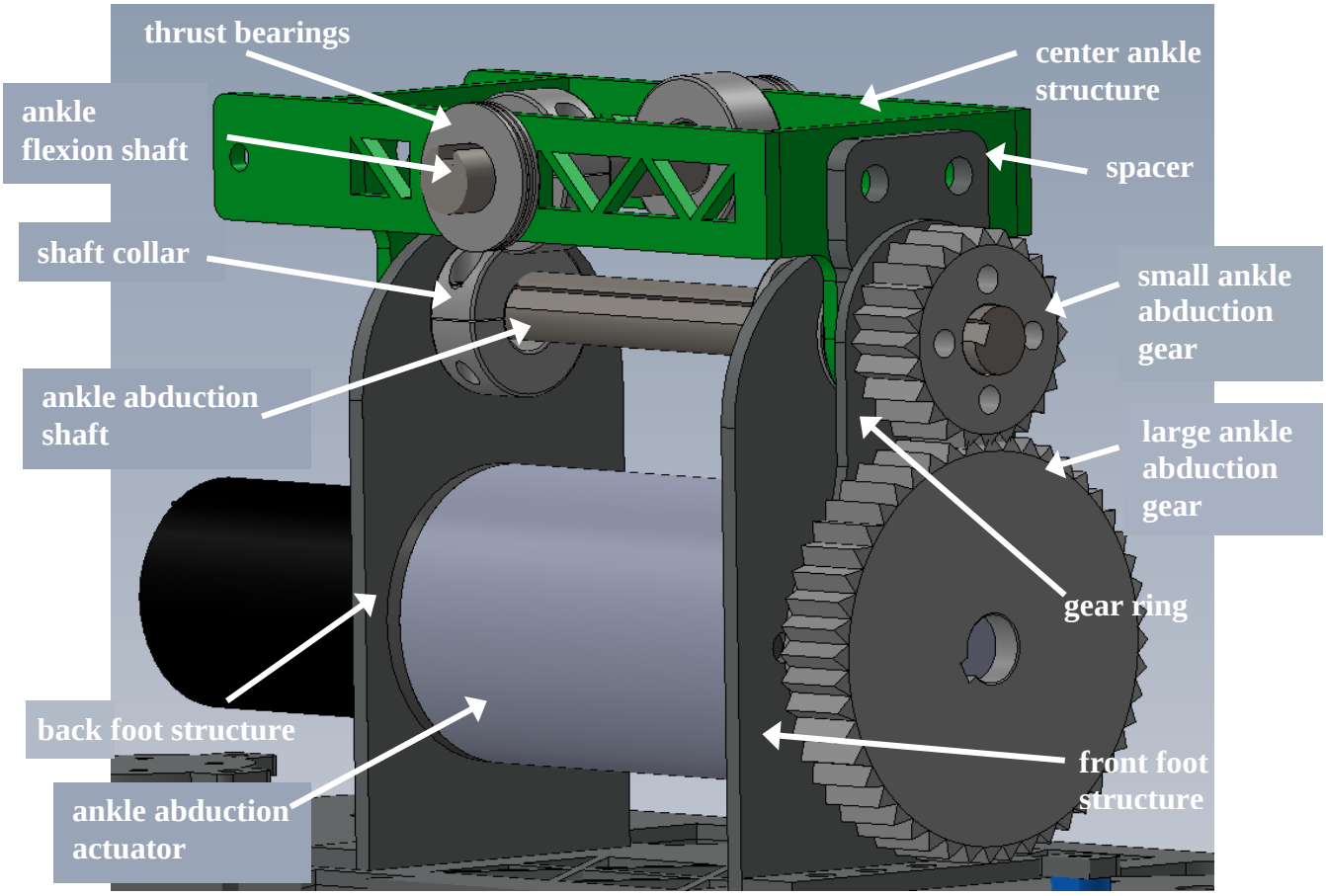


**Figure 2.2.18. Lower ankle assembly. The ankle roll motor rotates the whole foot around the smaller spur gear when actuated. The gears are on the front side of the foot.**

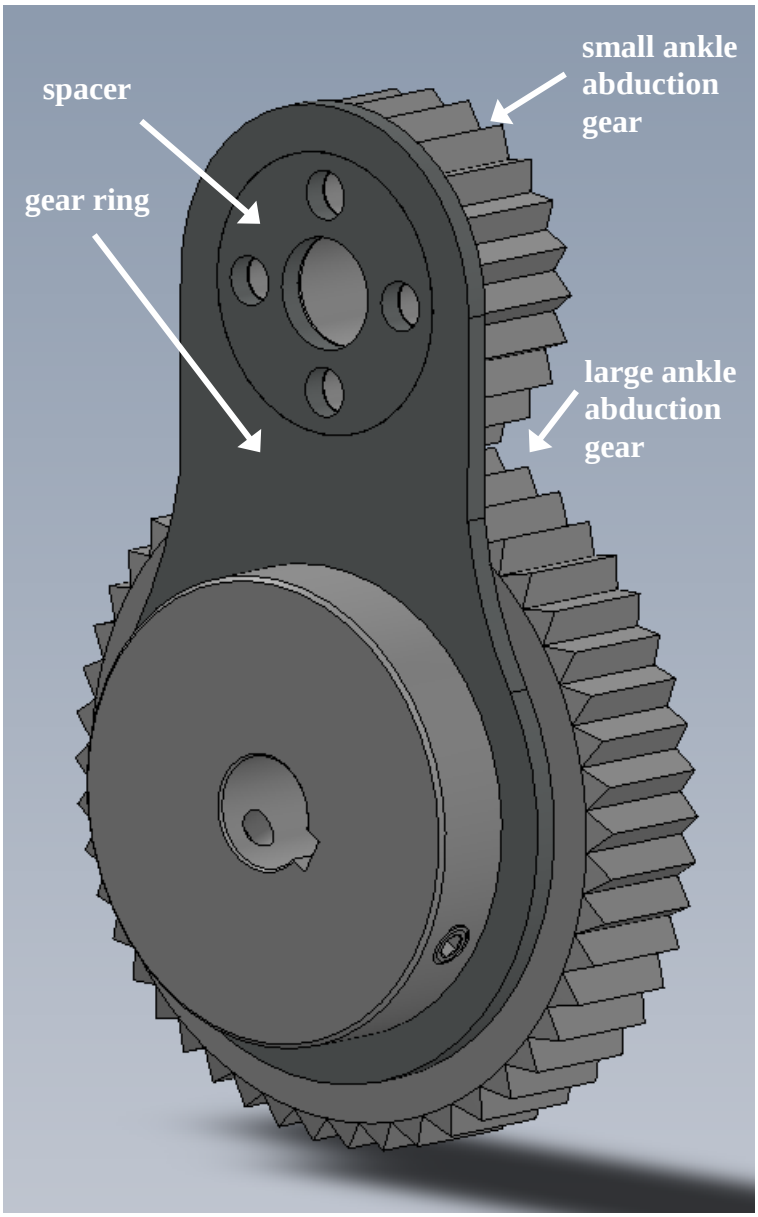


**Figure 2.2.19. Ring to reduce the gear head shaft loading. The ring goes around the outside of the large gear hub and the spacer on the smaller gear shaft.**

To simplify the balancing during initial testing, a large foot was designed to increase the base of support. Cut outs were again used to reduce weight, as shown in Figure 2.2.20. The force sensors were mounted on the feet, and a total of seven locations on each foot were created for mounting, which allowed for two sensors in the front of the foot in two different locations and either one or two sensors on the back of the foot. This would allow different sensor configurations to be tested to determine which configuration would provide the best data for the

zero moment point. Figure 2.2.21 shows the bracket that was attached to each sensor and the spacers between the bracket and the foot plates. A screw makes contact with the sensor and passes through the three layers of the foot plates, so that the only part of the foot that should be touching the ground at any time are the screws. This allows all the force to be transmitted into the screw and read by the sensors, which will be further discussed in Chapter 3.

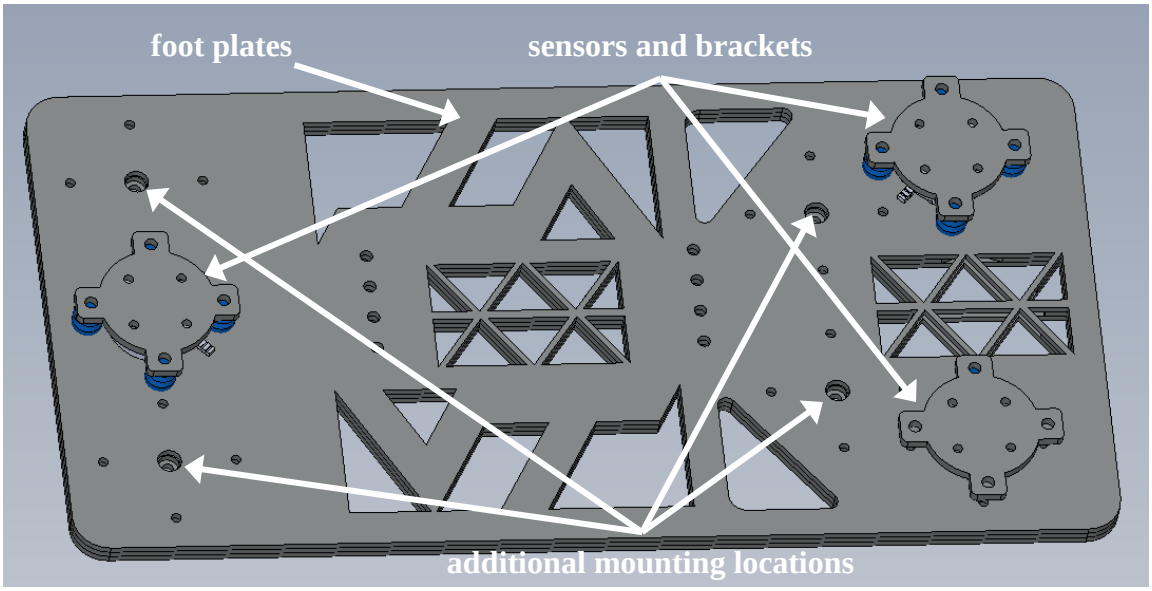


**Figure 2.2.20. Foot with force sensors. This figure shows two sensors mounted on the front of the foot at the position further from the center of the foot. Moving them to the closer position would reduce the effective size of the foot, since the foot only contacts the ground at the sensor locations.**

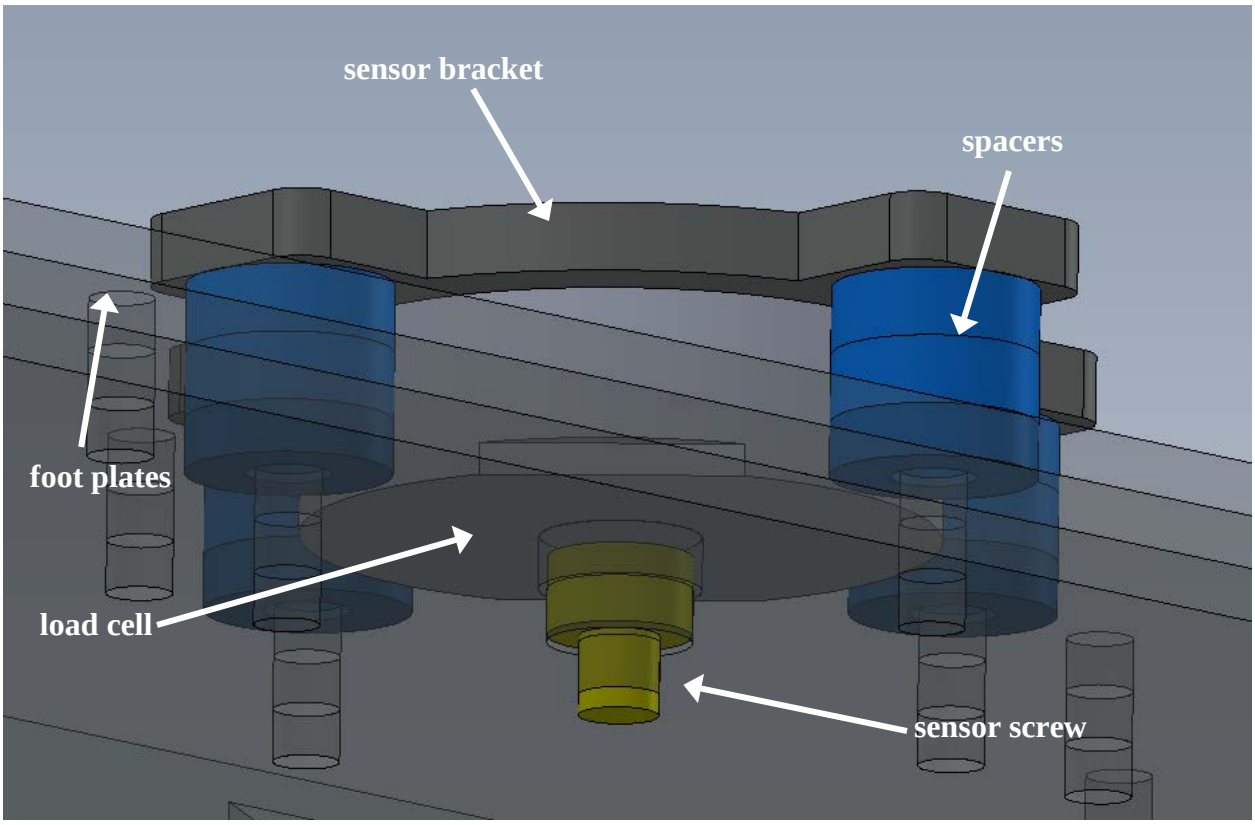


**Figure 2.2.21. Sensor assembly. Each sensor has two screws that pass through the bracket into the sensor. The three layers of the foot plate keep the screw contacting the sensor from falling out when the foot is lifted off the ground, since the bottom hole is just large enough for the screw threads to pass through.**

## 2.9 Overall Design Results

The final design achieved the goal of developing a pair of robotic legs with a human-like appearance and capability for a minimal cost. The completed design is shown in Figure 2.2.22 through Figure 2.2.28.

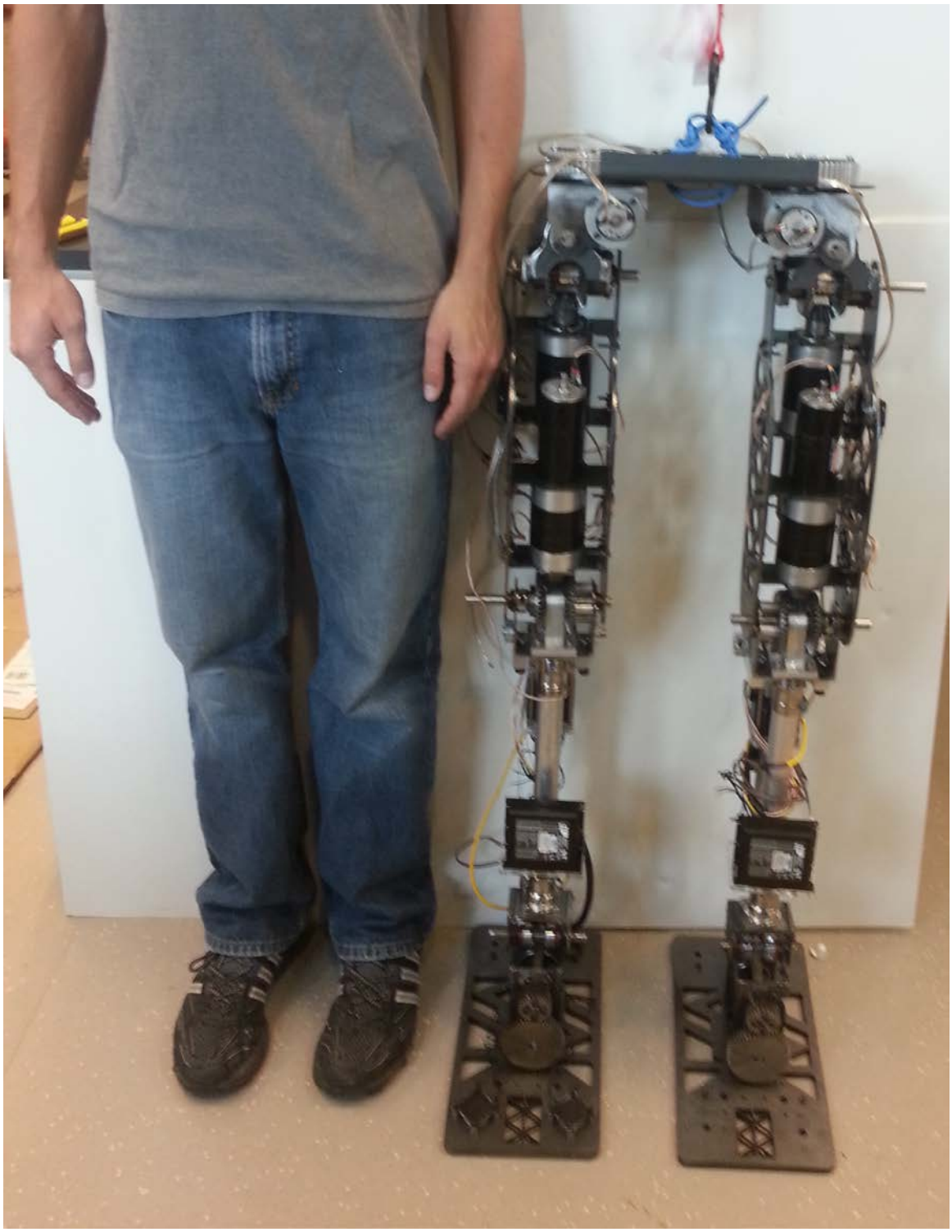

**Figure 2.2.22. Final design from the front standing next to person with height of 183 cm. The axis of the hip pitch joint is aligned with the same axis of the person.**

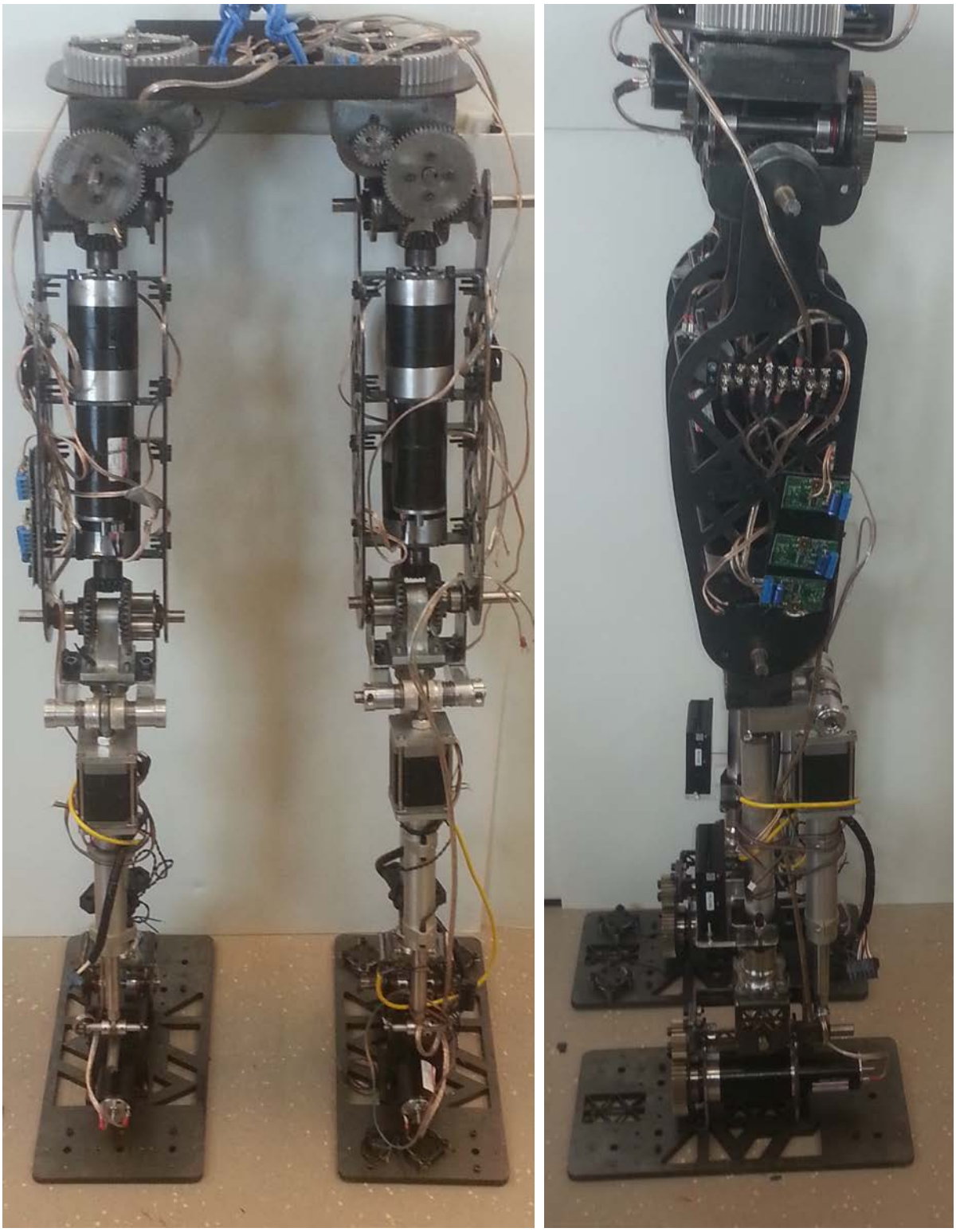

**Figure 2.2.23. Final design from behind and from the left side. The electronics can be seen mounted to the outside of the hip plate on the right.**

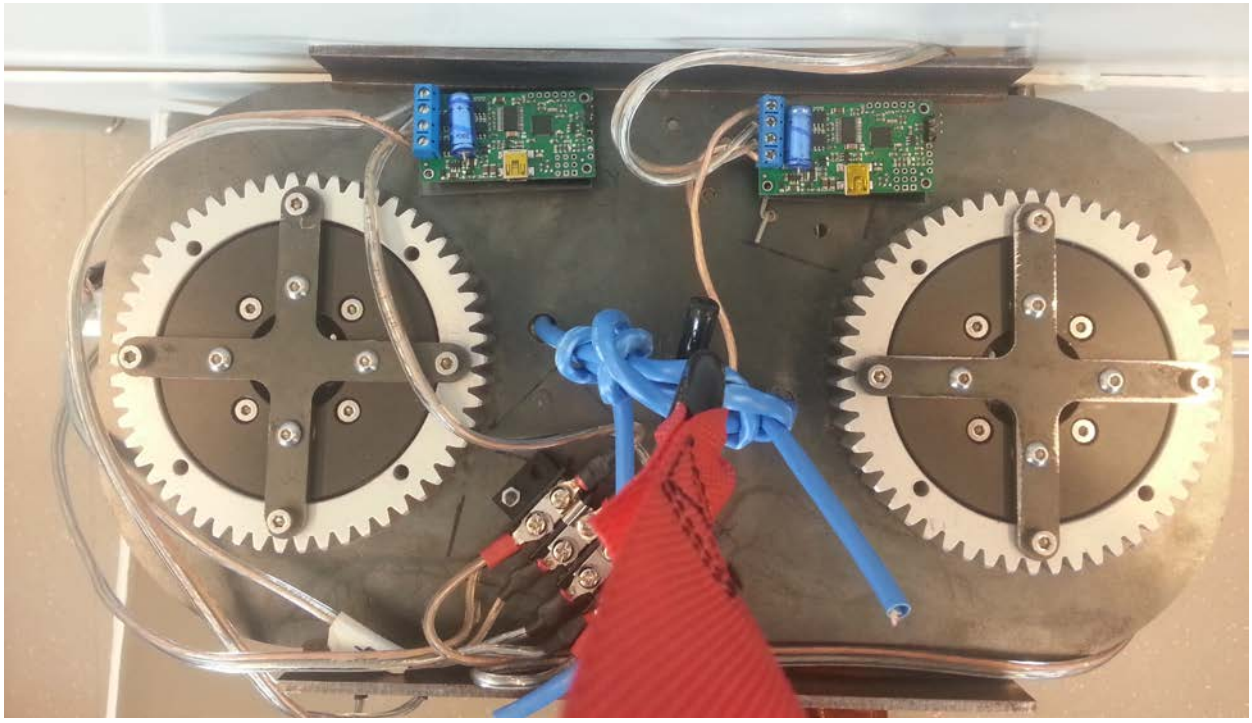

**Figure 2.2.24. Hip plate from above. The locking structures were installed to keep the hip from moving during early development, so the rotation motors are not in place.**

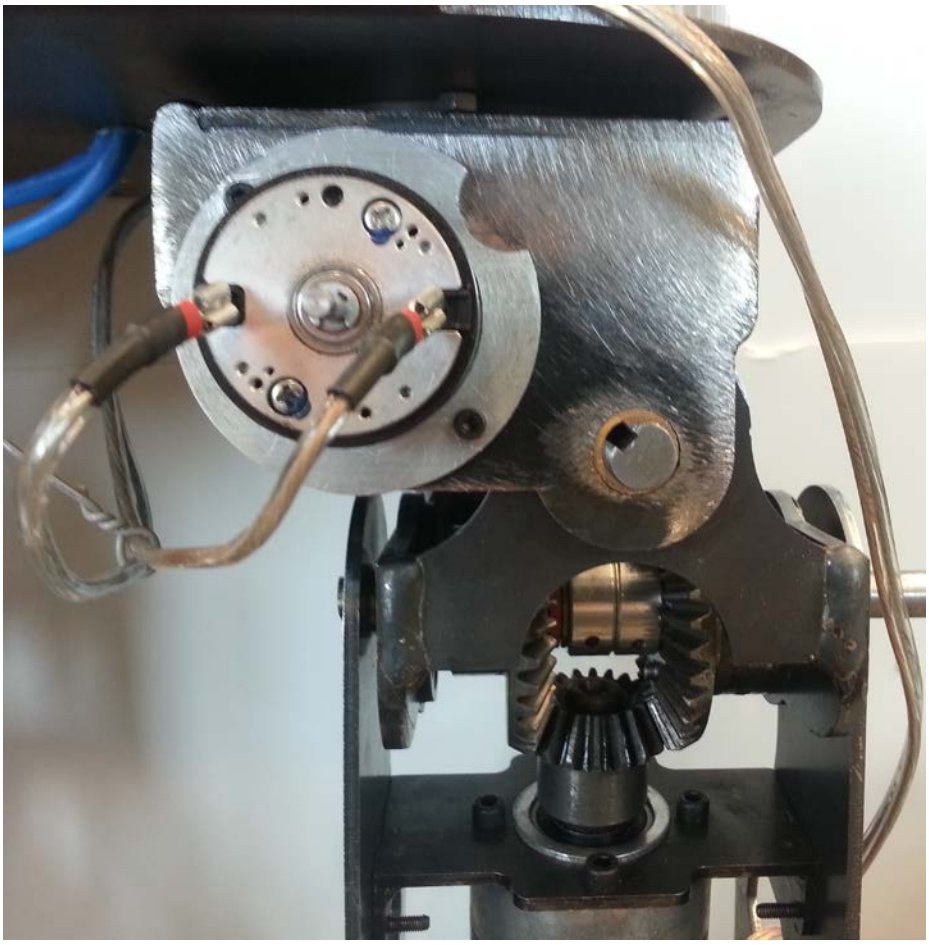

**Figure 2.2.25. Hip joint from the front.**

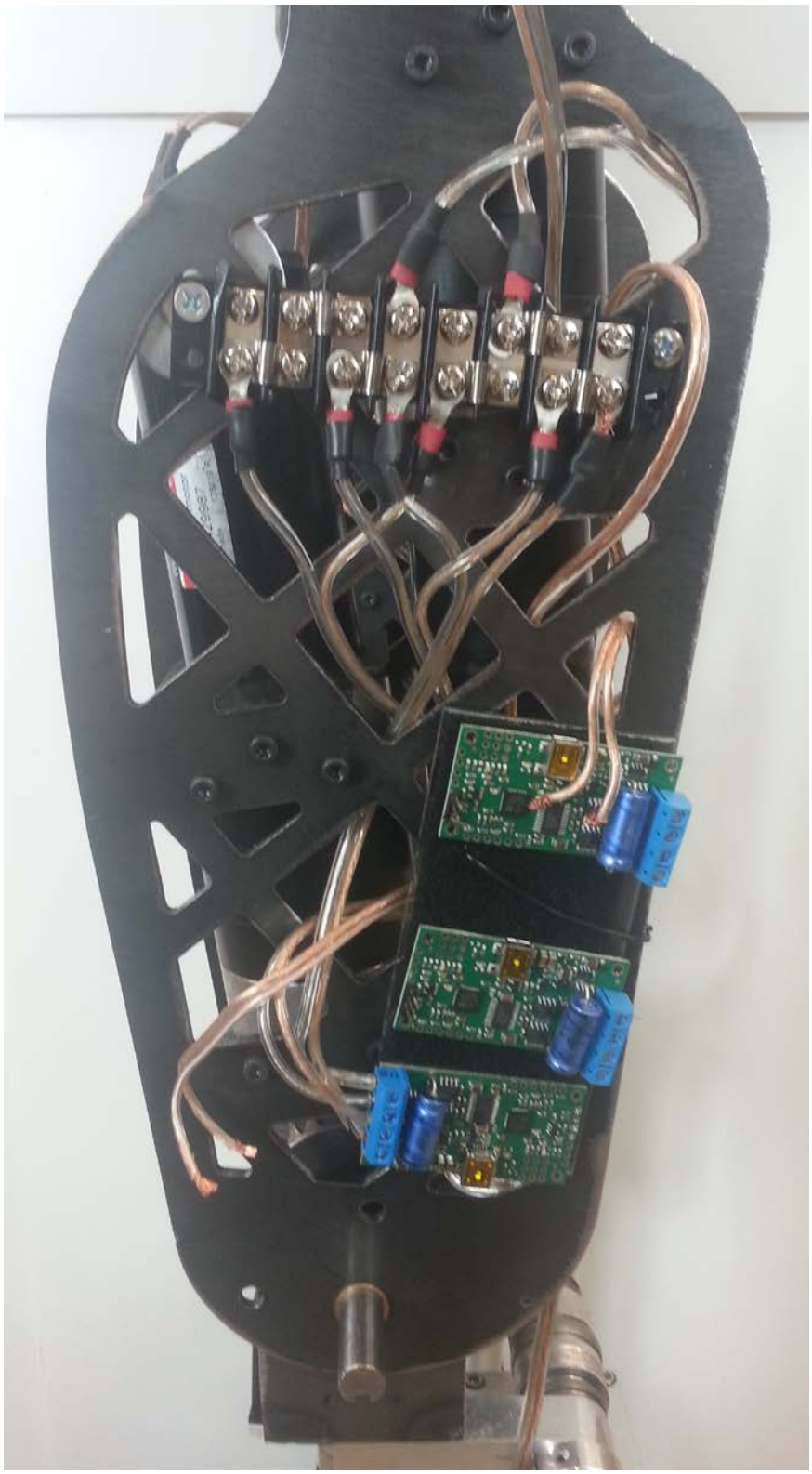

**Figure 2.2.26. Left side plate with DC motor controllers installed.**

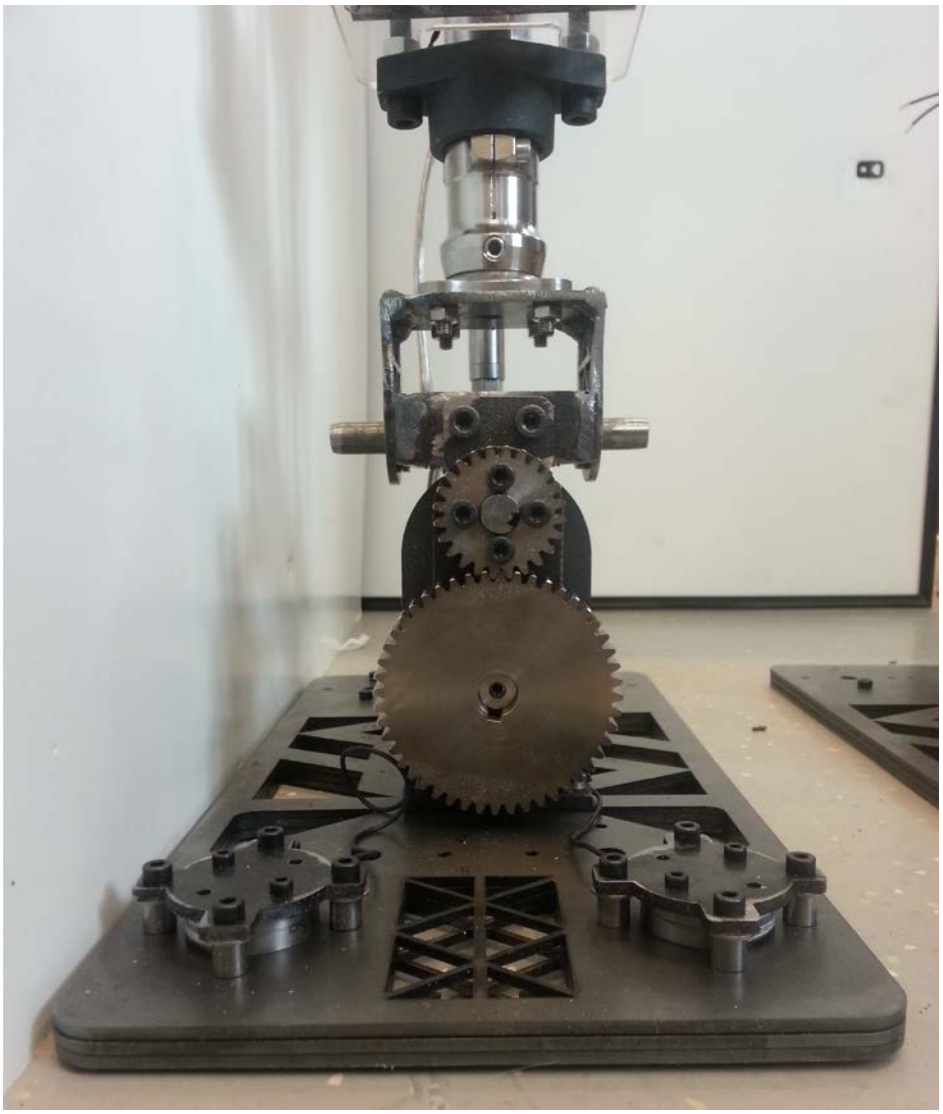

**Figure 2.2.27. Foot and ankle from the front. The force sensors are installed in the position furthest from the center of the foot.**

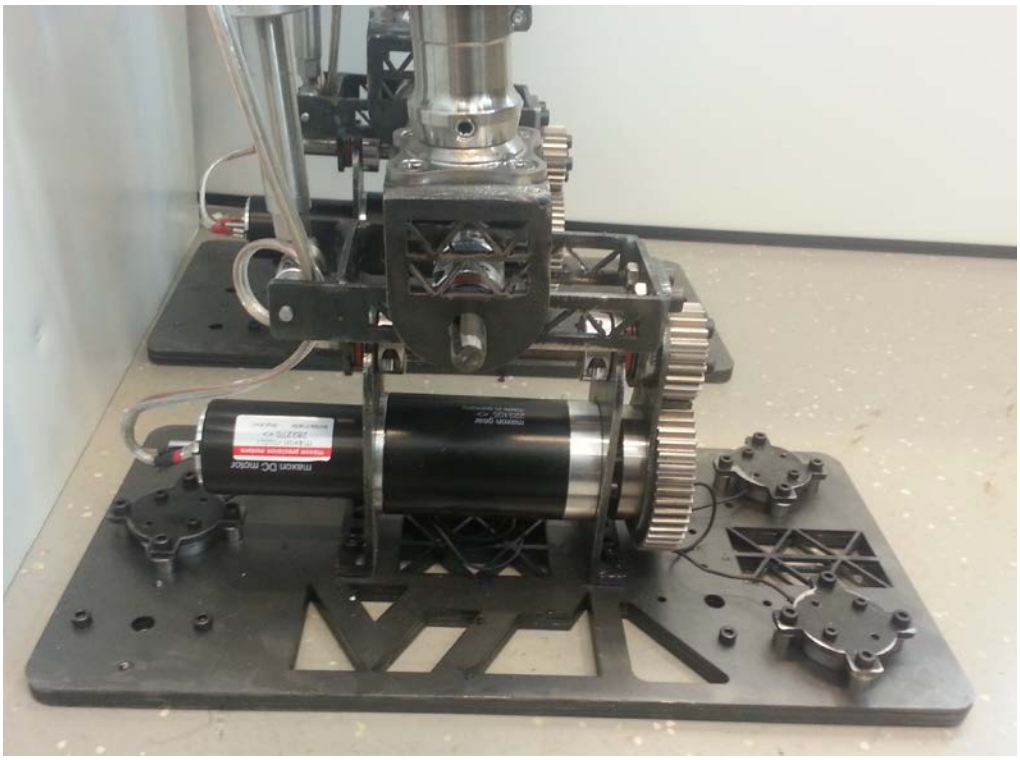

**Figure 2.2.28. Foot and ankle from the right side.**

The overall height is 94.2 cm from the bottom of the foot to the axis of the hip pitch. The length of each system segment was similar to that of a human, with the ankle being taller to accommodate the roll actuator and the thigh being smaller to most closely match the overall hip height. The weight of the full system (excluding the electronics which are relatively light) was 44.3 kg. Table 2.2.5 shows the mass of each of the actuation components (motors and gears), which make up approximately 38% of the total system weight. The structural weight was driven by the need to support the weight and actuation of these components, which were designed to have very high peak torques as previously mentioned, and the weight of an upper body.

**Table 2.2.5. Design goals for the robotic leg segment lengths**

| Segment | Desired Segment Length (cm) | Final Segment Length (cm) |
|---|---|---|
| **Total Height** | 183.0 | N/A |
| **Ground to Hip** | 97.0 | 94.2 |
| **Thigh** | 44.8 | 38.1 |
| **Shank** | 45.0 | 43.0 |
| **Foot (ground to ankle)** | 7.1 | 13.1 |

NOTE: The total system height was dependent upon the size of the upper body.

**Table 2.2.6. Weight of motors and gears**

| Motors/Gearhead/Gears | Quantity | Mass (g/unit) | Total Mass (g) |
|---|---|---|---|
| **Hip** | | | |
| RE-40 (Maxon 148866) | 2 | 480 | 960 |
| GP 42 (Maxon 203126) | 2 | 460 | 920 |
| 60 Tooth Gear (SDP/SI S10T12M060S1012) | 2 | 336.58 | 673.16 |
| 24 Tooth gear (SDP/SI S10T12M024S1012) | 2 | 61.53 | 123.06 |
| **Thigh** | | | |
| RE-50 Motor (Maxon 370355) | 2 | 1100 | 2200 |
| GP 62 Gear Head (Maxon 110507) | 2 | 1500 | 3000 |
| Pinion Gear (SDP/SI A 1C 3MYK20018H) | 8 | 110.12 | 880.96 |
| Bevel Full Hub (SDP/SI A 1C 3MYK20036) | 2 | 311.96 | 623.92 |
| Bevel No Hub (SDP/SI A 1C 3MYK20036) | 4 | 214.92 | 859.68 |
| Bevel Partial Hub (SDP/SI A 1C 3MYK20036) | 2 | 263.67 | 527.34 |
| **Lower Leg** | | | |
| Linear Actuator (UltraMotion D-B.125-HT23-4-2NO-PRBC3/RBC3) | 2 | 1515 | 3030 |
| **Foot** | | | |
| RE-40 (Maxon 148867) | 2 | 460 | 920 |
| GP52 (Maxon 223105) | 2 | 920 | 1840 |
| Large Spur Gear (Misumi GEAKBG1.5-48-15-B-12N-KC120) | 2 | 81.13 | 162.26 |
| Small Spur Gear (Misumi GEAHBG1.5-24-15-A-12-KFC21-K5.0) | 2 | 12.16 | 24.32 |
| | | **Total** | 16744.7 |

The range of motion (ROM) of each joint met or exceeded each of the human ranges. Although many of the robots only use a portion of the ROM of each joint for most tasks, just as humans do, it was considered important not to limit the capability of the system as much as possible.

**Table 2.2.7. Typical leg joint ROM of males 30-40 years of age (Roass & Andersson, 1982)**

| Joint | Motion | Human ROM (degrees) | Design ROM (degrees) |
|---|---|---|---|
| Hip | Extension | 9.4 | 52.6 |
| | Flexion | 120.3 | 90 |
| | Abduction | 38.8 | 64.3 |
| | Adduction | 30.5 | 16.8 |
| | Internal Rotation | 32.6 | 45 |
| | External Rotation | 33.6 | 45 |
| Knee | Extension | -1.6 | 0 |
| | Flexion | 143.8 | 90 |
| Ankle | Dorsiflexion | 15.3 | 45 |
| | Plantar flexion | 39.7 | 45 |
| | Eversion | 27.6 | 45 |
| | Inversion | 27.7 | 45 |

An important set of parameters for control of the legs will be the mass of each segment. The leg was divided into sections by the components that rotate together as shown below in Table 2.2.8.

**Table 2.2.8. Size of each leg segment**

| Segment | Weight per Leg (g) | Total Weight (g) |
|---|---|---|
| **Hip plate (without rotation motors)** | 4090 | 4090 |
| **Lower hip** | 1837 | 3670 |
| **Thigh** | 7808 | 15620 |
| **Lower leg** | 4583 | 9170 |
| **Foot** | 5856 | 11710 |
| **Total System Weight** | | **44260** |

One of the major design goals was to develop a system that was relatively inexpensive. The total estimated cost of the mechanical system was estimated at $14,510. Of this cost, the actuation components (actuators and gears) cost 87% of the price, with the prosthetic components being valued at an additional 8%. The total system price was increased by the sensors and control components. A summary of the mechanical costs is shown below in Table 2.2.9.

**Table 2.2.9. Cost of mechanical components by section (without hip rotation)**

| Component or Group | Quantity | Price($/unit) | Total Cost ($) |
|---|---|---|---|
| **Misc Adapters and Hardware** | 1 | $ 800.00 | $ 800.00 |
| **Steel Structure** | 1 | $ 100.00 | $ 100.00 |
| **Prosthetic Components** | 1 | $ 1,000.00 | $ 1,000.00 |
| **Hip** | | | |
| RE-40 Motor (Maxon 148866) | 2 | $ 485.38 | $ 970.76 |
| GP 42 Gear Head (Maxon 203126) | 2 | $ 359.75 | $ 719.50 |
| 60 Tooth Spur Gear (SDP/SI S10T12M060S1012) | 2 | $ 39.92 | $ 79.84 |
| 24 Tooth Spur Gear (SDP/SI S10T12M024S1012) | 2 | $ 18.60 | $ 37.20 |
| **Thigh** | | | |
| RE-50 Motor (Maxon 370355) | 4 | $ 592.38 | $ 2,369.52 |
| GP 62 Gear Head (Maxon 110507) | 4 | $ 728.75 | $ 2,915.00 |
| Pinion Gear (SDP/SI A 1C 3MYK20018H) | 4 | $ 47.84 | $ 191.36 |
| Bevel Gear (SDP/SI A 1C 3MYK20036) | 8 | $ 80.41 | $ 643.28 |
| **Lower Leg** | | | |
| Linear Actuator (UltraMotion D-B.125-HT23-4-2NO-PRBC3/RBC3) | 2 | $ 1,255.00 | $ 2,510.00 |
| **Foot** | | | |
| RE-40 Motor (Maxon 148867) | 2 | $ 485.38 | $ 970.76 |
| GP52 Gear Head (Maxon 223105) | 2 | $ 517.25 | $ 1,034.50 |
| Large Spur Gear (Misumi GEAKBG1.5-48-15-B-12N-KC120) | 2 | $ 52.60 | $ 105.20 |
| Small Spur Gear (Misumi GEAHBG1.5-24-15-A-12-KFC21-K5.0) | 2 | $ 31.66 | $ 63.32 |
| | | **Total** | $ 14,510.24 |

## 2.10 Future Work

As mentioned at the beginning of this chapter, this is the third of three designs of the robotic legs. Several problems that arose with earlier designs—including weak structure, gear play, overall stiffness, and lack of bearings—were addressed in this final version. However, several other improvements could be incorporated in a future design:

1. Decrease the gear ratio of the knee and hip pitch actuators to increase speed output.
2. Increase the use of aluminum components instead of steel to decrease weight.
3. Remove the prosthetic components to decrease cost.
4. Choose a gear head for the ankle roll that has a lower gear ratio to decrease ankle height by modifying the current external gear ratio.
5. Decrease the weight of the foot.

Future versions of the leg will include these improvements to decrease weight and increase the overall performance.

## 2.11 Overall Conclusion

The focus on this chapter was to develop a pair of robotic legs that could have torque, velocity, and size similar to that of a human while maintaining a low financial cost. A 12-DOF leg system was designed to be comparable to the capabilities of other robots and humans, with an emphasis on maximum torque output over other performance factors. Other human data on was also researched as a guide for creating legs that will match anatomy studies. Five DC brushed motors with planetary gear heads and external gearing were chosen for five joints, and a stepper motor-driven linear actuator was responsible for one DOF. The overall design used similar components throughout, particularly the knee and hip pitch which were designed very similarly. The final size and range of motion of the fabricated system was comparable to that of a human, and its final cost was kept relatively low. This design could be improved in several ways, but the overall design goals were met and the system is theoretically capable of being used to implement various balancing and walking algorithms, which will be the focus of Chapter 3.

# Chapter 3

# Electrical Design and Control of the Legs

## 3.1 Introduction

The control system for the legs was developed in conjunction with the mechanical design. Several components were considered for controlling the different actuators and providing the position feedback from the joints. A ZMP sensor was designed to allow the implementation of a balancing algorithm. An overall control architecture was designed for close loop control of the legs and a Simulink simulation code was developed to evaluate the different walking gaits.

## 3.2 Control and Feedback Components

### 3.2.1 Motor Drivers

The selection of the brushed DC motors allowed simpler and lower cost drivers to be integrated into the control system than would have been required with other electric motors. Although cost and size could have been minimized by creating a custom motor control board, these benefits were outweighed by the time to design, build, and troubleshoot such a board and the simplicity of COTS components. The Pololu Simple Motor Controller was very compact, met the voltage and current requirements, and used a simple serial communication protocol. The 24V12 model was used for each DC motor. Key specifications for this board are summarized in Table 3.2.1. The PWM frequency was high enough to eliminate the audible noise and the voltage resolution was greater than 11 bits in each direction. The driver output can be controlled by several methods including serial communication and serial over a USB connection. Two 12-bit analog-to-digital converters were available on the board and could be used in the future implementations for feedback or as limit switches. A picture of the driver can be seen in Figure 3.2.1.

**Table 3.2.1. Pololu Simple Motor Controller 24V12 parameters**

| Parameter | Value |
|---|---|
| Size (inches) | 2.1 x 1.1 x 0.2 |
| Model | 24V12 |
| Max Supply Voltage (volts) | 40 |
| Max Continuous Output Current (amps) | 12 |
| Voltage Resolution (volts) | Max Supply Voltage / 3200 |
| Max PWM Frequency | 21.77 kHz |
| Max Update Speed (Hz) | 1000 |

Note: Data from (Pololu, 2012).

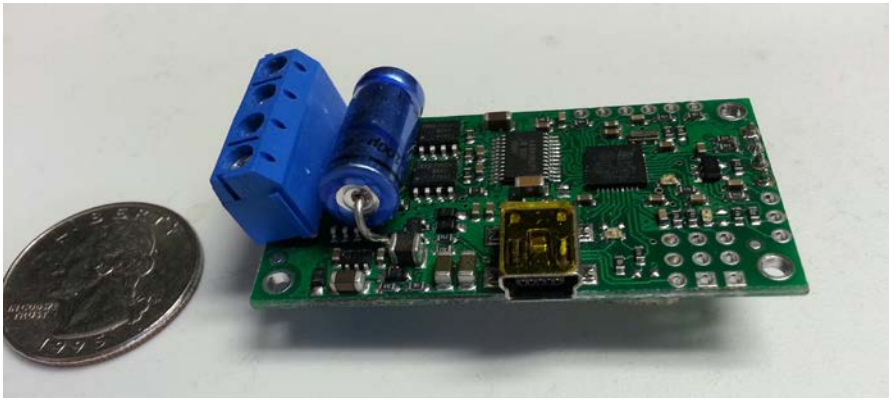

**Figure 3.2.1. The Pololu Simple Motor Controller was used as the DC motor driver. A micro USB connection allows the board to be programmed and/ or controlled over USB.**

Control of the stepper motors in the linear actuators is more complex and required a controller. Because the motor is rated at 4.24 amps per phase, a large controller was necessary and eliminated many of the inexpensive COTS controllers. The ST5-S controller from the same manufacturer as the motor, Applied Motion Products, was selected because it met the current rating and had several control inputs including RS-232 serial and an analog voltage speed control. Although the serial communication method, which commanded the number of steps to move, was initially used to test the actuator, the velocity control using the analog input was simpler in the full implementation because a speed and direction could be specified in a similar method to the DC drivers. The largest drawback with the ST5-S, which is shown in Figure 3.2.2,

was its high price, but since only two were needed in the system the features compensated for the cost. It is also considerably larger than the DC drivers, measuring 3.65 x 3 x 1.125 inches.


**Figure 3.2.2. The Applied Motion Products ST5-S stepper driver. The driver was programmed using an RS-232 connection but then can be driven using several different methods.**

### 3.2.2 Position Sensor

To acquire position feedback from the joints, several sensors were considered. Encoders were the most common feedback sensor, as mentioned in the survey in Chapter 1, and are typically mounted on the motor shaft directly. The widespread use of encoders is likely due to their being a digital sensor and therefore less sensitive to outside interference. Measurement of the motor movement before the gear head will provide a very fine resolution after the gear multiplication. However, most encoders measure relative positions and require a homing routine to initialize their position, and being positioned on the motor shaft means that any backlash between the motor and joint will cause error in the position readings which can compile over time. Encoders are a bit expensive.

A more inexpensive method in comparison to encoders is potentiometers, which is analog sensor that acts as a variable voltage divider. The potentiometers experimented in this work provided absolute position by a corresponding varying voltage output. They are simple, requiring only a power, ground, and signal connection, and theoretically have infinite resolution. In practice the actual resolution is dependent upon the noise of the system and the quality of the sensor's mechanical design. Potentiometers are also inexpensive and small in volume. By connecting the potentiometer directly to the joint shaft, the actual joint position was measured

despite any backlash in the system (assuming no backlash in the potentiometer connection). The drawback to potentiometers for this design is that the analog reading from the sensor is more susceptible to noise than digital sensors, and the large amount of current drawn by the motors could create interference and impact the reading. However, the cost savings and simplicity of potentiometers outweighed complexities that had to be accounted for in analog signal degradation. Being a contact sensor, potentiometers also may have a shorter life cycle than encoders, but life cycle analysis was outside the scope of this work.

## 3.3 ZMP Sensor

As discussed in section 1.1.2, the zero moment point (ZMP) is the location where all the inertial forces on the body sum to zero, and a body will be stable if this point is located within the base of support (BOS), which is a polygon formed by the points of contact with the ground. If the overall system orientation, the segment positions, velocities, and accelerations, and the surface of the ground were known, the ZMP could be computed without the need for other sensing. Due to the variability of conditions during walking and the complexity of calculating the whole body dynamics, an additional sensor is often implemented to measure the actual ZMP directly for use in the control system.

### 3.3.1 Calculating ZMP

In order to determine the ZMP, a set of single-axis force sensors were implemented in the design. One method of calculating the ZMP would be to use knowledge of the position and acceleration of each segment of the body. However, this methodology is dependent upon knowledge of the whole body orientation, does not account for outside disturbances or increases in mass (such as if something is picked up), and is very computationally intensive. If sensors are used to measure the ZMP directly, these issues can be avoided at the cost of additional components and accommodating the sensors into the design. Although several different types of sensors are employed, a similar method can be used to compute the ZMP for all force sensors. Since the ZMP is a measurement of the location of the summed forces acting between the ground and the body that produces no moment, the forces and moments applied are measured. Since the sensors are measuring force from the ground, the ZMP in the z-direction (vertical) can be

assumed to be on the ground and is therefore ignored in computation. The ZMP can be calculated generally using Equations 3.3.1 and 3.3.2.

$$ZMP_X = \frac{\sum M_Y}{\sum Fz} \quad \textbf{3.3.1}$$

$$ZMP_Y = \frac{\sum M_x}{\sum Fz} \quad \textbf{3.3.2}$$

The moments about the x- and y-axis, the forces in the z-axis, and the ZMP in the x- and y-planes are represented as $M_X$, $M_Y$, $F_Z$, $ZMP_X$, and $ZMP_Y$, respectively (Bertec, 2012; Erbatur et al., 2002).

### 3.3.2 ZMP Sensor

Many of the robots surveyed in Chapter 1 used a force-torque sensor similar to the one shown in Figure 3.3.1 which measure forces in the x-, y-, and z-directions and the moments around these three axes. When the sensor is placed as the connection between the ankle structure and the foot, as shown in Figure 3.3.1, all the forces applied by the body to the ground are transmitted through the sensor. The drawback to this orientation is that the sensors tend to be large and therefore limit how close the ankle rotation can be to the ground. The important advantage is that since all the loads can be measured by the sensor, the orientation or location of contact between the foot and the ground will not prevent the sensor from sensing the load. However, these sensors also tend to be very expensive.

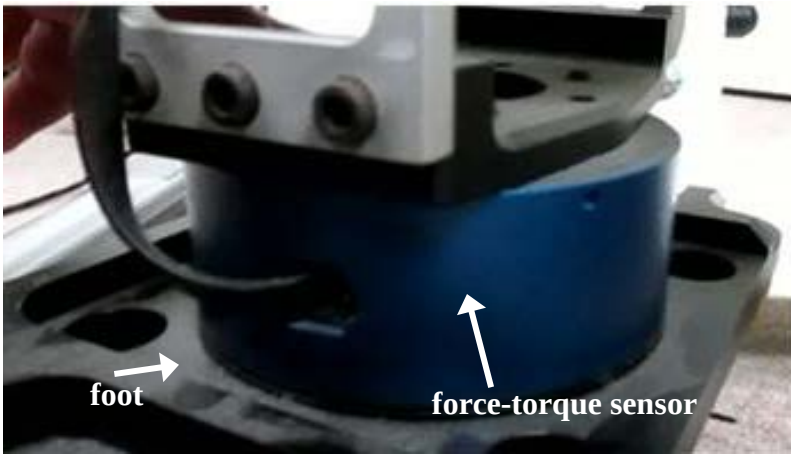


**Figure 3.3.1. An example of a six DOF force-torque sensor in a robotic foot. The foot is rigidly connected to the outside structure of the sensor while the ankle section is connected to the center section of the sensor. The loads are transmitted through the connection between these two sections on the inside of the sensor, which is measured to produce the output.**

Because six DOF sensors are very expensive, a more inexpensive sensor system was designed. The goal was to use multiple single-axis force sensors to measure loads in the z-direction only, similarly to the work performed by Erbatur et al. (2002). A key is that the foot must be designed so that the sensors only experience loads in the z-direction (vertical). Because the location of the sensors is known, the force can be multiplied by the distance to a given axis to find the moment around that axis. Figure 3.3.2 shows an example of loads seen on the foot.

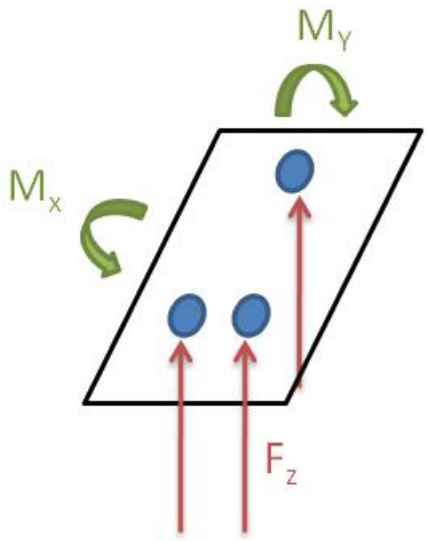


**Figure 3.3.2. Example of forces and moments applied to force sensors on bottom of the foot. The moments around the x-and y-axis are $M_X$ and $M_Y$, and the forces in the z-axis are $F_Z$.**

Using this methodology, the actual ZMP can be found using Equations 3.3.3 and 3.3.4 (Erbatur et al., 2002).

$$ZMP_X = \frac{\sum^i F_{Zi} * d_{Xi}}{\sum^i F_{Zi}} \quad \textbf{3.3.3}$$

$$ZMP_Y = \frac{\sum^i F_{Zi} * d_{Yi}}{\sum^i F_{Zi}} \quad \textbf{3.3.4}$$

where $d_{Xi}$and $d_{Yi}$ are the distances from a given location in the x- and y-direction, respectively, and $i$ is the sensor.

As mentioned previously in Chapter 2, the foot was designed to accommodate several different sensor arrangements. The best number or orientation of the components would be too difficult to compute due to uncertainties with the sensing and robot design. Being able to test various configurations allows four sensors to be used, which provides a larger base of support and more contact points to acquire data, or three sensors, which reduces the financial and computational cost. The different sensor placements are illustrated in Figure 3.3.3. When the front sensors are mounted close to the center of the foot, the effective foot size is decreased, and if this arrangement was found to yield acceptable results the foot weight could be reduced.

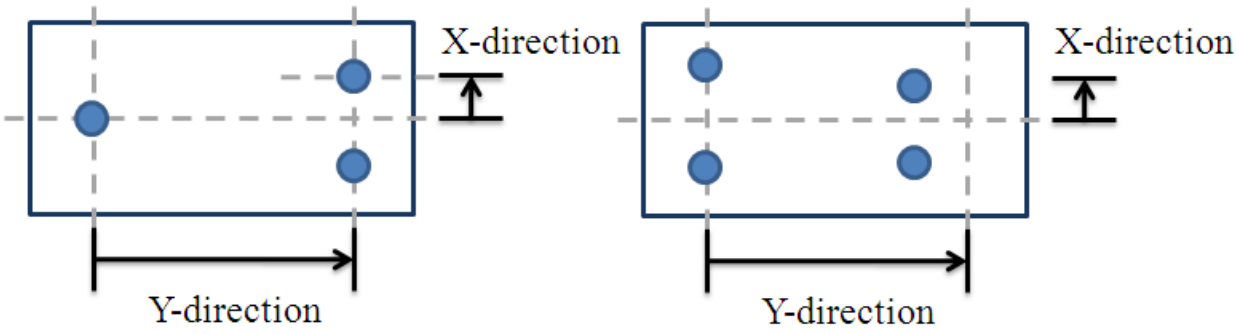


**Figure 3.3.3. Arrangement of force sensors on the foot. Several sensor arragements are possible for testing, with one or two sensors in the back of the foot and two different locations for two sensors in the front.**

Several different types of force sensors are available, including capacitive, resistive, and force sensing resistors. Capacitive sensors depend on frequency output and are more difficult to read than resistive sensors, which typically output an analog voltage signal. Force sensing resistors are inexpensive and very thin but are not designed for precision measurements (Erbatur et al., 2002). Therefore, the FC-23 resistive sensor from Measurement Specialties was chosen, and its performance parameters are shown below in Table 3.3.1 (Measurement Specialties, n.d.).

**Table 3.3.1. Specifications of FC-23 force sensor**

| Manufacturer | Measurement Specialties, Inc. |
|---|---|
| Model | FC23-1-1-0000-0250 |
| Force range | 0-250 pounds |
| Accuracy | +/-1% full scale |
| Output Voltage | 100 mV |
| Zero Force Output Voltage | +/-20 mV |
| Response Time | 1 ms |
| Max Overload Force | 2.5X max load |

To prevent damage, the force sensor needed to be able to accommodate the load of the robot moving dynamically. Since this line of sensors were available in 100 lbf and 250 lbf units, the 250 lbf max overload of the former would be close to the assumed worst load case scenario- where the full force is applied to a single sensor. This limited the accuracy, which is rated at +/- 1% of the full-scale of the sensor, but since the goal was to determine the relative load of each

sensor this was acceptable. The zero force output voltage can vary for each unit by an amount that is significant compared to the total voltage range, so calibration must be performed on each load cell individually. Calibration of the sensors is shown in Figure 3.3.4. The update rate of 1 ms matched that of the Pololu DC motor controllers. The mounting of these sensors was shown in Chapter 2, with a screw passing through the foot to make contact with ground and transmitting the force to the sensor.

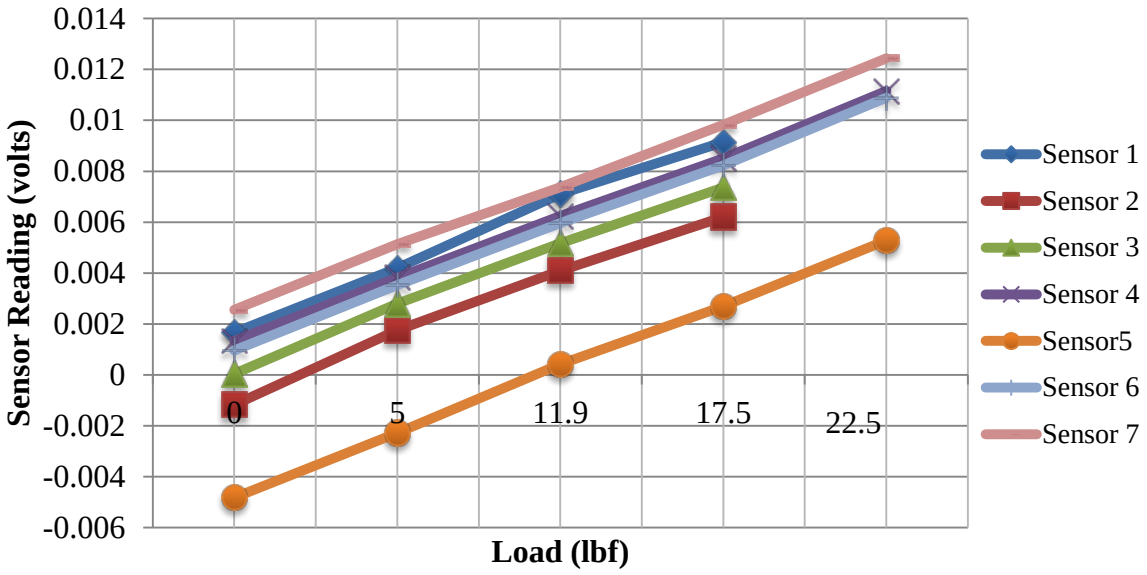


**Figure 3.3.4. Calibration outputs from the FC-23 sensors. All the sensors were in line with the manufacturer datasheet in terms of no-load offset and slope of the curves.**

## 3.3.3 ZMP Testing and Calibration

The next phase of this project will focus on testing of the sensors to determine which arrangement is optimal and if any calibration curve between the force readings and the actual ZMP is necessary. One method to perform the tests would be to place the bottom plates of the robot foot with the sensors mounted onto a force plate, and then have a person stand on the force plate and/or walk normally on the foot plate. This would give a dynamic ZMP that could be measured by the force plate directly and compared to the force sensor readings. Additionally, both feet could be placed on the force plate and similar tests could be performed. Erbatur et al. (2002) connected their sensor to the bottom of a person's foot and acquired data, and this method could also prove useful for the current design. Once the data has been acquired, a set of

calibration curves could be constructed to compute the actual ZMP from the readings of the foot sensors, with the possibility of having one calibration if both feet are experiencing load and a different one when only one foot is loaded. However, performance of these tests is outside the scope of the current work.

## 3.4 Proposed Control Architecture

Several different architectures were considered for the closed loop control of the legs. With the increasing speed of embedded processors, less computation is necessary on computers. In the proposed control architecture, which is shown in Figure 3.4.1, the overall control is performed on a PC with a real-time operating system. This is where the balancing algorithm would be executed, the safety checks would be performed, the user interface would be run, and the desired joint positions would be calculated and sent to the BeagleBone microcontroller. The BeagleBone is a very power miniature computer that also has low-level I/O capability. This would be used to perform the high-speed control loops on the position of each joint and communicate with the motor drivers. The output of the potentiometers and force sensors would be read by an Arduino microcontroller on each leg, which would then transmit the sensed data back to the computer. The distributed control would keep the computation demand low on each component. Serial communication would be used for the transmission of data between devices. Although parts of this control system have been tested, the full implementation is outside the scope of this work.

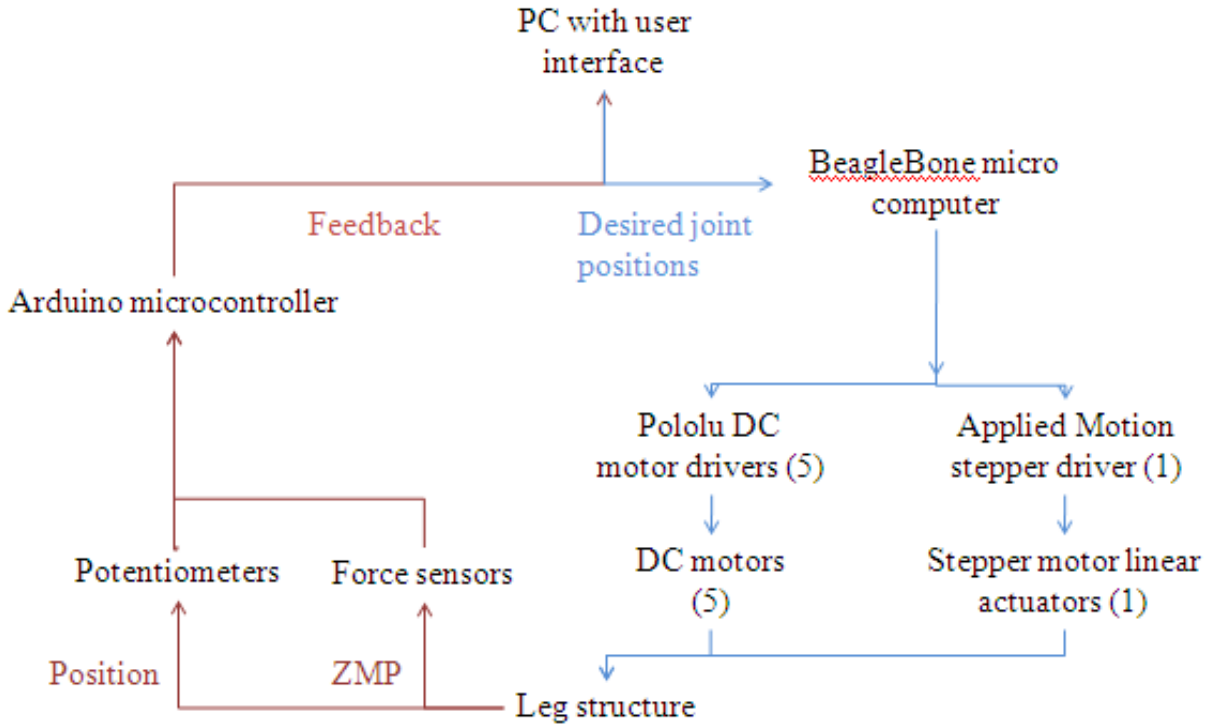


**Figure 3.4.1. Control structure for one leg. The same PC and BeagleBone microcontroller would be used for both legs, but the remaining components would be duplicated.**

## 3.5 Balance Simulations

In order to begin developing control equations for the legs, a Simulink simulation was developed to model the system dynamics. The SimMechanics package is used to model multi-body mechanical systems in the Simulink environment. This handles the kinetic computation for the model and includes blocks for friction, gearing, damping, and many other mechanical properties in addition to the capabilities of Simulink. The joint blocks allow torques, positions, velocities, or accelerations to drive the movement. A sagittal plane model (viewed from the side) was created for initial simulations with each leg consisting of three joints—hip, knee, and ankle pitch. The model was driven by supplying the joint angles at each step in time. A visualization window was included that allowed the movement to be observed in three dimensions. The simulation tracks the torque output of each joint as well, so that during a prescribed movement, evaluation can be performed to determine if a parameter limitation has been exceeded. The right

foot is always rigidly connected to the ground, so only one gait cycle can be modeled. Figure 3.5.1 shows images of the model during a simple walking gait with a step time of two seconds and a step length of 30 cm, and Figure 3.5.2 and Figure 3.5.3 show the joint angles and torques of each leg during the simulation.

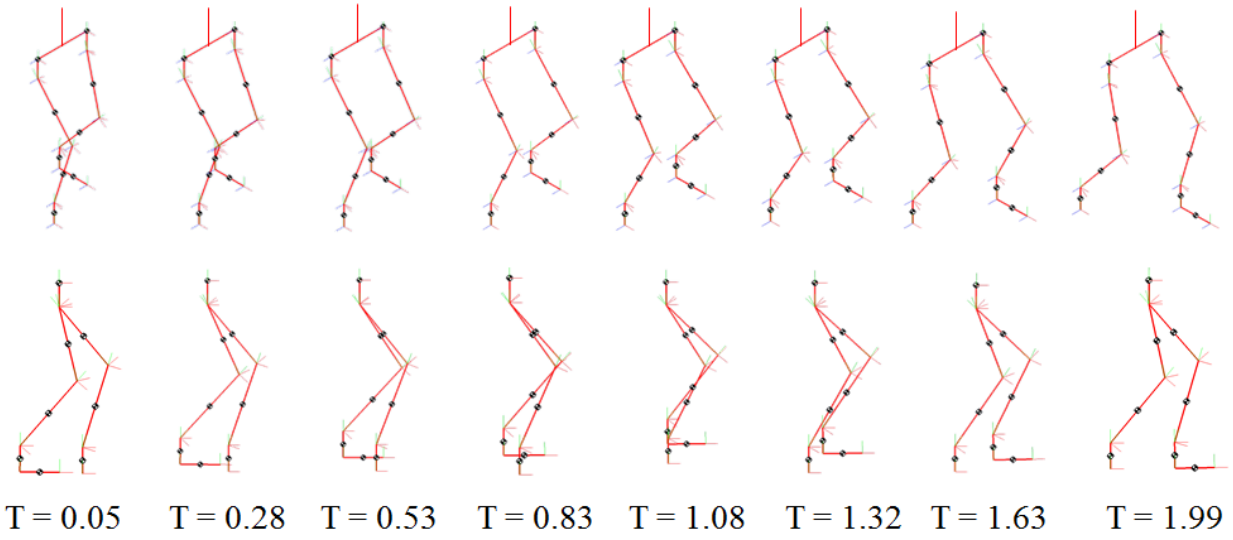


**Figure 3.5.1. Visualization from Simulink simulation. The motions are shown from both an isometric and side view at different steps in time, which are shown in seconds.**

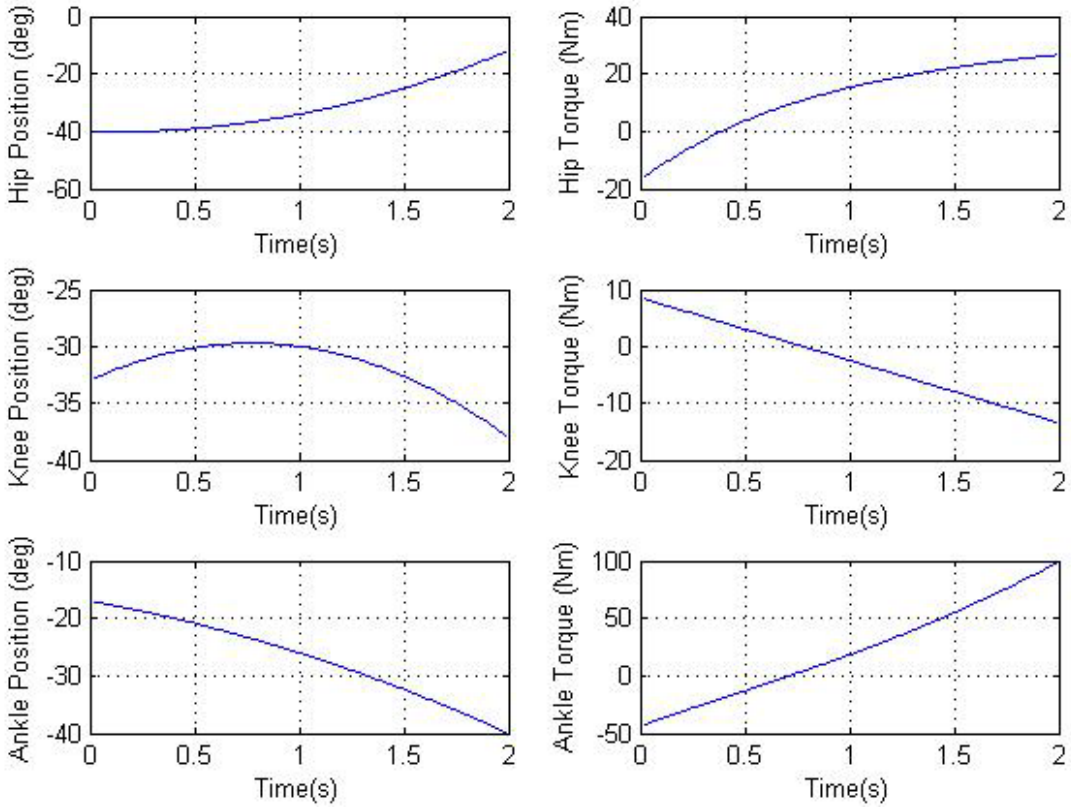


**Figure 3.5.2. Right leg angles and torques in simulation. In the model, the right leg is rigidly connected to the ground and is the loaded leg during the single support phase. This particular gait uses a very large amount of ankle torque and therefore would likely be refined to more evenly distribute the load.**

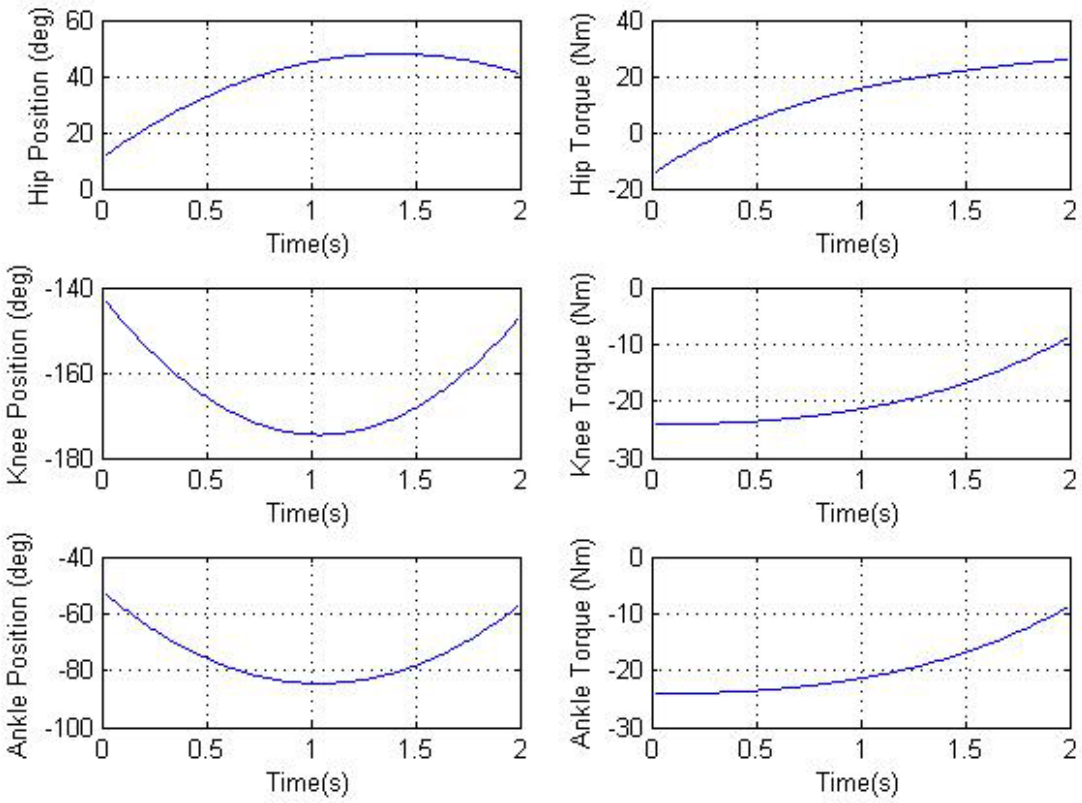


**Figure 3.5.3. Left leg angles and torques during simulation.**

This simulation will allow walking gaits of various forms to be evaluated before implementation on the robot. The computational power of Simulink would allow the simulation to be expanded to incorporate motor dynamics, friction in the gears, and the control algorithms to be used on the physical hardware. The legs are a nonlinear, unstable system that is heavy and could cause damage if it falls, so being able to model the performance of a controller before implementation is an important tool. The backlash in the gear heads also may complicate the control, and modeling this behavior would be the first step in decreasing its impact. Additionally, this model can be used to determine how modifications in future units hardware redesigns, such as different actuators or reduced weight, will impact the system performance.

## 3.6 Conclusions

In addition to the building of the robotic legs, a control architecture was developed to allow the robot to achieve locomotion. The motor drivers and position sensors were selected to reduce the cost and complexity using COTS components. A ZMP sensor was designed and an

algorithm for calibration was proposed, as was an overall electrical system for the future implementation of a balancing/ walking algorithm. As part of this next step, a software model of the legs was developed which can be used to test and evaluate various control methodologies.

# Chapter 4

# Servo Control of a Low-Cost Hydraulic Solenoid Valve

In the initial stages of the design of the legs, hydraulic cylinder actuators were strongly considered due to their high strength and power density. Because the legs must be able to carry the weight of the upper body, force output was one of the important considerations. A test system was designed to evaluate the appropriateness of hydraulics. A control system was developed to use an on/off solenoid as a servo valve for position control.

## 4.1 Introduction and Literature Review

### 4.1.1 Justification for Hydraulics

Hydraulic actuators have many advantages in robotics. The greatest advantages are their torque /mass and power/mass ratios, which are higher than electric motors (Hollerbach et al., 1992). They also offer the advantage of having the force created remotely by a pump generating pressurized fluid which can flow over a relatively long distance to the cylinder. The actual structure near the joint only has to bear the weight and size of the cylinder itself. Some small cylinders are also capable of providing high magnitude of force in a very small size, as in the system that will be described here. Hydraulic fluid is virtually incompressible which makes these systems faster than pneumatics and does not introduce compliance that can increase complexity (Hollerbach et al., 1992). The fluid also acts as a lubricant for the moving components.

However, there are some drawbacks to hydraulics as well. Leakage of the fluid can create complications when used with other electrical components and thus requires extra care in handling. Size within the robot can be an issue because a pump is required in addition to the cylinder, while electric motors only need the wiring to actuate. Depending on the work environment, filters may be necessary to maintain the fluid quality, adding weight and taking up

additional space. The lack of compliance in hydraulics can also be a drawback if the situation calls for an actuator that can handle sudden loads.

Hydraulic valves are known to be nonlinear and difficult to control (Chevallereau et al., 2009; Hollerbach et al., 1992). The valves typically incorporate an electrical solenoid that moves to change the fluid flow direction. Hollerbach et al. (1992) state that the "servovalves exhibit complex high-order, nonlinear dynamics, such as hysteresis of the electromagnetic valve element, variation of the orifice fluid-impedance with flow and fluid characteristics, change in orifice discharge coefficient with pressure ration, and sliding friction for spools" (p. 312). Although considerable gains have been made in valve control, the complexity along with leakage issues remain obstacles to be overcome for hydraulics to find acceptance in robotics.

The goal in this chapter was to demonstrate a low-cost, on/off electric solenoid valve as a servomechanism with position feedback. These components typically operate "bang-bang," meaning they are completely-on or completely-off. This presents difficulty in operation as the orifice opening cannot be controlled proportionally. Using a commercial off-the-shelf (COTS) solenoid valve may provide an option where higher level control is possible at a lower cost than more precise proportional servo valves. This also allowed the viability of hydraulic actuation to be evaluated for the leg design without significant financial investment.

### 4.1.2 Literature Review

Substantial research has been performed on the control of the position of hydraulic valves using various methods. Most of the control has been performed using servo valves (Niksefat & Sepehri, 2011; Wu, Sepehri, & Ziaei, 1998; Niksefat & Sepehri, 1999; Gamble, 1993; Šitum, Petrić & Crneković, 2003), which proportionally control the flow into the actuator. These valves are popular largely because common control methods such as PID can be used. The drawback is the typically high cost of these valves. Others have used on/off solenoid valves and performed pulse-width modulation, in which the valve is cycled on and off at a high rate at a varying duty cycle in order to act perform like a servo valve (Varseveld & Bone, 1997; Ahn & Yokota, 2005). This method is typically employed by DC motor drivers, but a major separation is that motor drivers use a low current signal to modulate, while hydraulic spools must overcome friction and internal pressure and therefore require significant energy for the switching. The switching time

also must be very fast to employ this method, which can drive up the valve cost. Other control methods use complex modeling of the system, but this requires in-depth knowledge of the valve parameters either from the manufacturer or from experimentation (Niksefat & Sepehri, 1999; Becan, 2007). Nguyen, Leavitt, Jabbari, and Bobrow (2007) developed a sliding mode controller without pulse-width modulation, but they also used an on/off valve with fast switching speed. No prior literature was found on controlling slow on/off valves for proportional control. Thus, this study provides a step towards developing low cost actuation system by addressing the control issues related to the slow on/off valves.

## 4.2 Directional Valve Characteristics

### 4.2.1 Valve Specifications

A basic hydraulic system is composed of four primary components - the pump, tank, directional valve, and cylinder, as shown in Figure 4.2.1. The pump is typically connected to a motor (electric or gasoline are most common) and pulls low pressure fluid from the tank and outputs a high pressure flow. The fluid then flows to a directional valve, which controls the path of the fluid that flows to the cylinder. The cylinder contains a piston that moves as fluid moves into either side A or side B, as shown in Figure 4.2.1. Cylinders come in two primary forms: single-acting, where fluid flows into only one side and is pushed out typically by a spring, and double-acting where fluid flows into one side and out the other at any given time. If fluid flows from the pump through the valve and into side A of the cylinder, then fluid would flow out back to the valve and then to the tank, and vice-versa. The tank serves as a reservoir for the fluid and is typically at atmospheric pressure to reduce the resistance in the flow from the valve.

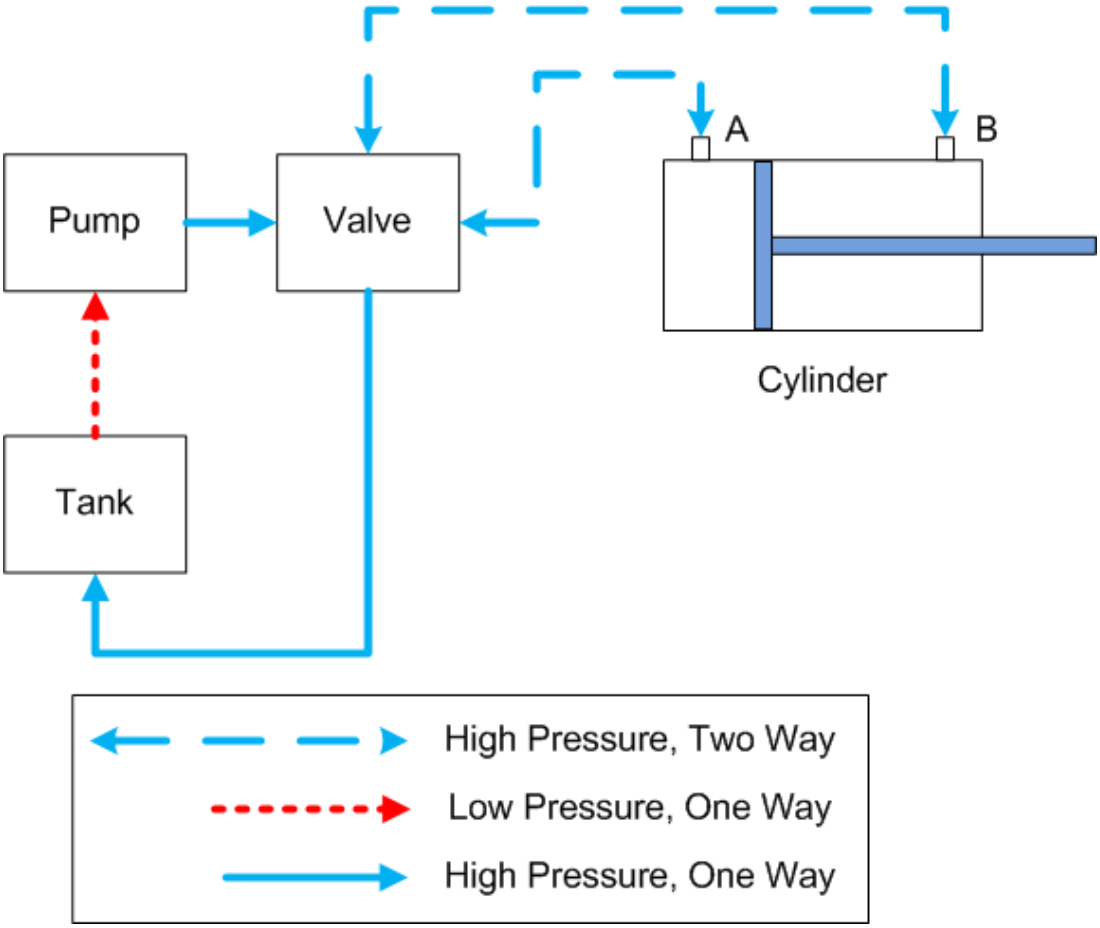


**Figure 4.2.1. Schematic of the basic hydraulic system. The large dotted lines indicate a high-pressure flow that can go in either direction. The small dotted lines indicate a low pressure flow that travels only in one direction. The solid lines indicate high pressure flow which travels in one direction.**

The goal of using a COTS valve to perform control led to the selection of a widely available direction valve from Northman Fluid Power. The specific valve chosen was the SWH-G02-C6-D12-10 model, which is a four-way, three-position tandem spring-centered spool valve. The four way means that fluid flows from the pump into the valve and then either back to the tank, to side A of the cylinder, or to side B of the cylinder. The three positions and the tandem refer to fluid flowing from the pump directly back to the tank but sides A and B are locked when in the center position, into side A and out of side B when in one on-position, or into side B and out of side A when in the other on-position. Figure 4.2.2 illustrates the flow path of this valve. When electricity is not applied to the solenoids, springs are used to center the spool, the moving

component which directs the flow. This valve is operated by applying a 12 volt DC signal to one of the solenoid coils, creating a magnetic field to move the spool. Table 4.2.1 summarizes some of the important parameters of the valve which were acquired from the Northman Fluid Power website (Northman Fluid Power. (n.d.).).

**Table 4.2.1. Reported valve parameters from manufacturer**

| **Parameter** | **Reported Value** | **Unit** |
|---|---|---|
| Weight | 2 | kg |
| Max Operating Pressure | 310 | BAR |
| Rated Flow Capacity | 50 | LPM |
| Maximum Frequencies of Operation | 300 | cycles per minute |
| Hydraulic Fluids Viscosity | 10-400 | cST |
| Temperature Range | -25 - +90 | ˚C |
| Rated Voltage | 12 | VDC |
| Voltage Range | +/-10% rated | VDC |
| In-rush Current | 2.2 | A |
| Holding Current | 2.2 | A |
| Switching On Delay | 0.02-0.06 | s |
| Switching Off Delay | 0.02-0.04 | s |

The high flow rate and operating pressure of this valve provides a large operating range, although plans for the study did not include coming close to these limitations. The frequency of operation refers to the rate at which the valve can be switched from off, to fully on in one direction, to fully on in the opposite direction, and finally off again. The valve was specified to turn on when 10.8-13.2 volts was applied. The switching on delay refers to the time required for the spool to move from the center off-position to completely on in one direction once voltage has been applied. The switching off delay refers to the time required for the spool to move back to the center once the voltage has been shut off. If the maximum delays were seen in operation, the valve would take 0.20 seconds to complete a cycle, coinciding with the 5Hz switching frequency. Figure 4.2.3 below shows the dimensions of the valve.

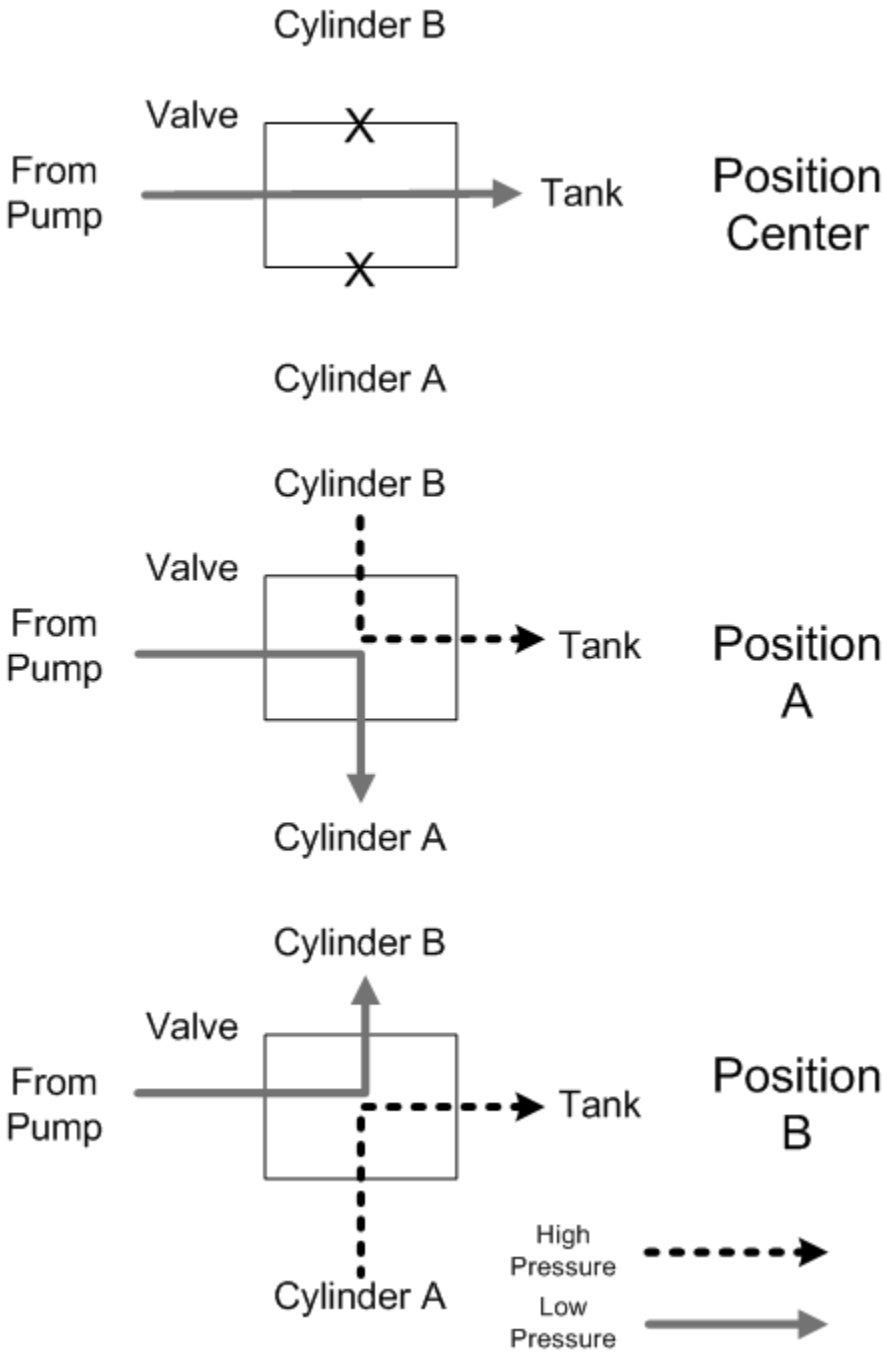


**Figure 4.2.2. Flow diagram for a four-way, three position valve.**

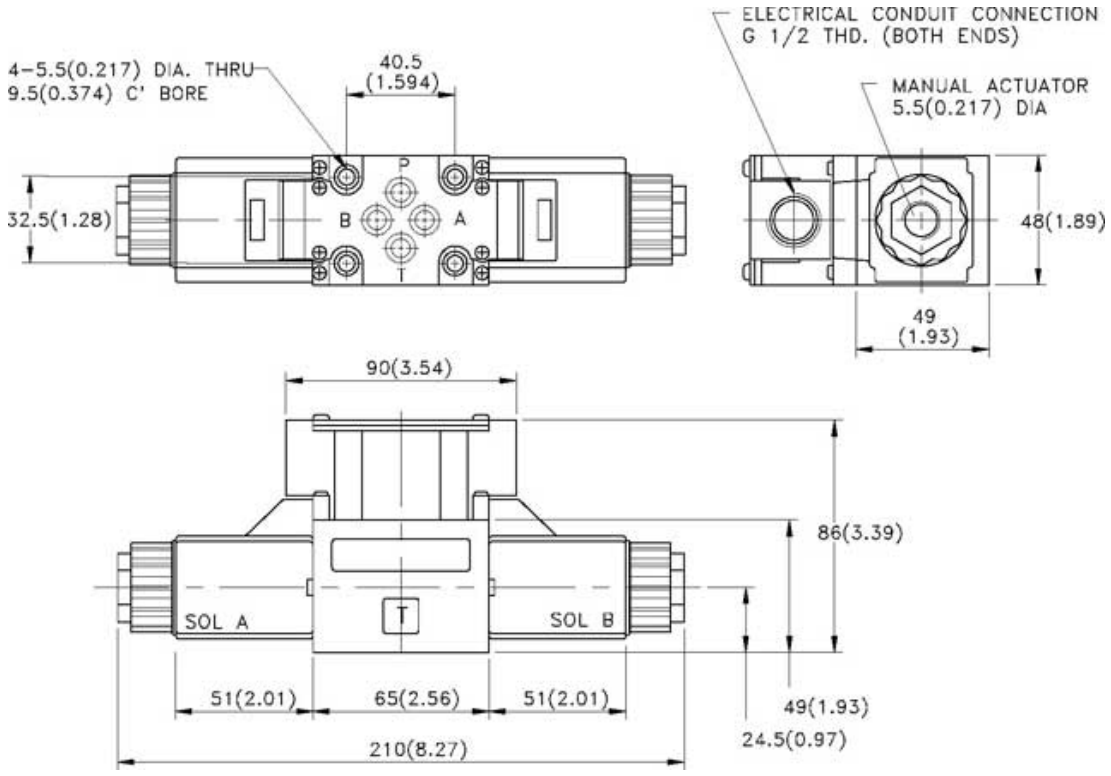


**Figure 4.2.3. Dimensions of the directional control valve. Figure was taken from (Northman Fluid Power, n.d.).**

## 4.2.2 Valve Operation

As previously mentioned, the valve uses a pair of solenoids in order to move the spool and control the flow. The solenoid itself is a wire coil which creates a magnetic field when energized. The field applies a force to the steel spool, and when the field strength is great enough it moves the spool and changes the direction of fluid flow within the valve. When the energy supplied to the solenoid is removed, the spring pushed the spool back to the center position. To change the fluid direction, the solenoid must overcome the force of the spring, friction between the spool and the rest of the valve, and the force of the fluid flowing through the valve housing. Figure 4.2.4 shows the forces involved in the movement of the spool.

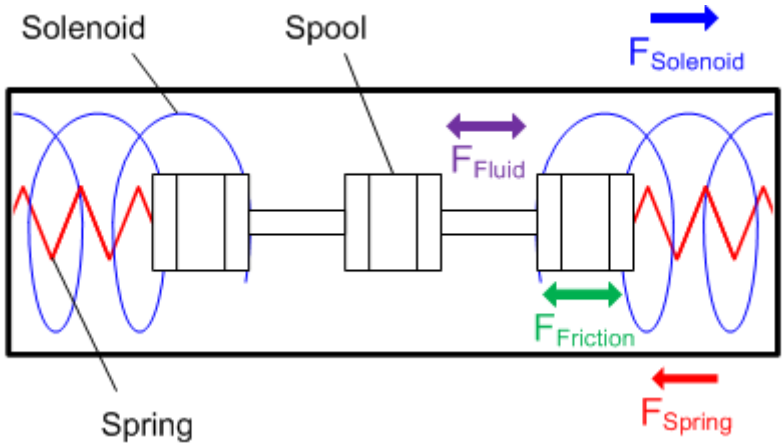


**Figure 4.2.4. Diagram of forces on valve spool.**

The manufacturer lists the valve as being on-off, meaning that the valve must be 100% open in one direction or the other or completely closed in the center position; it is not designed to be open any intermediate amount. The delays in opening and closing the valve, as previously mentioned, mean that one cycle from closed to open to closed could take as long as 0.1 seconds, limiting the sped of operation of the valve. When the valve is open, the speed of the piston will be directly proportional to the flow rate into the directional vale. Therefore, a slow closing time would have the potential to limit either the accuracy of positioning or the usable flow rate. As a result, three methods of improving the valve control were proposed to meet the goal of developing a position control system:

1. Can a proportional range of operation for the valve be found and used for control?
2. Can the switching speed be increased?
3. Can the dynamics of the valve after it has been shut off be predicted well enough to accurately control the valve position?

If a proportional range could be found, then more conventional control methodologies could be implemented. This would mean that over some input range, the valve can be made to open a varying amount depending on the input power. If such a range cannot be found, then the ability to increase the valve speed would be investigated. With high enough speeds, pulse width modulation (PWM) could be attempted. If it is found that the performance of the valve cannot be modified, then the task would turn to controlling the piston movement based on knowledge of the valve behavior, where the valve could be turned off at the right point to achieve the desired

position. This method is limited by the repeatability of the system dynamics and the quality of the model of those dynamics, the sensory feedback available, the fluid flow rate (and therefore the piston speed), and the acceptable steady-state error.

## 4.3 Test System Development

In order to evaluate the directional valve, a test system was constructed to control a robotic joint. The mechanical design featured a coupled two-joint system using a four-bar mechanism. The hydraulic system used all commercial components that allowed for flexibility in parameter design. Several different position feedback sensors were evaluated before a linear potentiometer was finally chosen.

### 4.3.1 Mechanical Design

Because the goal was to determine if the hydraulics were a viable option for actuation in the leg design, a simple joint was chosen as the basis for a hand-like design rather than developing a leg which would introduce the complexity of a balancing. The central component to the mechanical design was the cylinder. High force output was desired for a small length and diameter, so a custom short-stroke cylinder from Mack Corp was selected because of the high pressure rating (10.3 MPa) and the custom stroke length. The line of pistons with the smallest diameter was chosen, and a kinematic model was used to determine the desired stroke length of the piston.

#### 4.3.1.1 Kinematic Model

The model of the joint allowed the force output, speed, and possible stroke lengths to be varied to find the joint lengths and stroke length. Figure 4.2.5 shows the simplified geometry of the proposed joint. The finger would be attached to a base, as would the cylinder itself. The length of the cylinder body was dependent upon the stroke length of the piston, which was available in 0.254 cm (0.1 in) increments. The desire of using this model was to find the necessary extension length of the finger, or "*a*" in Figure 4.2.5, and the required stroke length, "s".

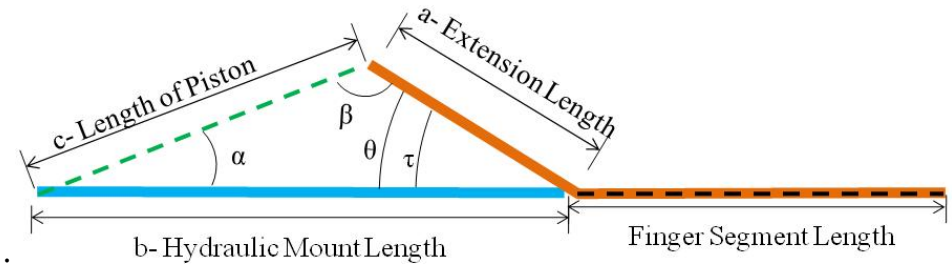


**Figure 4.2.5. A sketch of the finger components. The orange line is the finger being designed, while the light blue line is the length from the finger rotation point to the cylinder attachment. In this diagram, the piston is at the minimum length, $c_{min}$.**

As the extension length *a* increases, the length of the piston increases more quickly, as described by the law of cosines in Equation 4.2.1.

$$c^2 = a^2 + b^2 - 2 * a * b * \cos(\theta) \quad \textbf{4.2.1}$$

where "*b*" is the mounting distance of the piston, or the distance where the piston connects to the previous joint and the pivot point. However, as "*c*" gets longer, the hydraulic piston must also have a longer stroke length in order to allow the finger to make a full 90° rotation. The stroke length was found by using Equation 4.2.2:

$$s = c_{max} - c_{min} \quad \textbf{4.2.2}$$

where "s" is the stroke, "$c_{max}$" is the length of c at a 90° bend, as in Figure 4.2.5, and $c_{min}$ is *c* when the finger is completely straight, as in Figure 4.2.6. The length of the actual piston is dependent upon the stroke length, as seen in Figure 4.2.7 and in Equation 4.2.3:

$$c_{max} = 2s + r \quad \textbf{4.2.3}$$

where "*r*" is the base length of the hydraulic not including stroke.

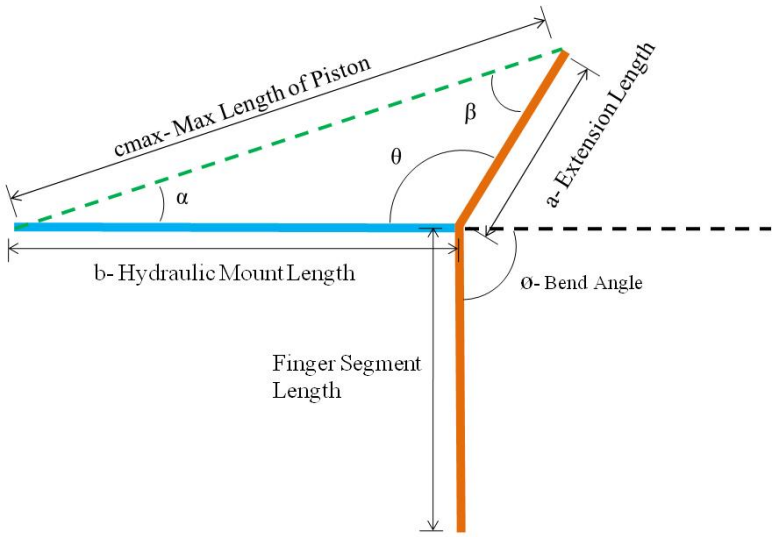


**Figure 4.2.6. The finger is fully bent at 90°. Angle $\phi$ represents the bend angle from horizontal. In this position, the piston would be fully extended.**

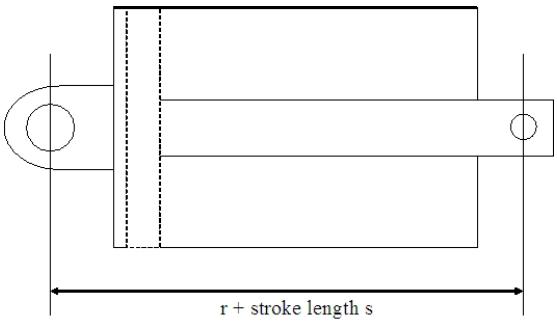


**Figure 4.2.7. A sketch of the hydraulic piston fully retracted. The fully retracted length is the set length *r* plus the length of the piston.**

The model was designed to always produce the maximum force at a 45° bend by adjusting *b*, as *a* was varied. The joint segment length was chosen to be 10.2 cm (4 in). The design also had to minimize *a* because the thickness of the joint, the vertical direction in Figure 4.2.6, increases proportionally to the length of *a*. Therefore a mounting distance of 9.4 cm was chosen to achieve a stroke length of 2.03 cm (0.8 in) and an extension length of 1.44 cm, which led to the selection of the S6558-(8)-LS cylinder from Mack Corp. The datasheet for the cylinder can be seen in Appendix D. Table 4.2.2 shows some key dimensions of the cylinder.

**Table 4.2.2. Summary of cylinder geometry**

| Parameter | Value | Unit |
|---|---|---|
| Piston diameter | 19.05 | mm |
| Stroke | 20.3 | mm |
| Retracted length | 82.6 | mm |
| Extend area | 276 | mm^2 |
| Retract area | 178.7 | mm^2 |
| Extend volume | 5.61 E -3 | L |
| Retract volume | 3.63 E -3 | L |

#### 4.3.1.2 Four-bar Mechanism

After the geometry had been determined, the segments of the hand were designed. Because only one joint limits the functionality, the original design was to have two individually-actuated joints, with the desired to have three linkages total in the shape of a large claw-like structure, as seen in Figure 4.2.8. However, due to the complexity of the valve control and the cost of six cylinders, the design was modified to only actuate the first joint for testing and use a crossed four-bar mechanism to actuate the second segment. The finalized mechanism can be seen in Figure 4.2.9.

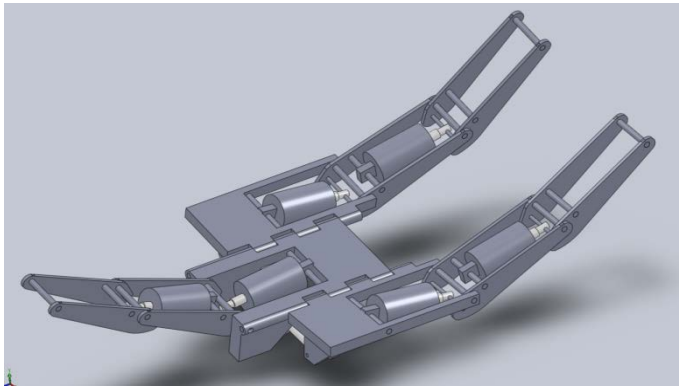

**Figure 4.2.8. Completed original design of hand with six cylinders.**

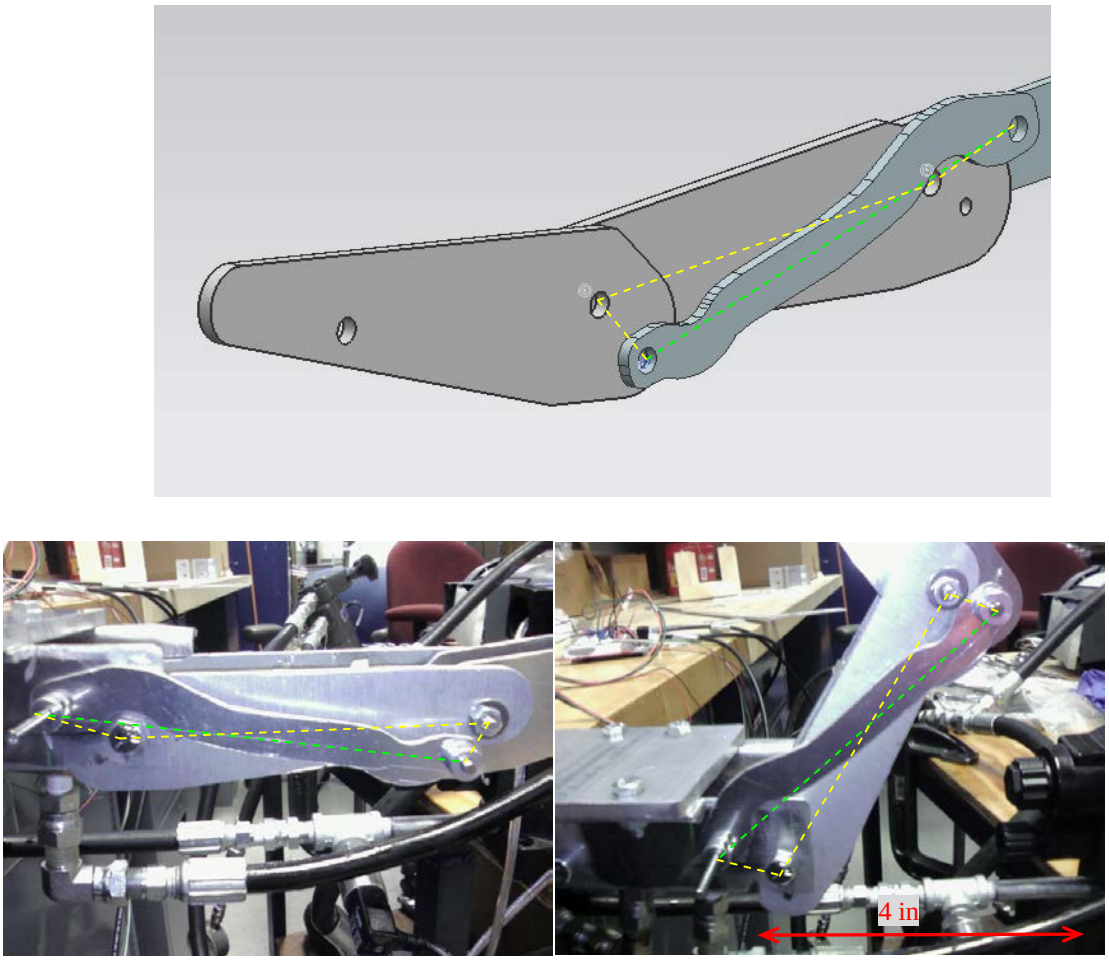


**Figure 4.2.9. Four-bar mechanism in joint. The kinematics of the four-bar were designed such that the following (second) joint would reach a 90 degree bend angle at the same point as the leading (first) joint. The yellow dotted lines show the static bars while the green line shows the crossing bar.**

### 4.3.1.3 Sensor Selection

To perform the position feedback, several different sensors were evaluated to measure the bend angle of the joint. Because the two joints were coupled, only the angle of the first joint was measured. The first sensor evaluated was the STRX-02 Flex Stretch Sensor by Images Scientific Instruments, which is composed of a special material with a resistance that increases when strained. Figure 4.2.10 shows the sensor mounted on the joint. The benefit of these sensors is that they are simple varying resistors that allow for simple integration into a system. However, the

manufacturer states that the sensor exhibits hysteresis and does not immediately return to the starting resistance when the sensor is relaxed and may temporarily remain as much as 10% above the starting value, but specific time response was not supplied (Image Scientific Instruments, 2013). Because of the slow operation of the valve, the stretch sensors were tested despite the hysteresis. The resistance was found to change linearly when strained, as seen in Figure 4.2.11. The time response was found to be much less acceptable, as shown in Figure 4.2.12. The sensor did not return to its original relaxed resistance in over 80 sec and thus was eliminated from consideration.

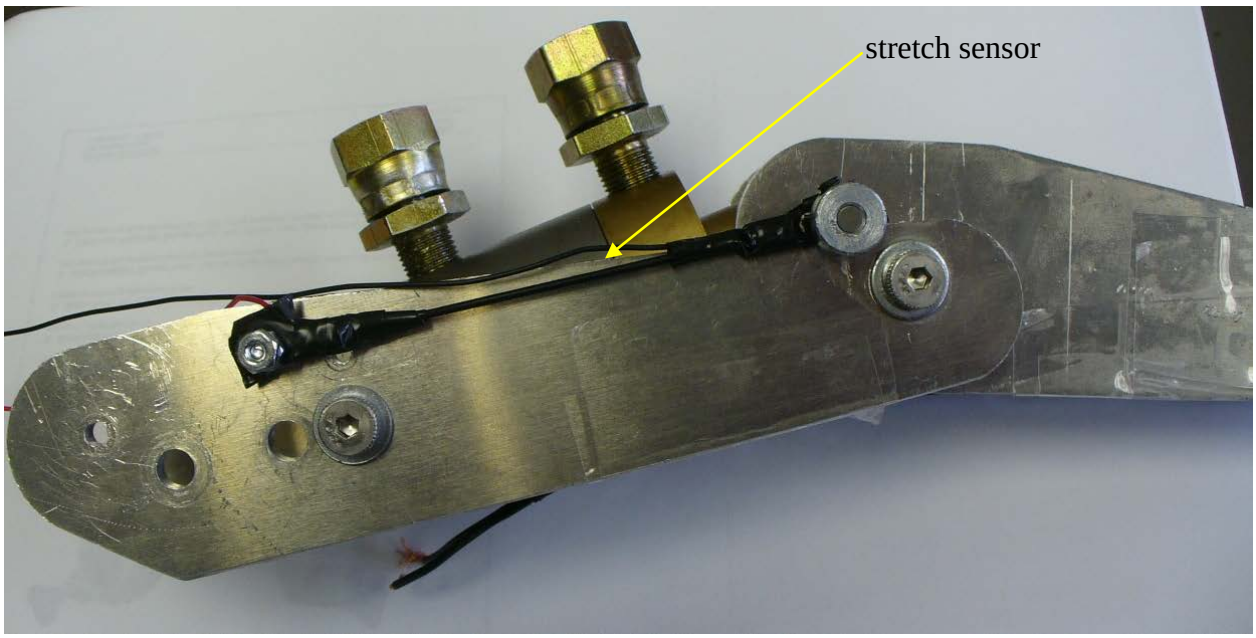


**Figure 4.2.10. The stretch sensor was attached on the outside of the joint. The ends were covered in electrical tape to prevent them from contacting the metal joints.**

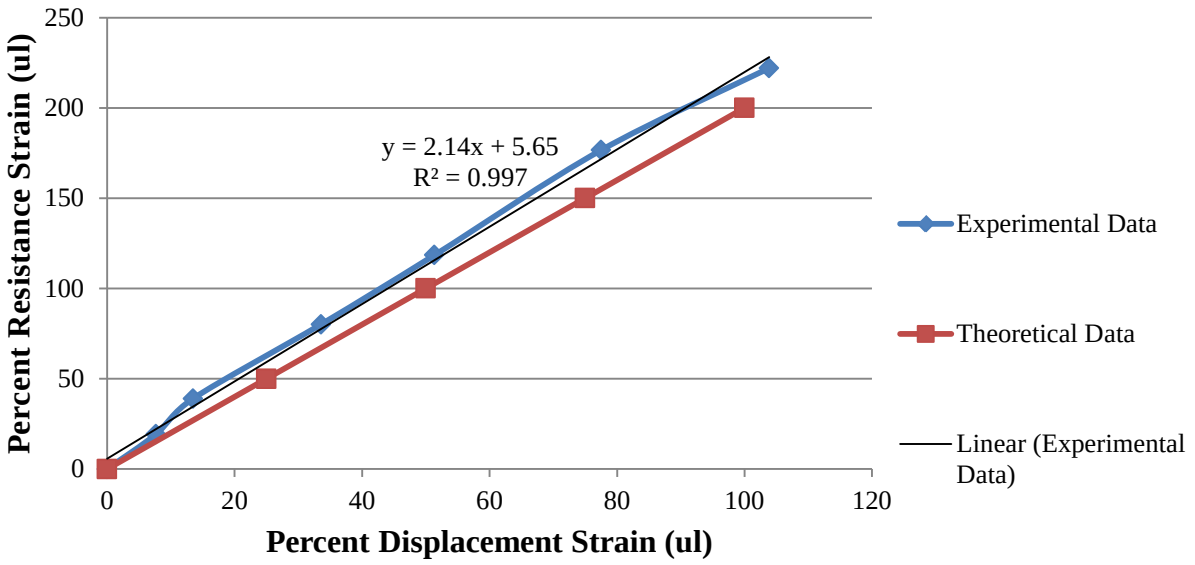


**Figure 4.2.11. Strain test of the stretch sensor. The y-axis shows the resistance strain, which is the change in resistance divided by the original resistance. The manufacturer claims that the resistance doubles when the length is stretched to 150% of its original length (Image Scientific Instruments, 2013), which was used as the theoretical sensor response.**

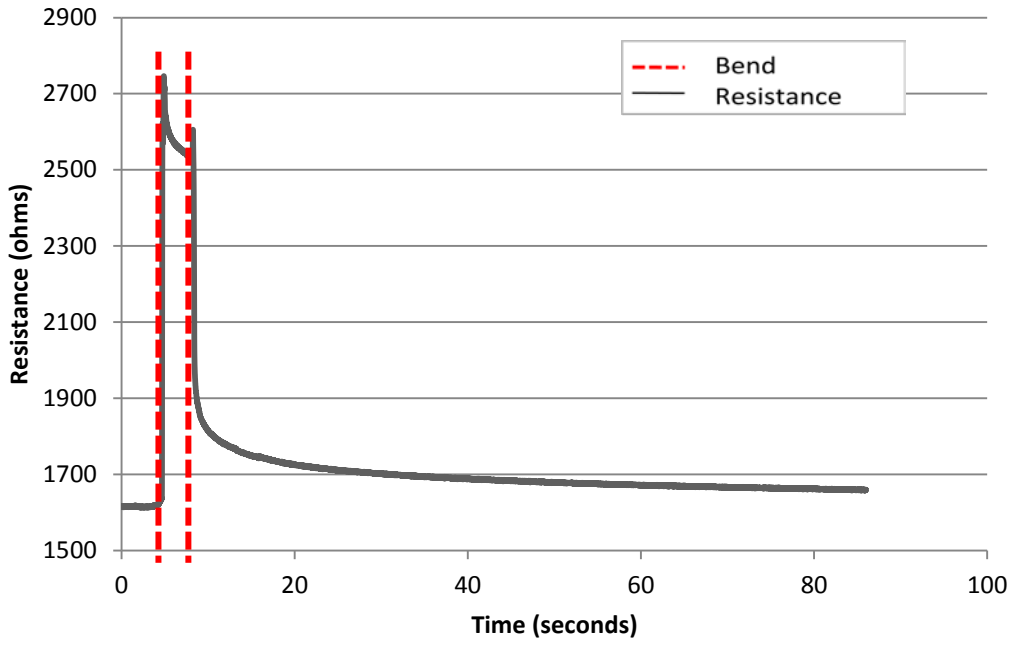


**Figure 4.2.12. Time response of the stretch sensor. The joint was bent from completely straight to completely bent and back. The approximate time of when the joint was bent is shown by the first dotted line, and the approximate time of retraction is shown by the second dotted line.**

The next sensor that was evaluated was a string potentiometer. The potentiometer is made up of a conventional potentiometer with a spring and string attached. As the string is pulled, the shaft of the potentiometer is rotated and the output voltage changes. Two main issues were found with the sensor. First, because the stroke length of the sensor was greater than 15 cm, but only about 20 mm of the stroke were being used. This made the change in sensor output very small and noisy through the range of motion. Second, the string pot was very large and expensive. While this sensor would work in a test apparatus for one joint, it was too large for use in a practical system and it was not financially viable to use on more than one joint. However, during the initial testing the string potentiometer was used.

The final sensor evaluated was a slide potentiometer. These linear sensors are both inexpensive and simple, as their movement provides a change in resistance. Many precision models were considered that would have been very rigid and had a high life cycle, but a less expensive potentiometer was chosen due to the nature of the project to achieve a cost-effective

system. Figure 4.2.13 shows the potentiometer mounted onto the joint. This sensor is linear and has no hysteresis and was connected with rigid bar to the first joint segment.

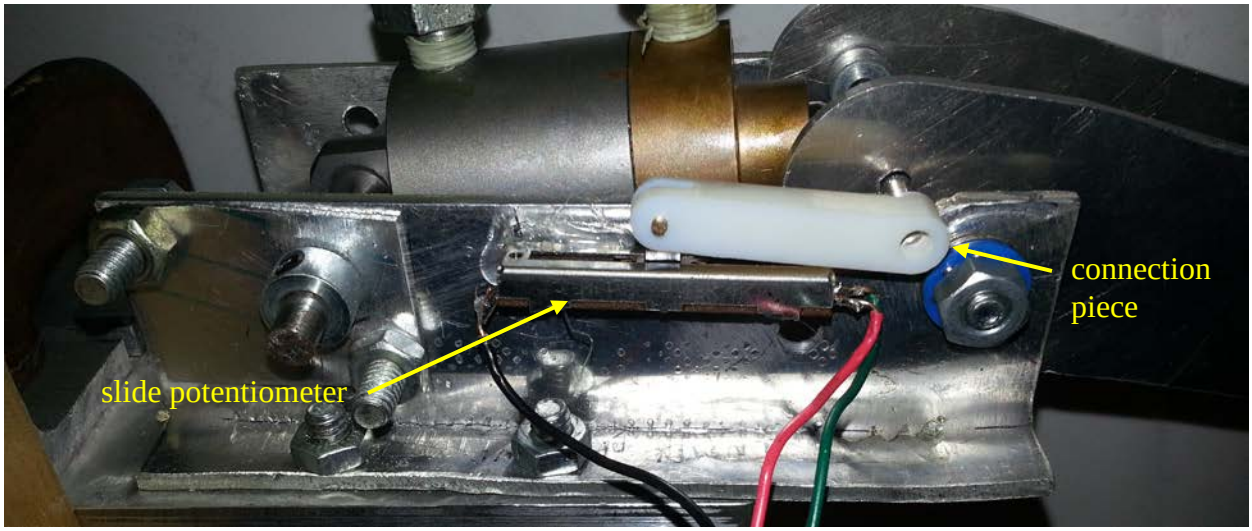


**Figure 4.2.13. Slide potentiometer attached to the joint. A rapid prototyping machine was used to create the connection piece. Because the sensor saw little loading, it is glued in place.**

## 4.3.2 Hydraulic Design

In addition to the mechanical components, the hydraulic system was developed to evaluate the directional valve and hydraulics as a whole. A combined tank-motor-pump system was used to supply flow, a variable pressure regulator was used to control the pressure, and a variable flow control valve was used to adjust the flow rate. A pair of manifolds was used to distribute or control flow. Although the testing was only performed on one actuator, the system was designed to allow expansion to multiple cylinders in the future.

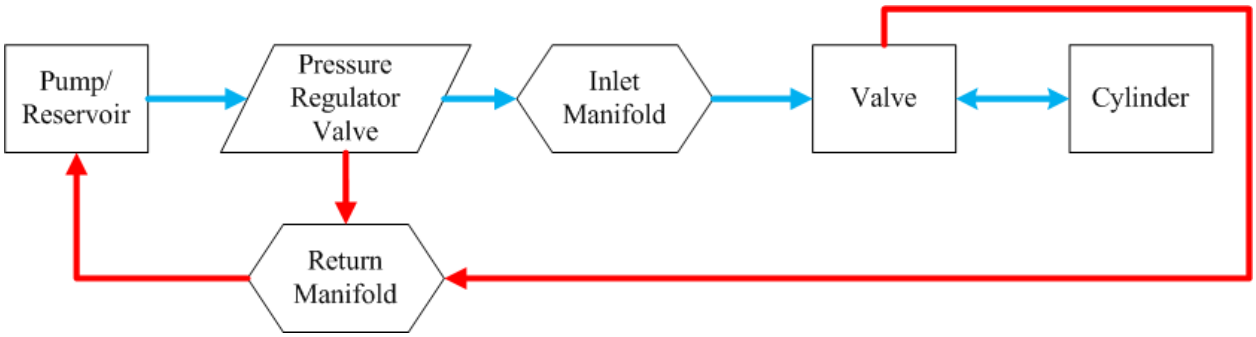


**Figure 4.2.14. Schematic of the hydraulic system.**

The tank-motor-pump system from Bucher Hydraulics (model M-4304) was chosen because of its simplicity. It is rated at 3.5 LPM flow rate and 20.7 MPa pressure. With the cylinder chosen, the pump nominally outputs 16 times of the cylinder retract volume per second, which would be far too fast to control. For this reason, two other components were incorporated in the system. Because the output pressure of the pump was higher than that desired for initial testing, the PRV-T03 pressure regulator made by Northman Fluid Power was included. This has an internal valve that directs fluid to the return manifold to maintain the desired pressure. The output is adjustable from 0.69-3.45 MPa (100-500 psi). Most of the testing was done at the lowest pressure. To adjust the speed of the piston movement, the flow rate was adjusted by using the MT-02W-K flow control valve made by Northman Fluid Power. Each side of the valve is individually adjustable, meaning that the flow to each side of the piston can be altered independently, which is important because the piston does not have the same volume on each side due to the piston shaft. Although the pressure regulator does decrease the flow rate, the pump output is still high enough that it would make control very difficult without this flow control valve. For safety purposes, the BioFlo FG by BioBlend hydraulic fluid was used because it is food grade and biodegradable. Its specific gravity is 0.913 and its kinematic viscosity is 46 cST at 40˚C.

## 4.4 Control Design

As previously stated, three questions were considered for developing a method for controlling the directional valve to achieve the best possible performance, progressing from a high amount of control authority to a low amount of authority. The first question deals with finding a proportional range of the valve, the second with increasing the switching speed, and the

third with predicting accurately the valve dynamics in order to control the position. To implement any scheme, the electrical circuitry had to be developed to address each of these three questions. Then the valve was tested to evaluate which, if any, control method could be applied. Throughout the whole process, the desire remained to perform the control with only joint position feedback rather than adding other types of sensors to measure parameters such as pressure or flow to reduce cost and maintain relative electrical simplicity. An additional simplification was that the flow control valve was used to significantly slow the volumetric flow rate leaving the directional valve to the sides of the cylinder. Both sides were adjusted to approximately the same speed- which means that the side of the cylinder with the piston rod would receive less flow due to the smaller volume. The pressure entering the directional valve was maintained at 100 psi.

### 4.4.1 Electrical Circuit Design

To implement the control, the electrical circuitry had to be developed. Since each side of the valve has its own solenoid to apply force on the spool, the current applied was individually controlled. During initial testing, an Arduino Mega 2560 microcontroller was used with a pair of MOSFETs to direct the electricity, as seen in Figure 4.2.15. Digital signals from the microcontroller were used with pulse-width modulation (PWM) to change both the direction and effective amplitude of the current flow into the solenoids. However, the resolution on the duty cycle was limited to 8-bits, and therefore did not provide a fine enough range to evaluate if a proportional range was existent over voltage changes less than 0.39 volts with a 10 volt power supply. The PWM frequency was only 470 Hz and presented a concern, as typical motor controllers are more than an order of magnitude faster, although no tests were conducted to evaluate the frequency's impact. An additional issue was seen when attempting to read the analog sensors previously mentioned, which may have been due to the microcontroller ground being connected to the power supply ground.

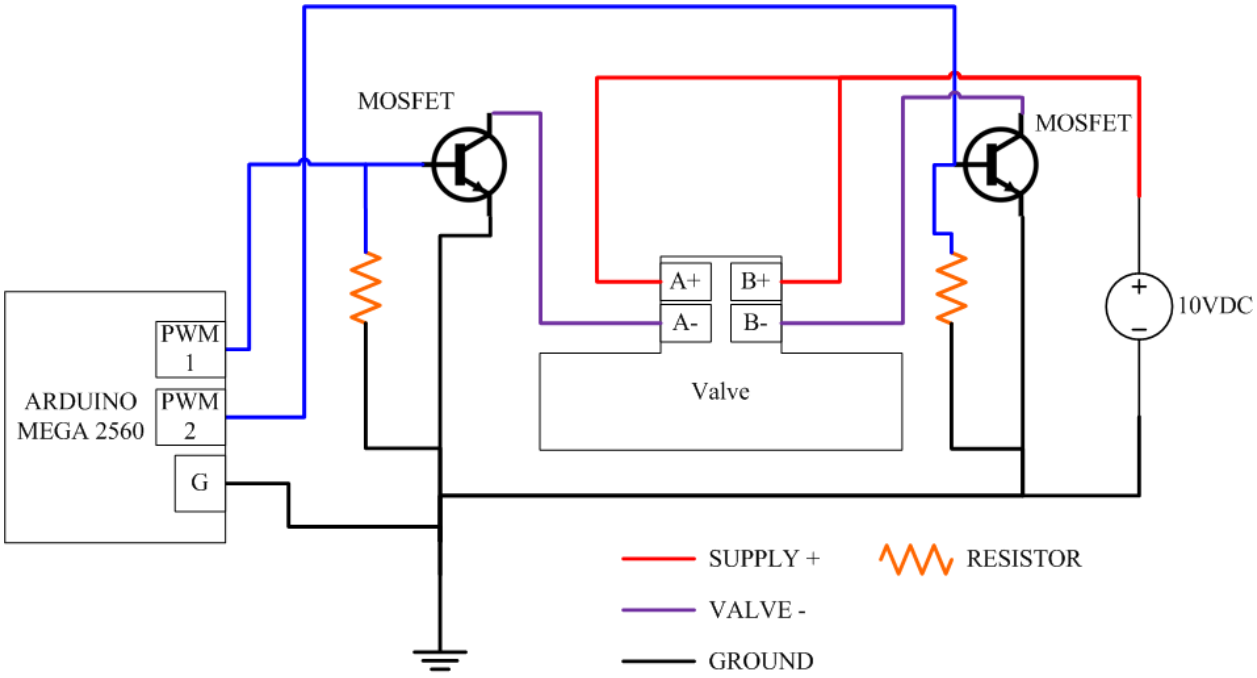


**Figure 4.2.15. First electrical circuit diagram. An Arduino Mega 2560 microcontroller was used to control a pair of NPN MOSFET transistors using a PWM output. The PWM signal sent to each transistor pulses at a frequency of approximately 470 Hz to control the voltage into the valve. The resistor is necessary to prevent a short. The grounds of the digital and power were connected.**

The second circuit that was developed replaced the MOSFETS with a pair of Pololu Simple Motor Controllers to control the output voltage, as seen in Figure 4.2.16. The same microcontroller was used, but delivered serial communication to control the output. The resolution of the Pololu controllers was approximately 11-bit each direction of current flow, although only one direction output was used. An input command range of 0-3200 corresponded to 0 volts to the input voltage. The PWM frequency was also significantly higher than the first circuit at 22 kHz.

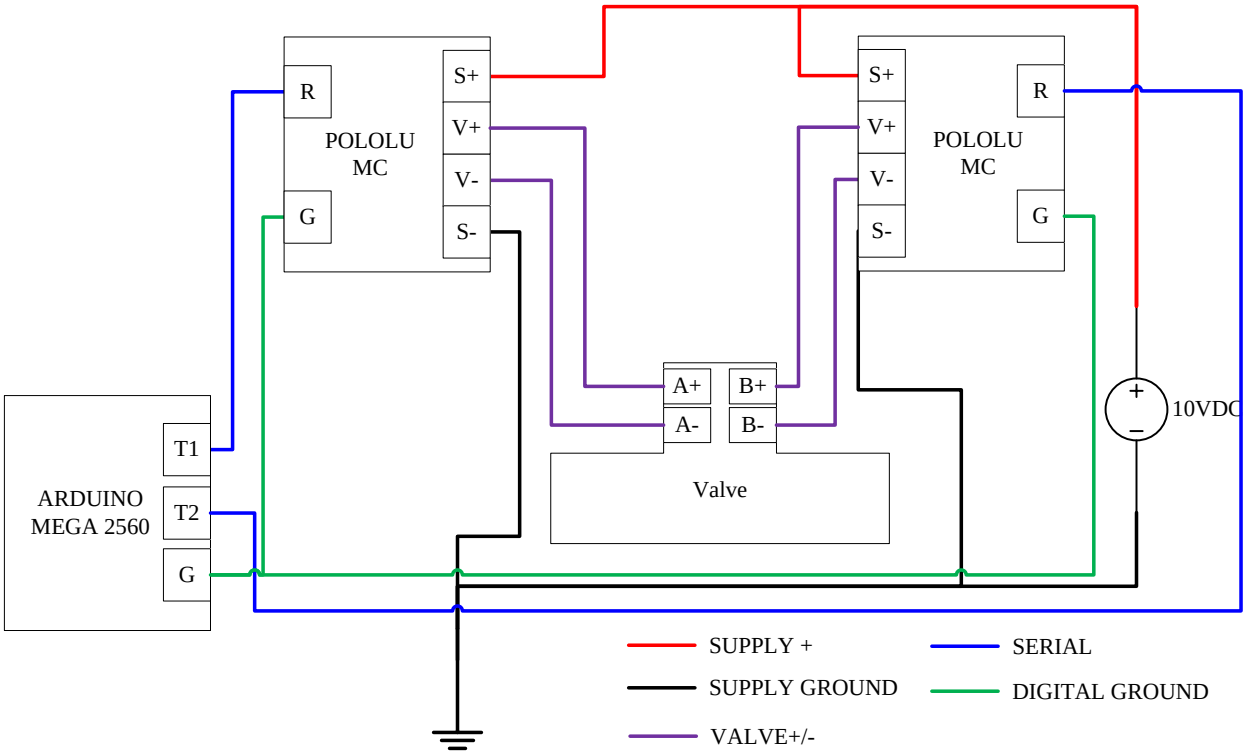


**Figure 4.2.16. Second electrical circuit diagram. The Arduino Mega 2560 microcontroller sends TTL serial commands to the two Pololu motor controllers (MC). Each controller is connected to the power supply. The MC then outputs a voltage to the valve in accordance to the command received from the Arduino. The digital and power grounds were not connected.**

The feedback of the control system was implemented on the Arduino microcontroller as well. Figure 4.2.17 shows the flow of signal transmissions in the system.

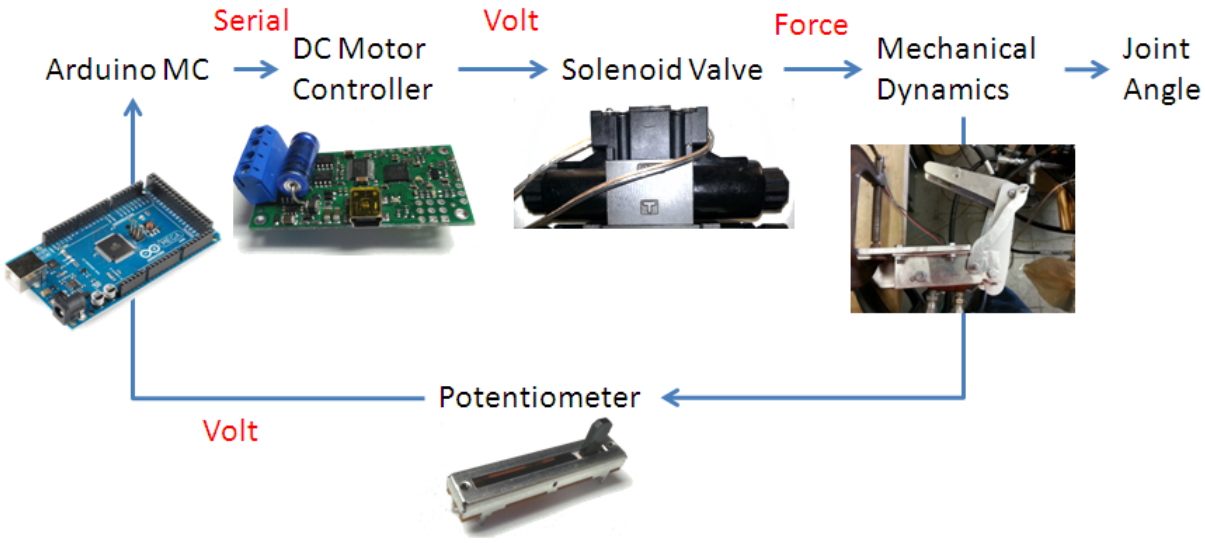


**Figure 4.2.17. Flow chart of information in the control system.**

## 4.4.2 Switching Time Testing

Once an effective electrical system was developed, the first two controls questions were tested together. First, the minimum voltage (On-Voltage) required to open the valve was tested, as initial testing seemed to show that the valve opened only after a threshold was met. Although fairly consistent results were seen, the On-Voltage did have some variability, as seen in Table 4.2.3and in Figure 4.2.18

**Table 4.2.3. Testing the on-voltage of each solenoid**

| **Test** | **1** | **2** | **3** | **4** | **5** | **6** | **7** | **8** | **9** |
|---|---|---|---|---|---|---|---|---|---|
| Sample Period (ms) | 20 | 20 | 50 | 50 | 50 | 50 | 500 | 500 | 500 |
| Solenoid 1 On-Voltage (volts) | 7.684 | 7.619 | 7.550 | 8.072 | 7.694 | 7.622 | 7.628 | 7.716 | 7.572 |
| Solenoid 2 On-Voltage (volts) | 5.566 | 5.559 | | | 5.650 | 5.669 | 5.638 | 5.569 | 5.541 |

Note: Results of the on voltage for solenoid 2 on tests 3 and 4 were not conducted.

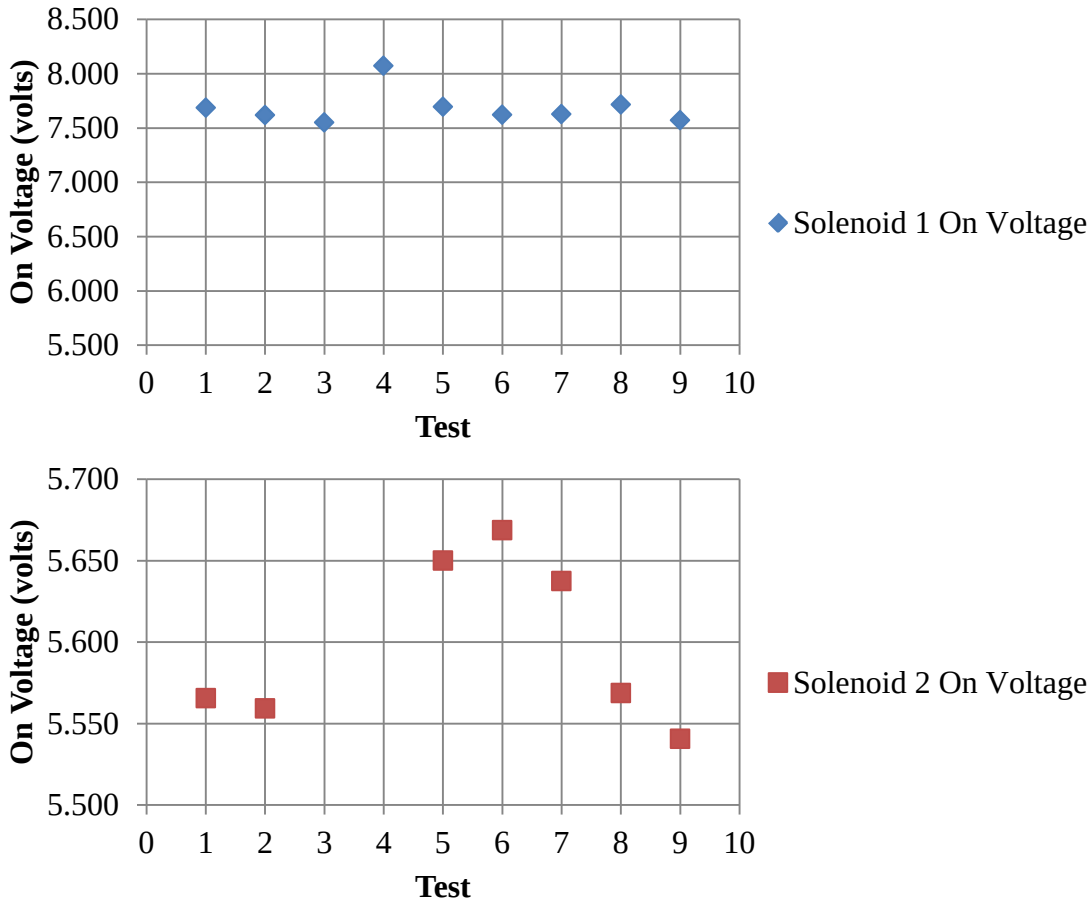


**Figure 4.2.18. Solenoid on-voltage.**

In order to evaluate the proportional range, testing was performed on the difference in joint speed when the valve had a voltage just above the threshold compared to when it received maximum voltage. The speed difference was not significant enough to conclude that a usable proportional range exists. Therefore, further testing of a proportional range was not conducted and attention shifted to increasing switching speed.

Using the previously examined On-voltage approximation, a series of tests were performed to determine if a method to speed up the valve switching could be implemented. It was theorized that if the solenoid was pre-loaded close to that threshold it would turn on more quickly since the valves only turn on when the threshold is crossed. Similarly, if the voltage was just above the threshold to turn the valve off, it would turn off more quickly. If the methodology proved to be effective, the pre-load could always be applied to increase switching speed at the cost of continuously applying energy.

The time delay between when the voltage changed to when the joint began to move was measured for three scenarios. Each scenario was tested for turning the valve on and turning the valve off. The valve was considered on as soon as movement was measured by the position sensor. Since the valves were designed to function on-off, the first test was used as a baseline and applied zero volts and then the max voltage. The second test consisted of first applying an offset voltage just below the On- Voltage thresholds in the open tests and just above the Off- Voltage threshold in the close test, and then applying the maximum voltage. The final test also applied an offset, but then applied a voltage just beyond the threshold. Table 4.2.4 shows the parameters used and results for the voltage used to open the valve while Table 4.2.5 shows the same for turning off the valve. The current was also measured throughout each test.

**Table 4.2.4. Testing of time required for valve to open using voltage offsets**

| | **Zero- Max On** | **Below Threshold- Max On** | **Below Threshold- Above Threshold** |
|---|---|---|---|
| **Start Voltage** | 0 | 6.875 | 6.875 |
| **End Voltage** | 10 | 10 | 7.750 |
| **Total Average for Pos Delay** | 0.25 | 0.23 | 0.38 |
| **StDev** | 0.018 | 0.027 | 0.053 |
| **St Dev %** | 7% | 12% | 14% |
| **Number of Tests** | 8 | 6 | 11 |

As theorized, pre-loading the valve with a voltage below the threshold did show the quickest switching time, but was very close to the switching time of the zero-to-max tests. These were approximately within one standard deviation for each test of one another, and the sample period was 0.02 seconds. The slowest switching time was seen in the final test, which was significantly slower and was less repeatable.

**Table 4.2.5. Testing of time required for valve to close using voltage offsets**

| | Max On- Zero | Above Threshold- Zero | Above Threshold- Below Threshold |
|---|---|---|---|
| **Start Voltage** | 10 | 3.531 | 3.531 |
| **End Voltage** | 0 | 0 | 3.297 |
| **Total Average for Pos Delay** | 0.16 | 0.13 | 0.18 |
| **Total StDev for Test Type** | 0.019 | 0.021 | 0.035 |
| **St Dev %** | 12% | 17% | 19% |
| **Number of Tests** | 12 | 8 | 8 |

Testing was also performed when turning the valve off, and similar results were seen. The above threshold-zero test was again the fastest and very close to the delay for the max-zero case. However, the test around the threshold was much closer, within approximately one standard deviation of the max-zero test results. The cause of the delay's existence was investigated by looking at the current being pulled by the solenoid for each case. Figure 4.2.19 shows the current response to a step voltage input. The delay between the voltage change and when the current reached steady state was measured for each test, as shown in Table 4.2.6 and Table 4.2.7.

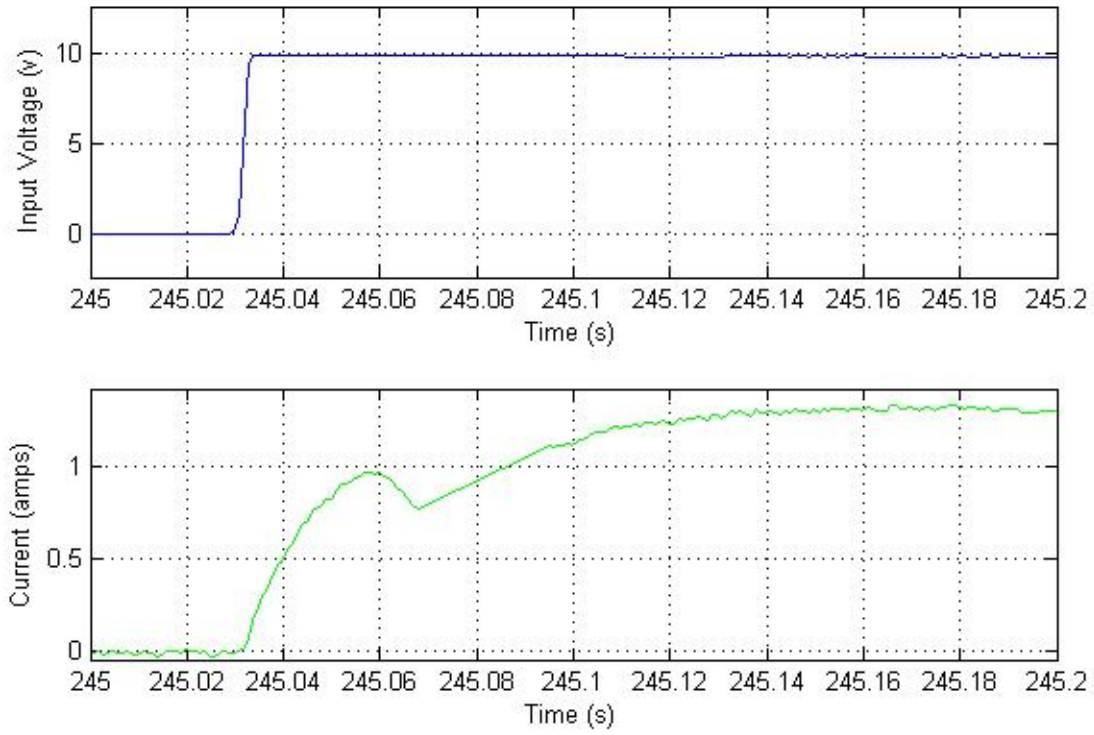


**Figure 4.2.19. The valve voltage and current response to a step voltage change. The current has a delay. The drop in current is seen for all tests except when the voltage was dropped to zero.**

**Table 4.2.6. Testing of current delay using voltage offsets when turning valve on**

| | **Zero- Max On** | **Below Threshold- Max On** | **Below Threshold- Above Threshold** |
|---|---|---|---|
| **Start Voltage** | 0 | 6.875 | 6.875 |
| **End Voltage** | 10 | 10 | 7.750 |
| **Total Average for Current Delay** | 0.10 | 0.07 | 0.23 |
| **Total StDev for Current Delay** | 0.013 | 0.010 | 0.033 |
| **St Dev %** | 13% | 14% | 14% |
| **Number of Tests** | 8 | 6 | 11 |

**Table 4.2.7. Testing of current delay using voltage offsets when turning valve off**

| | Zero- Max On | Below Threshold- Max On | Above Threshold- Below Threshold |
|---|---|---|---|
| **Start Voltage** | 10 | 3.531 | 3.531 |
| **End Voltage** | 0 | 0 | 3.297 |
| **Total Average for Current Delay** | -- | -- | 0.16 |
| **Total StDev for Current Delay** | -- | -- | 0.037 |
| **St Dev %** | -- | -- | 24% |
| **Number of Tests** | 12 | 8 | 8 |

The delay between the voltage change and the current steady state appeared to directly correlate with the position delay for the tests turning the valve on. The final test of below and above the threshold showed a significantly longer delay. When the valve was turned close and voltage dropped to zero, no current drop was seen because the current obviously could not drop anymore. However, a drop was seen in the test of above and below the threshold. As a result of all the tests on increasing the valve speed, it seemed that voltage pre-loading the valve did not have a significant impact on the switching speed. Because of the simplicity of controlling a system by applying either zero or maximum voltage, this method was used in further testing. Therefore, experiments to determine if the valve dynamics after voltage was removed could be predicted were conducted.

## 4.4.3 Valve Dynamics Prediction

The final question that was examined was if the movement of the valve could be predicted reliably enough to use in control. If it was known how far the joint would travel once the valve was turned off, then it would be possible to know when to turn off the valve to reach a desired position. To determine this, two test cycles were run in which the valve was turned on and then off six times in each test. All of the tests were normalized to the time when the position sensor first saw movement, so that all positions were relative to the position at this time. Since control was going to be performed using the position reading on the microcontroller, the calibration to angle was not applied. The average relative position at each relative sample time

was taken, both for the two tests and for all 12 times the valve was shut off. Figure 4.2.20 and Figure 4.2.21 show the results from each of the two tests.

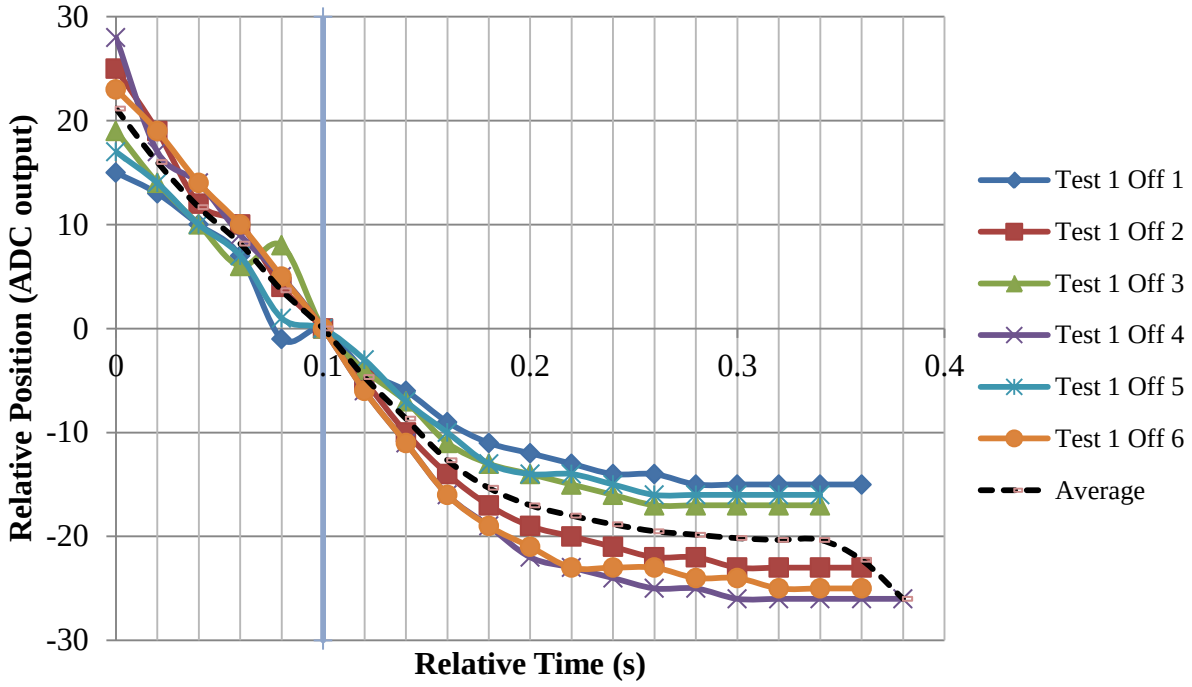


**Figure 4.2.20. The relative joint position for Test 1 after valve is shut off.**

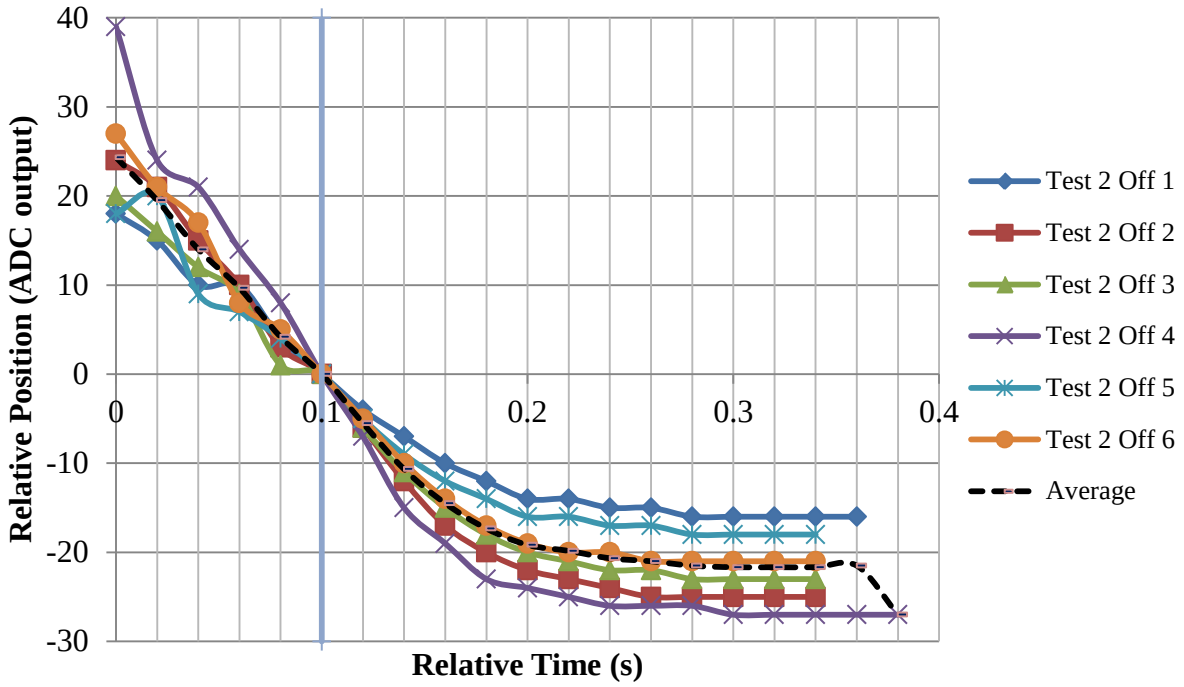


**Figure 4.2.21. The relative joint position for Test 2 after valve is shut off.**

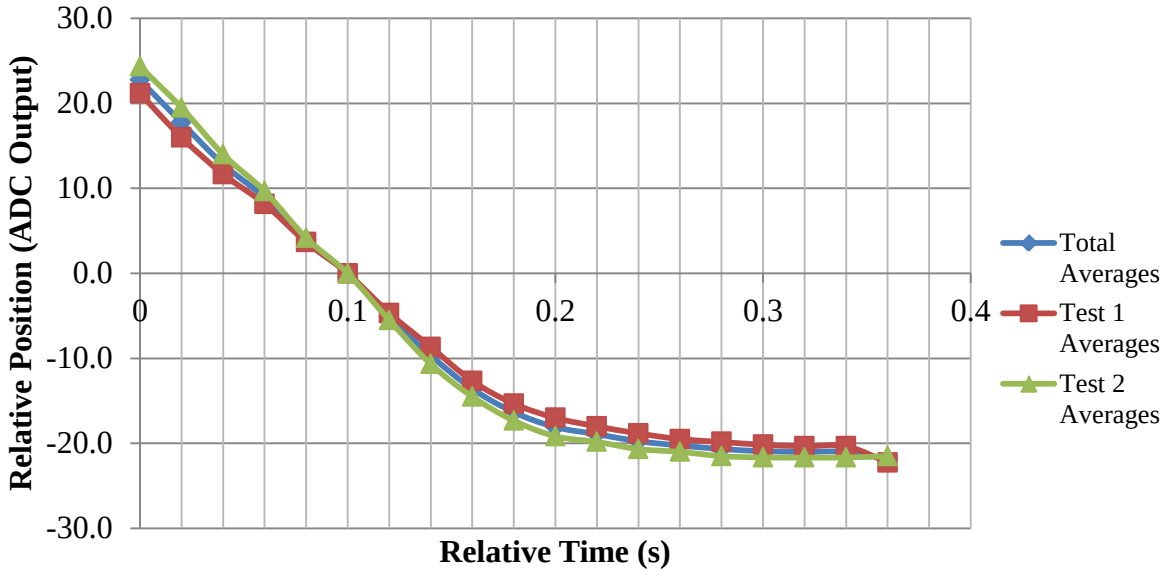


**Figure 4.2.22. Overall average relative position for all 12 tests.**

The time required for the movement to cease after the valve closes was relatively consistent for all twelve of the tests. The average movement after the valve stopped was 21

positions. Because the results showed high repeatability, it was decided to test an implementation of control using the predicted valve movement.

### 4.4.4 Control Design

The design of the controller was based around a simple closed loop scheme with a deadband. Because the valve was force to operate as an on-off actuator, the valve was turned off when the sensor had a reading within 2 degrees of the desired position. Additionally, because the valve would take 2 degrees to complete turn off, any position within this range would result in no output to the valve. Equations 4.2.4- 4.2.6 show the mathematical implementation.

$$e' = \theta_d - \theta \tag{4.2.4}$$

The error $e'$ is the difference between the desired angle of the joint, $\theta_d$ and the actual angle $\theta$. However, this error signal may be smaller than the minimum angle the joint will be able to move, $\theta_{min}$. Therefore, a conditional statement is applied.

$$e = \begin{cases} e', if \ \|e'\| < \theta_{min} \\ 0, else \end{cases} \tag{4.2.5}$$

The primary control law was then applied, as seen in Equation 1.4.3.

$$u = V_{max} sgn(e) \tag{4.2.6}$$

where $u$ is the input into the solenoid, $V_{max}$ is the supply voltage, and $sgn$ is the signum function, which gives the sign of the error. This was applied at a sampling rate of 50 Hz, which was well above the switching speed of the valve.

### 4.4.5 Control Results

The performance of the control equation was evaluated using three tests. The first gave random step changes in the desired position, as seen in Figure 4.2.23. The second test gave a sine wave desired position and is shown in Figure 4.2.24. The final test, seen in Figure 4.2.25, gave a varying trajectory for the valve to follow.

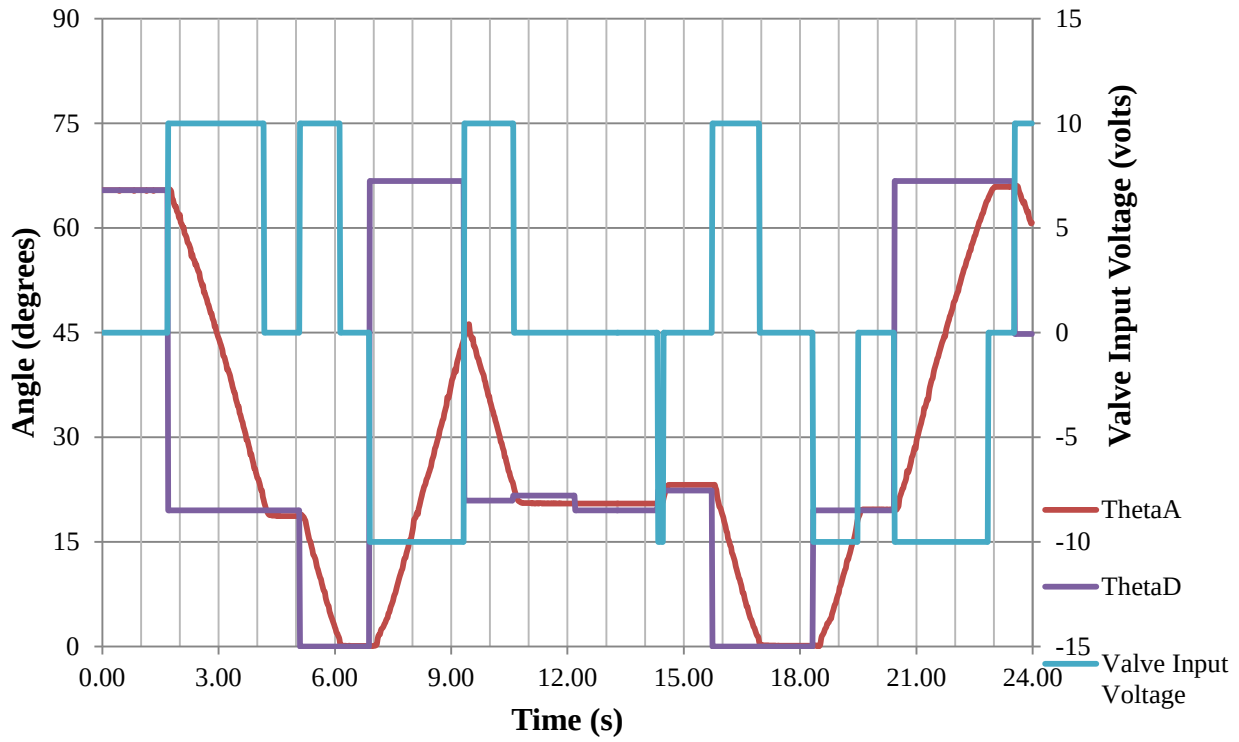


**Figure 4.2.23. Step set point control results. The desired angle was ThetaD and the measured angle was ThetaA. The valve input voltage is plotted using the right vertical axis.**

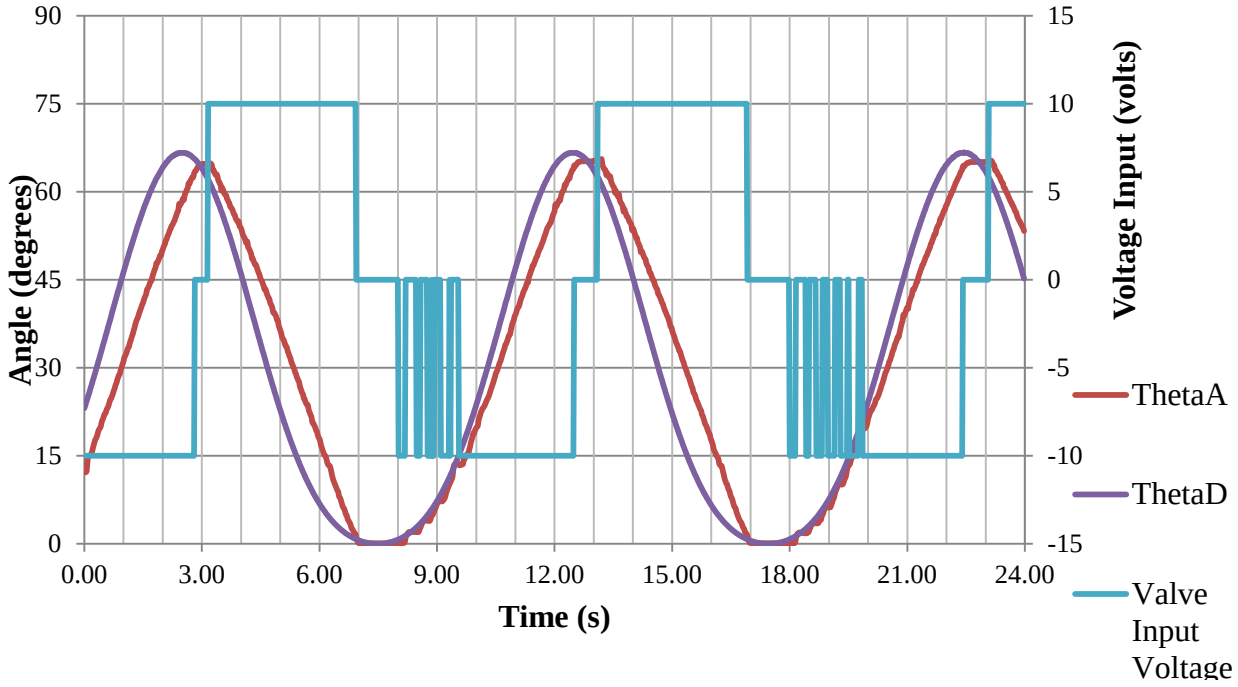


**Figure 4.2.24. Tracking a sine wave set point. The input sine wave had a frequency of 0.1 Hz, and amplitude of 450, and a DC offset of 450. The desired angle was ThetaD and the measured angle was ThetaA. The valve input voltage is plotted using the right vertical axis.**

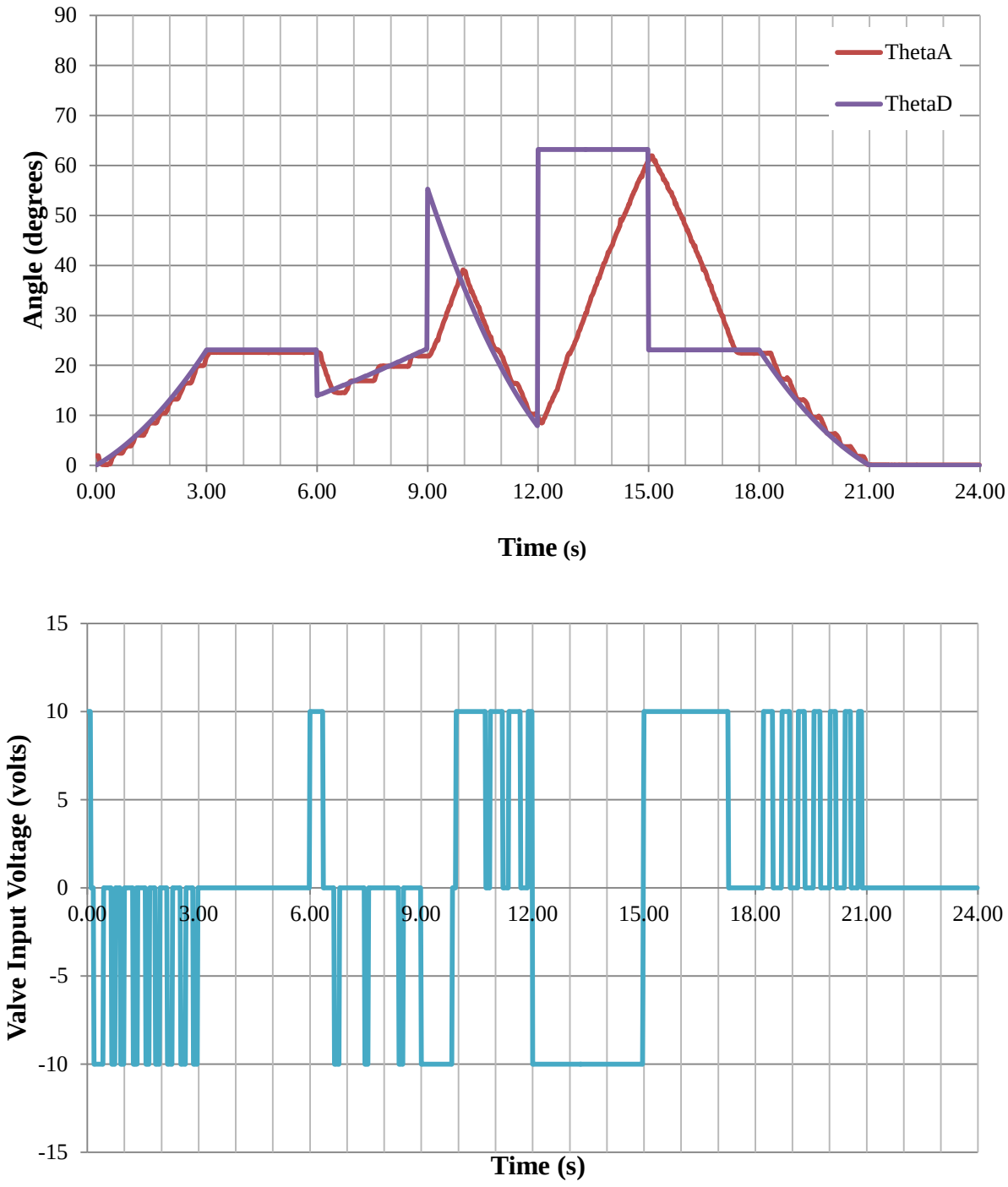


**Figure 4.2.25. Trajectory set point tracking results. The desired angle was ThetaD and the measured angle was ThetaA. The valve input voltage is plotted using the right vertical axis.**

The three tests showed that the control law is able to command the valve to the desired position. The first test, which used varying step changes in desired position, showed that the valve was consistently able to drive the system within 1 degree of the desired position. The greatest limitation seen was the max speed of the valve, which was shown to be fairly consistent around 20 degrees/ second. Similar results were seen for the other two tests as well. Overall, the valve was capable of controlling the joint position accurately, reliably, and repeatedly.

## 4.5 Conclusions

The goal with the hydraulic system was to control the position of the hydraulic piston using a low-cost, commercial direction valve. With limited information about the dynamic response of the component, several control questions were presented and evaluated. Both an electric and hydraulic circuit were developed that allowed various control strategies to be implemented. No proportional range was found for the valve, and pre-loading the valve did not seem to have a significant impact on switching time. The valve dynamics were predictable enough to implement a simple control strategy, which was able to follow a tracking input with relatively low steady-state error. The greatest limitation was the valve speed, which was determined by the adjustable flow control valve and therefore throttled the settling time of the valve to improve steady state error.

The next stage of this work would focus around creating an algorithm that is more adaptive to changes in the system. Some correlation between the velocity before the valve closed and the final amount of movement, but significantly more data would have been necessary to find a quantifiable trend which would have the possibility of reducing the steady state error and handling outside disturbances better. The control is also designed to handle the volumetric flow rate that was used for testing and may not be able to handle a wide range of flow rates. Re-testing could be performed, potentially automatically when the system starts up, to calibrate the control to a different flow rate. If combined with a correlation between valve speed and distance traveled once the valve is closed, a control algorithm could be developed that would be able to adapt to a range of hydraulic input parameters to position the piston.

In the overall scope of the project, the complexity of hydraulics was determined to outweigh the strength benefits when compared to electric motors. The nonlinearity proved to be

a non-trivial problem to control, and leaking was difficult to avoid. Additional components would likely be necessary to better control the valve as well, driving up the cost and weight. It is certainly important to note that if the hydraulic motor, pump, and valves were better sized for the system, a higher level of control would be possible. The use of proportional valves would also be an important change for improving performance that would always be limited for the valve used here. Although hydraulics were found to be more difficult than electric motors for the leg design, significant gains were made through the process of developing the hydraulic system, most importantly the basis for the electronics of the legs and a better understanding of joint control and kinematics.

# Chapter 5

# Conclusions

A pair of low-cost, biomimetic robotic legs based on the size of a 6 foot tall human were designed and fabricated. In order for humanoid robotics to transition from research environments to integration in daily life, the price of these systems must be greatly reduced. Currently many costly components and complex geometries are employed in other leg designs. Therefore the design of these new robotic legs focused on achieving comparable performance while remaining as inexpensive as possible.

Chapter 1 of this thesis provides a survey of the humanoid robotic legs that have been released between 2006-2012. Key design parameters for each robot were collected and presented. Trends in the total group and within series of robots developed by the same research group were discussed. Suggestions for improving the reporting of this data were laid out, and a discussion of future trends in robotic legs was also presented.

Chapter 2 focused on the design of the robotic legs, from the design parameters, to the component selection, and finally to the final design. Human anatomy data was researched to develop the metrics for the range of motion, length, and weight for each segment. To determine the joint torque and velocity, data from human walking and from another humanoid robot was considered, and actuators were chosen to match or exceed the torque of each. Planetary gear heads were used to reduce costs over more expensive drives that are commonly used in other robots. Brushed DC motors were chosen for five joints, and a linear actuator driven by a stepper motor was selected for the ankle flexion. The design of each joint segment was presented and showed how simple machined parts and off-the-shelf components that were used throughout the design saved cost on manufacturing.

Chapter 3 describes the electrical components and control architecture for the system. The rationale for the chosen motor drivers is discussed. Potentiometers were chosen as the position feedback sensors because they are absolute, inexpensive, and compact. The zero moment point is a common parameter derived from force sensor data, and a methodology using

three sensors was employed. Although several sensors were considered, a single-axis resistive load cell was chosen. An overall control architecture was presented, which used a PC for user interface and a series of microcontrollers to interface with the motor drivers and sensors. A Simulink model of the legs dynamics was created and used to simulate a walking gait. This model can be used to evaluate control algorithms and simulate disturbances.

Chapter 4 discusses the evaluation of hydraulics as an actuator for a robotic system by developing a control system for a single cylinder. A literature review showed that the common methodologies used to perform position control on a hydraulic valve would not work for a valve with slow switching speed. A low-cost flow control valve was selected and investigated to determine if the speed could be increased. The control electronics used in the valve control was used as a basis for developing the control architecture for the robotic legs. A voltage pre-load did not improve performance significantly and no proportional range of operation was found. However, the valve dynamics were found to be consistently predictable. Therefore, a predictive deadband controller was used to turn the valve off at the appropriate time to track the desired position. The controller had a steady state error of less than 1 degree and showed little overshoot.

# Summary of major achievements

A pair of low-cost, biomimetic legs with 12 degrees of freedom was developed for approximately $14,500, with cost savings being derived from less expensive

Analysis of methods for position control of a low-speed on-off hydraulic valve was performed and found that the system response after the valve closed was predictable and repeatable.

A predictive deadband control algorithm for the hydraulic valve was developed and was capable of tracking an input with a steady state error under 1 degree and with little overshoot.

# Appendix A

# Copyright Permissions

Figure 1.1.5


**Thesis / Dissertation Reuse**

**The IEEE does not require individuals working on a thesis to obtain a formal reuse license, however, you may print out this statement to be used as a permission grant:**

*Requirements to be followed when using any portion (e.g., figure, graph, table, or textual material) of an IEEE copyrighted paper in a thesis:*

1) In the case of textual material (e.g., using short quotes or referring to the work within these papers) users must give full credit to the original source (author, paper, publication) followed by the IEEE copyright line © 2011 IEEE.
2) In the case of illustrations or tabular material, we require that the copyright line © [Year of original publication] IEEE appear prominently with each reprinted figure and/or table.
3) If a substantial portion of the original paper is to be used, and if you are not the senior author, also obtain the senior author's approval.

*Requirements to be followed when using an entire IEEE copyrighted paper in a thesis:*

1) The following IEEE copyright/ credit notice should be placed prominently in the references: © [year of original publication] IEEE. Reprinted, with permission, from [author names, paper title, IEEE publication title, and month/year of publication]
2) Only the accepted version of an IEEE copyrighted paper can be used when posting the paper or your thesis on-line.
3) In placing the thesis on the author's university website, please display the following message in a prominent place on the website: In reference to IEEE copyrighted material which is used with permission in this thesis, the IEEE does not endorse any of [university/educational entity's name goes here]'s products or services. Internal or personal use of this material is permitted. If interested in reprinting/republishing IEEE copyrighted material for advertising or promotional purposes or for creating new collective works for resale or redistribution, please go to http://www.ieee.org/publications_standards/publications/rights/rights_link.html to learn how to obtain a License from RightsLink.

Figure 1.1.6


Copyright Clearance Center
RightsLink®
Home
Create Account
Help
Taylor & Francis
Taylor & Francis Group
Title: Study on Roller-Walker — Improvement of Locomotive Efficiency of Quadruped Robots by Passive Wheels
Author: Gen Endo, Shigeo Hirose
Publication: Advanced Robotics
Publisher: Taylor & Francis
Date: May 1, 2012
Copyright © 2012 Taylor & Francis
User ID
Password
Enable Auto Login
LOGIN
Forgot Password/User ID?
If you're a copyright.com user, you can login to RightsLink using your copyright.com credentials. Already a RightsLink user or want to learn more?
Thesis/Dissertation Reuse Request
Taylor & Francis is pleased to offer reuses of its content for a thesis or dissertation free of charge contingent on resubmission of permission request if work is published.
BACK
CLOSE WINDOW
Copyright © 2013 Copyright Clearance Center, Inc. All Rights Reserved. Privacy statement.
Comments? We would like to hear from you. E-mail us at customercare@copyright.com

# Appendix B

# Survey References


ASIMO

Honda Motor Company. (2013). *ASIMO (2011-): All-new ASIMO*. Retrieved from http://world.honda.com/ASIMO/technology/2011/index.html

ATOM

FutureBot Components. (2013). *FutureBots Humanoid Lab.* Retrieved from http://www.futurebots.com/walk.htm

BHR-2

Huang, T. (2011). Some recent advances in mechanisms and robotics in China–Beijing. *Technology Developments: The Role of Mechanism and Machine Science and IFToMM*, . 265-279. Springer Netherlands. doi:10.1007/978-94-007-1300-0_22

Xiao, T., Li, M., Huang, Q., Zhang, W., & He, L. (2007, August). Analysis of pushing manipulation by humanoid robot BHR-2 during dynamic walking. *Proceedings of the IEEE International Conference on Automation and Logistics*, 3000-3005. IEEE. Retrieved from http://ieeexplore.ieee.org/xpls/abs_all.jsp?arnumber=4339096

Zhang, L., Huang, Q., Lu, Y., Xiao, T., Yang, J., & Keerio, M. (2006, October). A visual tele-operation system for the humanoid robot BHR-02. *Proceedings of the IEEE/RSJ International Conference on Intelligent Robots and Systems*, 1110-1114. IEEE. Retrieved from http://ieeexplore.ieee.org/xpls/abs_all.jsp?arnumber=4058514

Zhang, L., Jiang, Z., Huang, Q., Lu, Y., & Xiao, T. (2007, December). A reconstruction method for working scene of humanoid robot BHR-02 teleoperation based on multiple information fusion. *Proceedings of the IEEE International Conference on Robotics and Biomimetics*, 745-750. IEEE. Retrieved from http://ieeexplore.ieee.org/xpls/abs_all.jsp?arnumber=4522256

BHR-3

Zhang, W., Chen, F., Li, M., & Huang, Q. (2010, December). Simulation of humanoid motion based on the foot with one active joint. *Proceedings of the IEEE International Conference on Robotics and Biomimetics*, 167-172. IEEE. Retrieved from http://ieeexplore.ieee.org/xpls/abs_all.jsp?arnumber=5723321

BHR-4

Yu, Z., Chen, X., Huang, Q., Wang, H., Zhang, S., Xu, W., . . . & Fan, N. (2012, June). Humanoid walking pattern generation based on the ground reaction force features of human walking. *Proceedings of the International Conference on Information and Automation,* 753-758. IEEE. Retrieved from http://ieeexplore.ieee.org/xpls/abs_all.jsp?arnumber=6246919

CB

Bentivegna, D. C., Atkeson, C. G., & Kim, J. Y. (2007, November). Compliant control of a hydraulic humanoid joint. *Proceedings of the 7th IEEE-RAS International Conference on Humanoid Robots,* 483-489. IEEE.

Cheng, G., Hyon, S. H., Morimoto, J., Ude, A., Hale, J. G., Colvin, G., ... & Jacobsen, S. C. (2007). CB: A humanoid research platform for exploring neuroscience. *Advanced Robotics*, *21*(10), 1097-1114.

Cheng, G., Hyon, S. H., Ude, A., Morimoto, J., Hale, J. G., Hart, J., ... & Kawato, M. (2008, May). Cb: Exploring neuroscience with a humanoid research platform. *International Conference on Robotics and Automation*, 1772-1773. IEEE.

Hyon, S. H. (2009). A motor control strategy with virtual musculoskeletal systems for compliant anthropomorphic robots. *IEEE/ASME Transactions on Mechatronics*, *14*(6), 677-688.

Stephens, B. J., & Atkeson, C. G. (2010, December). Push recovery by stepping for humanoid robots with force controlled joints. *Proceedings of the International Conference on Humanoid Robots,* 52-59. IEEE.

Stephens, B. J. (2011, May). State estimation for force-controlled humanoid balance using simple models in the presence of modeling error. *International Conference on Robotics and Automation,* 3994-3999. IEEE.

Stephens, B. (2011). *Push recovery control for force-controlled humanoid robots* (Doctoral dissertation, Carnegie Mellon University). Retrieved from https://www.cs.cmu.edu/afs/cs.cmu.edu/Web/People/bstephe1/papers/thesis.pdf

CHARLI-L and CHARLI-2

Han, J. (2012). *Bipedal walking for a full-sized humanoid robot utilizing sinusoidal feet trajectories and its energy consumption* (Doctoral dissertation, Virginia Tech). Retrieved from http://scholar.lib.vt.edu/theses/available/etd-05042012-155706/

COMAN

Colasanto, L., Tsagarakis, N. G., & Caldwell, D. G. (2012, June). A compact model for the compliant humanoid robot COMAN. *Proceedings of the IEEE RAS & EMBS International Conference on Biomedical Robotics and Biomechatronics, 4,* 688-694. IEEE. Retrieved from http://ieeexplore.ieee.org/xpls/abs_all.jsp?arnumber=6290765

Kormushev, P., Ugurlu, B., Calinon, S., Tsagarakis, N. G., & Caldwell, D. G. (2011, September). Bipedal walking energy minimization by reinforcement learning with evolving policy parameterization. *Proceedings of the IEEE/RSJ International Conference on Intelligent Robots and Systems,* 318-324. IEEE. Retrieved from http://ieeexplore.ieee.org/xpls/abs_all.jsp?arnumber=6094427

Li, Z., Vanderborght, B., Tsagarakis, N. G., Colasanto, L., & Caldwell, D. G. (2012, May). Stabilization for the compliant humanoid robot COMAN exploiting intrinsic and controlled compliance. *Proceedings of the IEEE International Conference on Robotics and Automation,* 2000-2006. IEEE. Retrieved from http://ieeexplore.ieee.org/xpls/abs_all.jsp?arnumber=6224705

DLR

Englsberger, J., Ott, C., Roa, M. A., Albu-Schaffer, A., & Hirzinger, G. (2011, September). Bipedal walking control based on capture point dynamics. *Proceedings of the IEEE/RSJ International Conference on Intelligent Robots and Systems,* 4420-4427. IEEE. Retrieved from http://ieeexplore.ieee.org/xpls/abs_all.jsp?arnumber=6094435

Ott, C., Baumgartner, C., Mayr, J., Fuchs, M., Burger, R., Lee, D., . . . & Hirzinger, G. (2010, December). Development of a biped robot with torque controlled joints. *Proceedings of the IEEE-RAS International Conference on Humanoid, 10,* 167-173. IEEE. Retrieved from http://ieeexplore.ieee.org/xpls/abs_all.jsp?arnumber=5686340

HRP-3

Kaneko, K., Harada, K., Kanehiro, F., Miyamori, G., & Akachi, K. (2008, September). Humanoid robot HRP-3. *Proceedings of the IEEE/RSJ International Conference on Intelligent Robots and Systems,* 2471-2478. IEEE. Retrieved from http://ieeexplore.ieee.org/xpls/abs_all.jsp?arnumber=4650604

HPR-4

Kaneko, K., Kanehiro, F., Morisawa, M., Akachi, K., Miyamori, G., Hayashi, A., & Kanehira, N. (2011, September). Humanoid robot hrp-4-humanoid robotics platform with lightweight and slim body. *Proceedings of the IEEE/RSJ International Conference on Intelligent Robots and Systems,* 4400-4407. IEEE. Retrieved from http://ieeexplore.ieee.org/xpls/abs_all.jsp?arnumber=6094465

KBHR

Lim, H. O., & Tajima, K. (2008, October). Mechanism and control of biped walking robot with 3 DOF waist. *Proceedings of the International Conference on Control, Automation and Systems,*2026-2031. IEEE.

Yamada, K., Sayama, K., Yoshida, T., & Lim, H. O. (2011, October). Mechanisms of biped humanoid robot and online walking pattern generation. *Proceedings of the International Conference on Control, Automation and Systems,* 1117-1122. IEEE.

KHR4-HUBO 2

Ali, M. A., Park, H. A., & Lee, C. G. (2010, October). Closed-form inverse kinematic joint solution for humanoid robots. *Proceedings of the 2010 IEEE/RSJ International Conference on Intelligent Robots and Systems, Taipei, Taiwan,* 704-709.

Carroll, J. M., Jiang, H., Rosson, M. B., Shih, S.- I., Wang, J., Xiao, L., & Zhao, D. (2011, May). *Supporting activity awareness in computer-mediated collaboration*. Paper presented at the IEEE International Conference on Collaboration Technologies and Systems, Philadelphia, PA.

Gross, R. J., & Oh, P. Y. (2010). A scalable software toolkit for miniature humanoids. *Proceedings of the International Conference on Automation, Robotics and Control Systems, Orlando, FL,* 1-6. Retrieved from http://dasl.mem.drexel.edu/~rjGross/wp-content/uploads/2011/07/A-Scalable-Software-Toolkit-for-Miniature-Humanoids.pdf

Lofaro, D. M. (2009a). *Jaemi Hubo (KHR4) users manual*. Retrieved from http://www.pages.drexel.edu/~dml46/DASL/Weekly_Update_2009-09-21_files/JaemiHubo_Manual_KHR4_R1_2009-09-24.pdf

Lofaro, D. M. (2009b). *Jaemi Hubo (KHR4) users manual*. Retrieved from http://www.pages.drexel.edu/~dml46/DASL/Weekly_Update_2009-10-08_files/JaemiHubo_Manual_KHR4_R1_2009-10-08.pdf

Lofaro, D. M. (2009c). *Jaemi Hubo (KHR4) users manual*. Retrieved from http://www.pages.drexel.edu/~dml46/DASL/HUBO/JaemiHubo_Manual_KHR4_R1_2009-12-22_0236.pdf

LOLA

Buschmann, T., Favot, V., Lohmeier, S., Schwienbacher, M., & Ulbrich, H. (2011). Experiments in fast biped walking. *Proceedings of the International Conference on Mechatronics, Istanbul, Turkey,* 863-868. IEEE.

Buschmann, T., Lohmeier, S., & Ulbrich, H. (2009). Humanoid robot LOLA: Design and walking control. *Journal of Physiology-Paris, 103*(3), 141-148.

Favot, V., Schwienbacher, M., Buschmann, T., Lohmeier, S., & Ulbrich, H. (2010, September). The Humanoid Robot LOLA—Experimental Results. *Proceedings of the International Conference on Numerical Analysis and Applied Mathematics, 1*, 398-401.

Lohmeier, S., Buschmann, T., & Ulbrich, H. (2009). Humanoid robot LOLA. *Proceedings of the International Conference on Robotics and Automation, Kobe, Japan,* 775-780. IEEE.

MAHRU 11

Oh, Y., Ahn, K. H., Kim, D., & Kim, C. (2006). An analytical method to generate walking pattern of humanoid robot. *Proceedings of the IEEE/IECON 32nd Annual Conference on Industrial Electronics, Paris, France,* 4159-4164.

MAHRU 111

Kwon, W., Kim, H. K., Park, J. K., Roh, C. H., Lee, J., Park, J., . . . & Roh, K. (2007). Biped humanoid robot MAHRU III. *Proceedings of the 7th IEEE-RAS International Conference on Humanoid Robots, Bled, Slovenia,* 583-588.

MAHRU R

Chang, Y. H., Oh, Y., Kim, D., & Hong, S. (2008). Balance control in whole body coordination framework for biped humanoid robot MAHRU-R. *Proceedings of the 17th IEEE International Symposium on Robot and Human Interactive Communication, Munich, Germany,* 401-406.

Hong, S., Oh, Y., You, B. J., & Oh, S. R. (2009). A walking pattern generation method of humanoid robot MAHRU-R. *Intelligent Service Robotics*, *2*(3), 161-171.

MAHRU-Z

Kim, K., Cha, Y. S., Park, J. M., Lee, J. Y., & You, B. J. (2011). Providing services using network-based humanoids in a home environment. *IEEE Transactions on Consumer Electronics*, *57*(4), 1628-1636.

Kim, K., Lee, J. Y., Kim, S. J., Jeong, M. H., & You, B. J. (2010). Network-based humanoid operation in home environment. *Proceedings of the 2010 IEEE International Conference on Robotics and Biomimetics, Tianjin, China*, 423-430.

REEM B

Tellez, R., Ferro, F., Garcia, S., Gomez, E., Jorge, E., Mora, D., . . . & Faconti, D. (2008). Reem-B: An autonomous lightweight human-size humanoid robot. *Proceedings of the 8th IEEE-RAS International Conference on Humanoid Robots, Daejeon, South Korea,* 462-468.

SURALP

Erbatur, K., Seven, U., Taskran, E., Koca, O., Ylmaz, M., Unel, M., . . . & Onat, A. (2009). SURALP: A new full-body humanoid robot platform. *Proceedings of the 2009 IEEE/RSJ International Conference on Intelligent Robots and Systems, St. Louis, MO,* 4949-4954. IEEE.

Seven, U., Akbas, T., Fidan, K. C., & Erbatur, K. (2012). Bipedal robot walking control on inclined planes by fuzzy reference trajectory modification. *Soft Computing, 16*(11), 1959-1976.

Running Robot

Ota, Y. (2010, May). Partner robots—From development to implementation. *Proceedings of the 2010 3rd Conference on Human System Interactions, Rzeszow, Poland,* 14-16.

Violin Playing Robot

Chestnutt, J., Takaoka, Y., Doi, M., Suga, K., & Kagami, S. (2010). Safe adjustment regions for legged locomotion paths. *Proceedings of the 2010 10th IEEE-RAS International Conference on Humanoid Robots, Nashville, TN*, 224-229. doi:10.1109/ICHR.2010.5686829

Tajima, R., Honda, D., & Suga, K. (2009). Fast running experiments involving a humanoid robot. *Proceedings of the 2009 IEEE International Conference on Robotics and Automation, Kobe, Japan,* 1571-1576.

WABIAN 2R

Hashimoto, K., Yoshimura, Y., Kondo, H., Lim, H. O., & Takanishi, A. (2011). Realization of quick turn of biped humanoid robot by using slipping motion with both feet. *Proceedings of the 2011 IEEE International Conference on Robotics and Automation, Shanghai, China,* 2041-2046.

Kang, H. J., Hashimoto, K., Nishikawa, K., Falotico, E., Lim, H. O., Takanishi, A., . . . & Berthoz, A. (2012). Biped walking stabilization on soft ground based on gait analysis. *Proceedings of the 2012 4th IEEE RAS & EMBS International Conference on Biomedical Robotics and Biomechatronics, Rome, Italy*, 669-674.

Ogura, Y., Aikawa, H., Shimomura, K., Morishima, A., Lim, H. O., & Takanishi, A. (2006). Development of a new humanoid robot WABIAN-2. *Proceedings of the 2006 IEEE International Conference on Robotics and Automation, Orlando, FL,* 76-81.

Ogura, Y., Shimomura, K., Kondo, A., Morishima, A., Okubo, T., Momoki, S., . . . & Takanishi, A. (2006). Human-like walking with knee stretched, heel-contact and toe-off motion by a humanoid robot. *Proceedings of the 2006 IEEE/RSJ International Conference on Intelligent Robots and Systems, Beijing, China,* 3976-3981.

# Appendix C

# Survey Robot Series References


ASIMO

Honda Motor Company. (2007). *ASIMO: Technical information.* Retrieved from http://asimo.honda.com/downloads/pdf/asimo-technical-information.pdf

HRP-2

Kaneko, K., Kanehiro, F., Kajita, S., Hirukawa, H., Kawasaki, T., Hirata, M., Akachi, K., & Isozumi, T., (2004). Humanoid robot HRP-2. *Proceedings of the IEEE International Conference on Robotics and Automation, Barcelona, Spain, 2,* 1083-1090. doi:10.1109/ROBOT.2004.1307969

Kaneko, K., Kanehiro, F., Morisawa, M., Yoshida, E., & Laumond, J. (2012). Disturbance observer that estimates external force acting on humanoid robots. *Proceedings of the 12th IEEE International Workshop on Advanced Motion Control, Trento, Italy, 12,* 1-6. Retrieved from http://ieeexplore.ieee.org/xpls/abs_all.jsp?arnumber=6197026

KHR-1

Kim, J. H., & Oh, J. H. (2004, April). Walking control of the humanoid platform KHR-1 based on torque feedback control *Proceedings of the International Conference Robotics and Automation, 1*, 623-628. IEEE.

KHR2

Kim, J. Y., Park, I. W., Lee, J., Kim, M. S., Cho, B. K., & Oh, J. H. (2005, April). System design and dynamic walking of humanoid robot KHR-2. . *Proceedings of the International Conference Robotics and Automation*, 1431-1436. IEEE.

KHR3 (Hubo)

Cho, B. K., Park, S. S., & Oh, J. H. (2009, December). Controllers for running in the humanoid robot, HUBO. *Proceedings of the International Conference on Humanoid Robots,* 385-390. IEEE.

Park, I. W., Kim, J. Y., Lee, J., & Oh, J. H. (2005, December). Mechanical design of humanoid robot platform KHR-3 (KAIST humanoid robot 3: HUBO). *Proceedings of the International Conference on Humanoid Robots*, 321-326. IEEE.

MAHRU 1

You, B. J., Kim, D., Kim, C., Oh, Y., Jeong, M., & Oh, S. (2008). Network-based humanoid 'MAHRU' as ubiquitous robotic companion. *Proceedings of the 17th World Congress, the International Federation of Automatic Control, Seoul, Korea*, 724-729. doi:10.3182/20080706-5-KR-1001.4257

# Appendix D

# Component Information

Mack Corp Hydraulic Cylinder

***SHORT STROKE HYDRAULIC ACTUATORS - HI-ENERGY® SERIES 1500-DA-SE-SP-LM***
***Double Acting-Single Ended Pistons-Side Ported-Lug Mounted***

**SPECIFICATIONS:**
**SERVICE, HYDRAULIC OIL**
**M.O.P. 1500 PSI**
**TEMPERATURE, -40 TO + 275 DEG. F.**
**MATERIALS:**
**COVER, BEARING BRONZE**
**BODY & PISTON, STAINLESS STEEL**
**FASTENERS, ALLOY STEEL**
**PISTON HEAD SEAL, "O" RING**
**ROD SEAL, LIP STYLE**

**NOTES:**
**DIMENSIONS ARE NOMINAL IN U.S.A. CUSTOMARY SPECIFICATIONS. METRIC VERSIONS ARE DIMENSIONALLY EQUIVALENT EXCEPT FOR CONVERSIONS IN MOUNTING DETAILS WHERE THREADS, FASTENERS, CLEARANCE HOLES AND COUNTERBORES ARE TO METRIC STANDARDS. THERE IS NO ADDED COST FOR METRIC VERSIONS.**

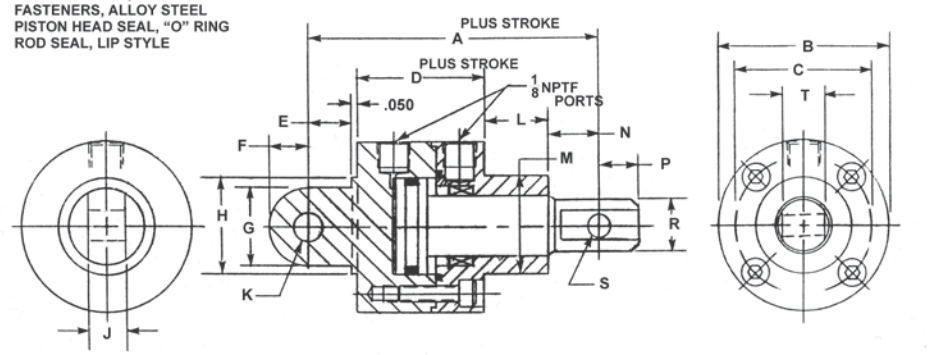


| BASIC PART NO. | A | B | C | D | E | F | G | H | J | K | L | M | N | P | R | S | T | EXT AREA (SQ.IN.) | RETR AREA (SQ.IN.) |
|---|---|---|---|---|---|---|---|---|---|---|---|---|---|---|---|---|---|---|---|
| S6558-(-)-LS | 2.452 | 1.500 | 1.142 | 1.253 | 0.375 | 0.313 | 0.625 | 0.750 | 0.313 | 0.250 | 0.433 | 0.750 | 0.341 | 0.189 | 0.378 | 0.156 | 0.313 | 0.428 | 0.277 |
| S6559-(-)-LS | 2.854 | 1.750 | 1.358 | 1.303 | 0.500 | 0.438 | 0.875 | 1.000 | 0.438 | 0.313 | 0.590 | 0.938 | 0.411 | 0.241 | 0.482 | 0.188 | 0.375 | 0.672 | 0.423 |
| S6560-(-)-LS | 3.122 | 2.000 | 1.575 | 1.353 | 0.500 | 0.438 | 0.875 | 1.125 | 0.438 | 0.375 | 0.745 | 1.125 | 0.474 | 0.304 | 0.608 | 0.250 | 0.500 | 0.982 | 0.610 |
| S6561-(-)-LS | 3.387 | 2.250 | 1.832 | 1.403 | 0.563 | 0.500 | 1.000 | 1.250 | 0.500 | 0.375 | 0.828 | 1.250 | 0.543 | 0.356 | 0.712 | 0.313 | 0.600 | 1.470 | 0.951 |
| S6562-(-)-LS | 3.952 | 2.500 | 2.067 | 1.453 | 0.750 | 0.625 | 1.250 | 1.563 | 0.500 | 0.500 | 1.062 | 1.563 | 0.637 | 0.450 | 0.900 | 0.375 | 0.750 | 2.010 | 1.226 |

**NOM. FORCE (lbs) = PRESSURE (psi) times AREA (sq.in.)**

**ORDERING INFORMATION:**

**HOW TO ORDER BASIC CYLINDERS:**
**A BASIC PART NUMBER consists of the letter "S" and four digits followed by a dash number to indicate piston stroke in increments of 1/10 (0.100) inch followed by the suffix -LS. Strokes to -20 (2.000) are standard products.**
**BASIC PART NO.**
**EXAMPLE = S6558-5-LS**
**Lip Seal Suffix**
**Indicates Piston Stroke**
**Letter & four digits from the table**

**HOW TO ORDER ALL STAINLESS STEEL CYLINDERS:**
**Add another letter "S" as a prefix to a BASIC PART NO.**
**Add 20% to the BASE PRICE.**
**EXAMPLE = S S6558-5-LS**
**BASIC PART NO.**
**All Stainless Steel Prefix**

**HOW TO ORDER METRIC VERSIONS:**
**A BASIC PART NO. FOR THE METRIC VERSIONS consists of the letter "S" and a four digit number from the table with a prefix "M" followed by a dash number to indicate stroke in millimeters followed by the dash number " - LS". Please see inside rear cover for metric thread and stroke conversions. There is no added cost.**
**EXAMPLE = M - S6558 - 20 - LS**
**Suffix**
**Stroke in millimeters**
**From the table**
**Metric prefix**

**HOW TO ORDER SERVICE KITS:**
**Specify the complete part number followed by the suffix "-SK".**
**EXAMPLE = S6558-LS-SK**
**Indicates service kit only.**
**Complete part number.**

MACK CORPORATION

***Data Sheet 2004-3***
***H-38***

# References

*Note: References from the survey performed in Chapter 1 are in Appendices B and C above.*


Ahn, K., & Yokota, S. (2005). Intelligent switching control of pneumatic actuator using on/off solenoid valves. *Mechatronics, 15*(6), 683-702. Retrieved from http://www.sciencedirect.com/science/article/pii/S0957415805000292

Applied Motion Products. (n.d.). *ST stepper drives.* Retrieved from http://www .applied-motion.com/sites/default/files/ST_Datasheet_925-0007.pdf

Beaglebone.org. (2012, May 9). *BeagleBone Rev A6 System Reference Manual*. Retrieved from http://beagleboard.org/static/beaglebone/latest/Docs/Hardware/BONE_SRM.pdf

Becan, M. R. (2005). Fuzzy boundary layer solution to nonlinear hydraulic position control problem. *Proceedings of the Third World Enformatika Conference WEC, Istanbul, Turkey, 5*, 206-208. Retrieved from http://citeseerx.ist.psu.edu/viewdoc/download?doi=10.1.1.193.1134&rep=rep1&type=pdf

Behnke, S. (2008). Humanoid robots–From fiction to reality? *Künstliche Intelligenz Heft, 4*(8), 5-9. Retrieved from http://www.ais.uni-bonn.de/papers/KI08_Behnke.pdf

Bertec Corporation. (2012). *Bertec Force Plates.* Retrieved from http://bertec.com/uploads/pdfs/manuals/Force%20Plate%20Manual.pdf

Besier, T. F., Sturnieks, D. L., Alderson, J. A., & Lloyd, D. G. (2003). Repeatability of gait data using a functional hip joint centre and a mean helical knee axis. *Journal of biomechanics*, *36*(8), 1159-1168. Retrieved from http://www.sciencedirect.com/science/article/pii/S0021929003000873

BioBlend. (2011). *BioFlo FG: Biodegradable food grade AW hydraulic fluid*. Retrieved from http://www.bioblend.com/templates/rt_panacea/pdf/foodgrade/BiofloFG_tds.pdf

Boston Dynamics. (2012). *PETMAN – BigDog gets a big brother*. Retrieved from http://www.bostondynamics.com/robot_petman.html

Bucher Hydraulics. (2010). *A.C. hydraulic power system: Monarch-dyna-pack M−450 Mini & M−400 series.* Retrieved from http://www.bucherhydraulics.com/bausteine.net/f/9349 /PowerPack_AC_500-P-000002-E-00.pdf?fd=3

Bräunl, T. (2008). *Embedded robotics: Mobile robot design and applications with embedded systems* (3rd ed.). Berlin, Germany: Springer-Verlag.

Caldwell, D. G., Medrano-Cerda, G. A., & Goodwin, M. (1995). Control of pneumatic muscle actuators. *Control Systems, IEEE, 15*(1), 40-48. Retrieved from http://ieeexplore.ieee.org/xpls/abs_all.jsp?arnumber=341863

Chaffin, D. B., Andersson, G., & Martin, B. J. (1999). *Occupational biomechanics* (3rd ed.). New York, NY: Wiley.

Chevallereau, C. (2009). *Bipedal robots: Modeling, design and walking synthesis*. London, UK: ISTE.

Chew, S., Tay, W., Smit, D., & Bartneck, C. (2010). Do social robots walk or roll? *Social Robotics, LNCS 6414,* 355-361.

Coradeschi, S., Ishiguro, H., Asada, M., Shapiro, S. C., Thielscher, M., Breazeal, C., . . . Ishida, H. (2006). Human-inspired robots. *IEEE Intelligent Systems, 21*(4), 74-85. Retrieved from http://ieeexplore.ieee.org/xpls/abs_all.jsp?arnumber=1667958

Defense Advanced Research Projects Agency (DARPA). (2012). *Broad agency announcement, DARPA robotics challenge, tactical technology office* (DARPA BAA-12-39). Retrieved from www.cs.cmu.edu/~cga/drc/pdfs/DARPA-BAA-12-39.pdf

Defense Advanced Research Projects Agency (DARPA). (2013). *DARPA robotics challenge (DRC).* Retrieved from http://www.darpa.mil/Our_Work/TTO/Programs/DARPA_Robotics_Challenge.aspx

Endo, G., & Hirose, S. (2012). Study on roller-walker—Improvement of locomotive efficiency of quadruped robots by passive wheels. *Advanced Robotics, 26*(8-9), 969-988. doi:10.1163/156855312X633066

Erbatur, K., Okazaki, A., Obiya, K., Takahashi, T., & Kawamura, A. (2002, July). A study on the zero moment point measurement for biped walking robots. *Proceedings of the 7th International Workshop on Advanced Motion Control, Maribor, Slovenia,* 431-436. doi:10.1109/AMC.2002.1026959

Gamble, J. B. (1993, Nov). Robust sliding mode control of hydraulic valves. *Proceedings of the IEEE Colloquium on Advances in the Application of Robust Controllers, London, UK,* 4/1-4/5. Retrieved from http://ieeexplore.ieee.org/xpl/articleDetails.jsp?reload=true&arnumber=287406 &contentType=Conference+Publications

Gouaillier, D., Hugel, V., Blazevic, P., Kilner, C., Monceaux, J., Lafourcade, P., . . . Maisonnier, B. (2009, May). Mechatronic design of NAO humanoid. *Proceedings of the IEEE International Conference on Robotics and Automation, Paris, France,* 769-774. doi:10.1109/ROBOT.2009.5152516

Hollerbach, J. M., Hunter, I. W., & Ballantyne, J. (1992). A comparative analysis of actuator technologies for robotics. In O. Khatib, J. J. Craig, & T. Lozano-Perez, (Eds.), *The robotics review 2* (pp. 299-342). Cambridge, MA: MIT Press.

Hoover, A. M., Steltz, E., & Fearing, R. S. (2008, September). RoACH: An autonomous 2.4 g crawling hexapod robot. *Proceedings of the IEEE/RSJ International Conference on Intelligent Robots and Systems, Nice, France,* 26-33. doi:10.1109/IROS.2008.4651149

Idaho National Laboratory. (n.d.). *Humanoid robotics*. U.S. Department of Energy and Battelle Energy Alliance. Retrieved from https://inlportal.inl.gov/portal/server.pt/community/introduction/536

Image Scientific Instruments. (2013). *Stretch sensor*. Retrieved from http://www.imagesco.com/sensors/stretch.pdf

Lebouvier, R. D. (2011). *Reflections in a robot's eye: A cultural history and epistemological critique of humanoid robotics* (Doctoral dissertation). Available from ProQuest Dissertations and Theses database. (UMI No. 3483269)

Mack Corporation. (2006). *Short stroke hydraulic actuators – Hi-energy ® series 1500-DA-SE-SP-LM*. Retrieved from http://www.mackcorp.com/Catalog/Hi_nrgy_pg38/hienergypage38.html

McDowell, M. A., Fryar, C. D., Ogden, C. L., & Flegal, K. M. (2008). *Anthropometric reference data for children and adults: United States, 2003-2006* (National Health Statistics Report No. 10). Retrieved from the Center for Disease Control and Prevention website: http://www.cdc.gov/nchs/data/nhsr/nhsr010.pdf

Measurement Specialties. (n.d.). *FC23 Compression Load Cell*. Retrieved from http://www.mouser.com/ds/2/261/FC23-196040.pdf

Muecke, K. J., & Hong, D. W. (2007, October). DARwIn's evolution: Development of a humanoid robot. *Proceedings of the IEEE/RSJ International Conference on Intelligent Robots and Systems, San Diego, CA,* 2574-2575. doi:10.1109/IROS.2007.4399177

National Institutes of Health (NIH). (1998). *Clinical guidelines on the identification, evaluation, and treatment of overweight and obesity in adults: The evidence report* (NIH Publication No. 98-4083). Retrieved from the National Institutes of Health website: http://www.nhlbi.nih.gov/guidelines/obesity/ob_gdlns.pdf

Nguyen, T., Leavitt, J., Jabbari, F., & Bobrow, J. E. (2007). Accurate sliding-mode control of pneumatic systems using low-cost solenoid valves. *IEEE/ASME Transactions on Mechatronics, 12*(2), 216-219. Retrieved from http://ieeexplore.ieee.org/xpls/abs_all.jsp?arnumber=4154710

Niksefat, N., & Sepehri, N. (1999, May). Robust force controller design for an electrohydraulic actuator based on nonlinear model. *Proceedings of the IEEE International Conference on Robotics and Automation, 1,*200-206. IEEE. Retrieved from http://ieeexplore.ieee.org/stamp/stamp.jsp?tp=&arnumber=769967

Niksefat, N., & Sepehri, N. (2001). Designing robust force control of hydraulic actuators despite system and environmental uncertainties. *Control Systems, IEEE*, *21*(2), 66-77. Retrieved from http://ieeexplore.ieee.org/xpls/abs_all.jsp?arnumber=918266

Northman Fluid Power. (n.d.). *Solenoid operated directional valve: SWH-G02 series features*. Retrieved from http://www.northmanfp.com/index.htm?var1=http://www.northmanfp.com/SWH-G02.htm

Ogura, Y., Aikawa, H., Lim, H. O., & Takanishi, A. (2004). Development of a human-like walking robot having two 7-DOF legs and a 2-DOF waist. *Proceedings of the IEEE International Conference on Robotics and Automation, New Orleans, LA,* 1, 134-139. Retrieved from http://ieeexplore.ieee.org/xpls/abs_all.jsp?arnumber=1307141&tag=1

Ogura, Y., Aikawa, H., Shimomura, K., Kondo, H., & Morishima, A. (2006, May). Development of a new humanoid robot WABIAN-2. *Proceedings of the 2006 IEEE International Conference on Robotics and Automation, Orlando, FL,* 76-81. Retrieved from www.mindtrans.narod.ru/pdfs/Wabian_2_walking.pdf

Ogura, Y., Kazushi, S. A., Kondo, A. M., Tatsu, O., Shimpei, M., Hun-ok, L., & Atsuo T. (2006, Oct). Human-like walking with knee stretched, heel-contact and toe-off motion by a humanoid robot. *Proceedings of the IEEE International Conference on Intelligent Robots and Systems, Beijing, China,* 3976-3981. Retrieved from https://www2.lirmm.fr/lirmm/interne/BIBLI/CDROM/ROB/2006/IROS%202006/pdfs /IROS06-646.pdf

Ott, C., Baumgartner, C., Mayr, J., Fuchs, M., Burger, R., Lee, D., . . . & Hirzinger, G. (2010, December). Development of a biped robot with torque controlled joints. *Proceedings of the IEEE-RAS International Conference on Humanoid, 10,* 167-173. IEEE. Retrieved from http://ieeexplore.ieee.org/xpls/abs_all.jsp?arnumber=5686340

Park, I. W., Kim, J. Y., Lee, J., & Oh, J. H. (2005, December). Mechanical design of humanoid robot platform KHR-3 (KAIST humanoid robot 3: HUBO). *Proceedings of the 5th IEEE-RAS International Conference on Humanoid Robots, Tsukuba,* 321-326. doi:10.1109/ICHR.2005.1573587

Pololu Corporation. (2012). Pololu simple motor controller user's guide. Retrieved from http://www.pololu.com/docs/pdf/0J44/simple_motor_controllers.pdf

Raz, G. (2008). *Why we love robots with Guy Raz/Interviewer: Matthew Battles*. Special Series: The Opinions Page, National Public Radio. Retrieved from http://m.npr.org/story/92292759

Roaas, A., & Andersson, G. B. (1982). Normal range of motion of the hip, knee and ankle joints in male subjects, 30-40 years of age. *Acta Orthopaedica*, *53*(2), 205-208. Retrieved from http://informahealthcare.com/doi/pdf/10.3109/17453678208992202

Riekert, M. (2005, August). Professor takes his robots at face value. *The Age*. Retrieved from http://www.theage.com.au/news/creative--media/professor-takes-his-robots-at-face-value/2005/08/07/1123353208817.html

Riskin, J. (2003). Eighteenth-century wetware. *Representations, 83*(1), 97-125. Retrieved from http://bod.sagepub.com/content/18/1/1.full.pdf

Shen, S. Y., Li, C. H., Cheng, C. C., Lu, J. C., Wang, S. F., & Lin, P. C. (2009, October). Design of a leg-wheel hybrid mobile platform. *Proceedings of the 2009 IEEE/RSJ International Conference on Intelligent Robots and Systems, St. Louis, MO, USA,* 4682-4687. Retrieved from doi:10.1109/IROS.2009.5353958

Šitum, Ž., Petrić, J., & Crneković, M. (2003, June). Sliding mode control applied to pneumatic servo drive. *Proceedings of 11th Mediterranean Conference on Control and Automation*. Retrieved from http://med.ee.nd.edu/MED11-2003/pdf/papers/t1-009.pdf

Stacey, J., & Suchman, L. (2012). Animation and automation: The liveliness and labours of bodies and machines. *Body & Society*, *18*(1), 1-46. Retrieved from http://bod.sagepub.com/content/18/1/1.short

Tak, S., Song, O. Y., & Ko, H. S. (2001). Motion balance filtering. *Computer Graphics Forum, 19*(3), 437-446. doi:10.1111/1467-8659.00436

Ultra Motion. (n.d.). *The Digit.* Retrieved from http://www.ultramotion.com/products/digit.php

USA Track & Field. (2012). *World open outdoor track & field records*. Retrieved from http://www.usatf.org/statistics/records/view.asp?division=world&location=outdoor%20track%20%26%20field&age=open&sport=TF

Van Varseveld, R. B., & Bone, G. M. (1997). Accurate position control of a pneumatic actuator using on/off solenoid valves. *IEEE/ASME Transactions on Mechatronics, 2*(3), 195-204. Retrieved from http://ieeexplore.ieee.org/xpls/abs_all.jsp?arnumber=622972

Wooden, D., Malchano, M., Blankespoor, K., Howardy, A., Rizzi, A. A., & Raibert, M. (2010, May). Autonomous navigation for BigDog. *Proceedings of the IEEE/RSJ International Conference on Intelligent Robots and Systems, Anchorage, AK,* 4736-4741. doi:10.1109/ROBOT.2010.5509226

Wu, G., Sepehri, N., & Ziaei, K. (1998, September). Design of a hydraulic force control system using a generalised predictive control algorithm. *Control Theory and Applications, IEE Proceedings, 145*(5), 428-436. Retrieved from http://ieeexplore.ieee.org/xpls/abs_all.jsp?arnumber=741972